TESIS DEFENDIDA POR

Luis Alberto Sánchez Pérez

Y APROBADA POR EL SIGUIENTE COMITÉ

Dr. Pratap Narayan Sahay Sahay

Director del Comité

Dr. Antonio González Fernández

Miembro del Comité

Dr. Pedro Gilberto López Mariscal

Miembro del Comité

Dr. Thomas Kretzschmar Gunter

Coordinador del programa de posgrado en Ciencias de la Tierra

Dr. David Hilario Covarrubias Rosales

Director de Estudios de Posgrado

18 de Marzo de 2010

CENTRO DE INVESTIGACIÓN CIENTÍFICA Y DE EDUCACIÓN SUPERIOR DE ENSENADA

PROGRAMA DE POSGRADO EN CIENCIAS

EN CIENCIAS DE LA TIERRA

REFLECTION AND TRANSMISSION IN POROELASTICITY

TESIS

que para cubrir parcialmente los requisitos necesarios para obtener el grado de

MAESTRO EN CIENCIAS

Presenta:

LUIS ALBERTO SÁNCHEZ PÉREZ

Ensenada, Baja California, México, Marzo de 2010

RESUMEN de la tesis de **LUIS ALBERTO SÁNCHEZ PÉREZ**, presentada como requisito parcial para la obtención del grado de MAESTRO EN CIENCIAS en CIENCIAS DE LA TIERRA con orientación en GEOFÍSICA APLICADA. Ensenada, Baja California, Marzo de 2010.

REFLEXIÓN Y TRANSMISIÓN EN POROELASTICIDAD

Resumen aprobado por:

Dr. Pratap Narayan Sahay Sahay

Director de Tesis

El objetivo de la sismología de reflexión es conocer el tipo de fluído presente en las rocas, su volumen (porosidad) y su capacidad de fluir (permeabilidad). En la teoría poro-elástica, la porosidad y permeabilidad están contenidas de manera natural en las ecuaciones constitutivas, y los componentes sólido y fluído tienen la misma importancia. Sin embargo, las condiciones de frontera para dos medios porosos en contacto aun no están bien definidas y esto es la razón por lo que la teoría poro-elástica aún no se aplica de manera importante en la sísmica de reflexión. En la literatura, existen dos conjuntos de condiciones de frontera, propuestas por Deresiewicz y Sakalak (1963) y de la Cruz y Spanos (1989). El primer conjunto le da más peso al contacto entre sólidos como frontera, mientras que la segunda asume que la frontera es aquélla en la cual la masa total es conservada.

En este trabajo se estudia el problema de valores a la frontera para el caso de reflexión y transmisión de ondas rápidas longitudinales y de corte en medios porosos. Para su solución se emplean las condiciones de fronteras previamente mencionadas. Para una onda rápida longitudinal incidente con ángulo normal a la superficie de contacto, se observa que en bajas frecuencias (debajo de la frecuencia crítica de Biot en ambos medios), los coeficientes de reflexión y transmisión son similares al emplear ambos conjuntos de condiciones de fronteras y estos son equivalentes a los coeficientes obtenidos con la teoría visco-elástica. Sin embargo, en frecuencias altas, los coeficientes obtenidos con la condiciones de fronteras en poroelasticidad están por debajo de los obtenidos con la teoría visco-elástica. Para el caso de una onda rápida de corte incidente con ángulo normal a la superficie de contacto, los resultados son completamente diferentes. Por un lado, al emplear las condiciones de fronteras propuestas por de la Cruz y Spanos (1989), éstas predicen una fuerte reflexión a diferencia de los coeficintes obtenidos al emplear las condiciones propuestas por Deresiewicz y Skalak (1963). Para el caso de una onda rápida de corte incidente con ángulo diferente al normal, los coeficientes obtenidos con ambas condiciones de fronteras son diferentes entre sí. Con base en resultados numéricos obtenidos en esta tesis, se proponen experimentos en laboratorio diseñados para validar los dos conjuntos de condiciones de frontera.

Palabras Clave: Propagación de ondas, poroelasticidad, condiciones de frontera

ABSTRACT of the thesis presented by **LUIS ALBERTO SÁNCHEZ PÉREZ**, in partial fulfillment of the requirements of the degree of MASTER IN SCIENCES in EARTH SCIENCES with orientation in APPLIED GEOPHYSICS. Ensenada, Baja California, March 2010.

REFLECTION AND TRANSMISSION IN POROELASTICITY

The ultimate aim of reflection seismology is to know the type of the saturating fluid, its volume (i.e., porosity) and whether it will flow (i.e., permeability). The poroelastic wave theory brings the role of the solid and fluid constituents on equal footing in a natural way. The porosity and permeability are also explicitly present in this theory. However, the applications of poroelastic theory to reflection seismology have not yet happened in a substantial way. It is because the boundary conditions for two porous media in contact are not yet well established. There are two competing schools of thought on poroelastic boundary conditions, namely, due to Deresiewicz and Skalak (1963) and due to de la Cruz and Spanos (1989). The former treats preferentially the solid/solid contact surface as the boundary. The later regards the boundary as the surface at which total mass is conserved.

In this work I have studied the reflection and transmission boundary value problems associated with incident fast compressional and shear waves for both sets of boundary conditions. For normal incident fast compressional wave, I observe that the reflection and transmission coefficients for both boundary conditions are similar. In the low frequency regime (defined by the Biot critical frequencies of the two media), they are akin to those for the equivalent visco-elastic framework. In the high frequency regime, they are below the response of the equivalent visco-elastic framework. For the fast shear wave case there are distinct differences. The later predicts a strong reflection for fast shear wave normal incident upon a planar fluid/fluid contact in a porous medium, whereas the former shows no such sensitivity. For non-normal incident case, the predicted trends for both boundary conditions are different from each other. Based upon numerical simulations that I have carried out, I have proposed a set of laboratory experiments to run validity check on the two sets of boundary conditions.

Keywords: Wave propagation, poroelasticity, boundary conditions

A Dios, por no haberme dejado solo nunca.

A Leticia, con todo mi amor, por su gran apoyo y comprensión.

A mis padres con mucho cariño: Flor de María y Bartolo.

Agradecimientos

Antes que nada quiero agradecer al Consejo Nacional de Ciencia y Tecnología (CONACYT), por el apoyo brindado durante estos dos años para la realización de este proyecto.

Al Centro de Investigación Científica y de Educación Superior de Ensenada (CICESE), por la facilidad en el uso en las instalaciones computacionales y a su personal.

A mi asesor el Dr. Pratap N. Sahay por su valiosa enseñanza durante su tutoría, así como a los miembros del comité de tesis por su valiosa colaboración: Dr. Antonio González Fernández y Dr. Gilberto López Mariscal.

Muchas gracias al Dr. Emitt Young por su valiosa ayuda para redactar mi tesis en Inglés.

A todos los investigadores, estudiantes y personal de la División de Ciencias de la Tierra por su enseñanza académica.

Y desde luego, a mis compañeros y amigos con los que he convivido durante los últimos dos años.

Contents

Page

Resumen en español **i**

Abstract **iii**

Dedicatoria **iv**

Agradecimientos **v**

Contents **vi**

List of Figures **ix**

List of Tables **xii**

I. INTRODUCTION **1**
- I.1 Reflection and transmission in poroelasticity: the next frontier 1
- I.2 Predicaments in the applications of poroelasticity to multicomponent seismology 3
- I.3 Objectives of the thesis and its outline 6

II. PLANE WAVE REFLECTION AND TRANSMISSION IN POROELASTICITY **9**
- II.1 Statement of the problems 9
- II.2 The solution 13
  - II.2.1 Decoupling of equations of motion 13
  - II.2.2 Decoupling of the matrix Helmholtz equation for potentials . 14
  - II.2.3 Plane wave solution for decoupled potentials 18
  - II.2.4 Expressions of displacements and stresses in terms of decouple potentials 19
  - II.2.5 Displacements and stresses associated with an incident downgoing P_I-wave for both media 22
  - II.2.6 Displacements and stresses associated with an incident downgoing S_I-wave for both media 24
  - II.2.7 Some Notations 25
  - II.2.8 8×8 system of equations for the DS09 boundary conditions: Incident fast P-wave 26
  - II.2.9 8×8 system of equations for the DS09 boundary conditions: Incident fast S-wave 28

Contents (continue)

Page

II.2.10 8×8 system of equations for the dCS09 boundary conditions: Incident fast P-wave . . . 29
II.2.11 8×8 system of equations for the dCS09 boundary conditions: Incident fast S-wave . . . 31
II.2.12 Reflection and transmission coefficients for potentials . . . 32
II.2.13 Displacement potential . . . 33
II.2.14 Energy flux . . . 34

III. SOME NUMERICAL RESULTS 38
III.1 Paradox on normal energy flux of the centre-of-mass component of the wave fields . . . 39
III.1.1 Normal incident fast shear wave . . . 46
III.2 Non-normal incidence case . . . 48
III.2.1 Incident fast compressional wave . . . 48
III.2.2 Incident fast shear wave . . . 48
III.2.3 Amplitude analysis angle-dependence . . . 51

IV. CONCLUSIONS 60

REFERENCES 62

A. SYMBOLS 63

B. VISCOSITY-EXTENDED BIOT THEORY 68
B.1 Biot Theory . . . 68
B.1.1 Constitutive equations by volume-averaging method . . . 70
B.1.2 Viscosity-extended Biot theory . . . 72
B.1.3 Viscosity-extended Biot theory in terms of natural dynamical fields . . . 75
B.1.4 Frequency domain representation . . . 80

C. SEISMIC BOUNDARY CONDITIONS IN POROUS MEDIA 82
C.1 Deresiewicz and Skalak (1963) boundary conditions . . . 84
C.1.1 Open pore case . . . 86
C.1.2 Partially open pore case . . . 87
C.1.3 Generalization of Deresiewicz and Skalak (1963) boundary conditions for fluid viscous stress tensor (DS09) . . . 89
C.1.4 DS09 boundary conditions in term of natural dynamical fields 90
C.2 de la Cruz and Spanos (1989) boundary conditions . . . 92
C.2.1 Continuity of total mass . . . 92

Contents (continue)

Page

C.2.2 Continuity of total linear momentum 93
C.2.3 Newton's third law of motion and balance of phasic forces . . 94
C.2.4 Reformulated de la Cruz and Spanos boundary conditions (dCS09) 95
C.2.5 dCS09 boundary conditions in terms of natural dynamical fields 97

D. PHYSICAL PROPERTIES 99

E. NATURE OF WAVE FIELDS 101

List of Figures

Figure		Page
1	Geometry and the incident and scattered wave fields. The solid black line is the incident fast compressional (P_I) wave (that can be fast shear (S_I) wave also). The solid and dash-dot blue line denote the scattered fast (P_I) and slow (P_{II}) compressional waves, respectively. The solid and dash-dot red line correspond to fast (S_I) and slow (S_{II}) shear waves, respectively.	10
2	Wave vector with respecto to the direction of propagation.	10
3	Sum of the normal energy fluxes of the centre-of-mass components of all scattered fields. The dashed blue line and dashed-dot red line correspond to the DS09 and dCS09 boundary conditions respectively. The values are scaled by the normal energy flux for the incident wave. The energy is conserved at low frequencies but not at high frequencies by both boundary conditions. The transition is around the Biot critical frequencies (plotted as red and blue triangles for top and bottom half-spaces respectively).	40
4	Total transmission for the water water contact.	42
5	Normal component of total energy flux of scattered fields (the sum of centre-of-mass and internal fluxes all reflected and transmitted waves) as the function of frequency showing how Deresiewicz and Skalak (1963), and de la Cruz and Spanos (1989) boundary conditions stand up to the principle of energy conservation. The centre-of-mass, internal component and total energy fluxes corresponding to DS09 are plotted as dashed blue line, dotted magenta line and dashdot green line, respectively. The centre-of-mass, internal component and total energy flux corresponding to dCS09 are plotted as dashdot red line, dotted yellow line and dashdot black line, respectively. The equivalent visco-elastic case is in dashdot green line.	43

List of Figures (continue)

Figure		Page
6	Normal component of the centre-of-mass part of the energy fluxes for scattered fields. Top and bottom panels on left-hand side correspond to the reflected and transmitted fast P-wave, while the top and bottom right-hand side panels correspond to the reflected and transmitted slow P-wave. It should be observed that as the energy fluxes of slow-wave processes are increasing, the energy fluxes in the fast-waves are decreasing as function of frequency.	44
7	Normal component of the internal parts of the energy fluxes for scattered fields. Top and bottom panels on left-hand side correspond to the reflected and transmitted fast P-wave, while the top and bottom right-hand side panels correspond to the reflected and transmitted slow P-wave. It should be observed that as the energy in the centre-of-mass part of fast waves (Figure 6, left hand-side panels) is decreasing as function of frequency, the internal energy part of slow-wave processes is increasing (right hand-side panels of this figure).	45
8	Energy flux for scattered S-wave.	47
9	In the four top panels, the energy flux corresponding to the centre-of-mass component for scattered P-wave, while in the four bottom panels the energy flux corresponding to the centre-of-mass component for an incident to scattered S-wave are shown.	49
10	In the top four panels the energy flux corresponding to the centre-of-mass component for scattered S-wave are presented, while in the bottom four panels the energy flux corresponding to the centre-of-mass component for scattered P-wave are shown.	50
11	Displacement amplitude and phases for scattered fast P-wave at 20 Hz.	52
12	Displacement amplitude and phases for scattered fast S-wave at 20 Hz.	53
13	Displacement amplitude and phases for scattered slow P-wave at 20 Hz.	54
14	Displacement amplitude and phases for scattered slow S-wave at 20 Hz.	55
15	Displacement amplitude and phases for scattered fast P-wave at 500 K Hz.	56
16	Displacement amplitude and phases for scattered fast S-wave at 500 K Hz.	57

List of Figures (continue)

Figure		Page
17	Displacement amplitude and phases for scattered slow P-wave at 500 K Hz.	58
18	Displacement amplitude and phases for scattered slow S-wave at 500 K Hz.	59
19	Open pore case, adapted from Deresiewicz and Skalak (1963)	87
20	Partially open pores, adapted from Deresiewicz and Skalak (1963)	87
21	Close pores, adapted from Deresiewicz and Skalak (1963)	88
22	Velocity and attenuation are shown, respectively, in solid and crossed curves. In all plots, the scales of velocities and phases are shown on the left and right vertical axes.	102
23	Amplitude and phase parts of the ratio of internal to center of mass associated with fast P-wave. The modulus and phases are plotted in solid and crossed lines, respectively. In all plots, the scales of modulus and phases are shown on the left and right vertical axes.	103
24	Amplitude and phase parts of the ratio of solid to fluid motions associated with fast P-wave plotted in solid and crossed lines, respectively. In all plots, the scales of modulus and phases are shown on the left and right vertical axes.	104

List of Tables

Table		Page
I	Notations for amplitudes of reflection and transmission potentials.	22
II	Displacement amplitude	33
III	Spectrum for seismic methods	39
IV	Biot theory field quantities	63
V	Dynamical field quantities	64
VI	Microscopic parameters	64
VII	Macroscopic parameters	65
VIII	Derived parameters	66
IX	Derived parameters (Continuation)	67
X	Solid-frame properties	99
XI	Fluid properties	100

Chapter I

INTRODUCTION

I.1 Reflection and transmission in poroelasticity: the next frontier

Seismic reflection processing and interpretation is about deducing the subsurface seismic structure to map geological structures and reservoir architecture. Historically, travel-time has been the geophysical observable in reflection seismology. The early era of seismic exploration started with the acquisition of the vertical component of the wave field. Since the measurement was a single component field, the acoustic (i.e. scalar) wave theory was used to analyze and model data. The acoustic model gave good results for non-complex geological structures, in particular, for near normal incidence in layered structures.

By early 1980s the demand for oil had become increasingly high, consequently, it led to the need to quantify new reservoirs in more complex geological areas. A new technology, namely, Amplitude Versus Angle of incidence (AVA) emerged to understand reflection coming of non-near normal incidence. The amplitude of a wave field has additional information about physical properties of materials from which it has been reflected. This information permits a better interpretation of data than the analysis based on travel-time alone. Indeed in a very short period, the seismic processing and interpretation incorporated the AVA analysis as a part of the routine workflow.

By late 1980's, with the innovation of the three component sensors to record the total wave field, a drastic change in reflection seismic practice took place. The capacity to record the wave field completely, which is called multicomponent seismic, has allowed the processing of data based on the elasticity (viscoelasticity) theory.

The elastic model proved to be a great improvement. It permits the analysis of converted waves, and gives a basis to model velocity anisotropy. Over the past two decades, based upon this theory, great steps have been made in the analysis of multicomponent seismic data. However, an elastic model assumes a solid rheology, but a reservoir rock is not exactly a solid. In fact, it is a solid matrix permeated by a network of pores saturated with fluid. Moreover, the ultimate aims of the reservoir/reflection seismology are to know what is the type of the saturating fluid (whether it is oil, or gas, or water), what is its volume (i.e., what is the porosity) and whether it will flow (i.e., what is the permeability). In any case, fluid properties, porosity and permeability, do not explicitly enter in the framework of elasticity (viscoelasticity) theory. In fact, in the framework of elasticity (viscoelasticity) theory, the seismic velocities and attenuations are assumed to be related to these parameters through empirical relations, which are based on laboratory studies carried out in the ultrasonic frequency band. On the other hand, the poroelastic wave theory brings the role of the solid and fluid constituents on equal footing in a natural way. The porosity and permeability are also explicitly present in this theory. Thus, applications of poroelastic wave theory, starting with plane wave reflection and transmission from a plane interface, are the next frontier in the analysis of multicomponent seismic data.

I.2 Predicaments in the applications of poroelasticity to multicomponent seismology

The applications of poroelastic theory to reflection seismology have not yet happened in a substantial way. It is because the boundary conditions for two porous media in contact are not yet well established.

A poroelastic medium is composed of two-interacting continua, so at an interface of two porous media there are four-interacting continua. Furthermore, from a pore-scale perspective, an interface comprise of fluid/fluid and solid/solid contact surfaces, which may separate out during deformation. In order to define the boundary conditions properly, an unique definition of interface (from a macroscopic point of view) and interactions among continua that take place at it must be firmly established, theoretically as well as experimentally. As of yet that has not happened. Consequently, the existing results of poroelastic reflection and transmission coefficients cannot be applied with confidence.

There are two competing schools of thought on poroelastic boundary conditions, namely, due to Deresiewicz and Skalak (1963) and de la Cruz and Spanos (1989). Both are based upon theoretical considerations, and neither has been subjected to a rigorous experimental corroboration.

Deresiewicz and Skalak (1963) boundary conditions are based upon conservation of total energy across the interface. This work preferentially treats the solid/solid contact surface as the interface and, on physical grounds, assumes the continuity of the normal component of so called "fluid filtration velocity" across it. Also, the two algebraic terms

constituting the expression of the energy flux are assumed to be individually continuous across the interface, since their sum is supposed to be continuous. No physical meaning can be ascribed to the separate continuity of these two terms, although, mathematically such a continuity is a possibility. Under these assumptions, continuity conditions on solid velocity field, normal component of fluid filtration velocity, and total stress and jump condition on fluid pressure are established. Furthermore, the jump condition on fluid pressure introduces so-called "interface permeability" which supposedly spans from zero to infinity. It can be viewed only as an adjustable parameter, because it cannot be measured independently.

de la Cruz and Spanos (1989) framework regards a boundary between two porous media as the surface across which total mass of poro-continuum is conserved. In here, by invoking the conservation of total mass and total momentum, continuity of the velocity field (associated with the total mass flux) and the total stress are established. Furthermore, by using the concept of alignment, how the stresses on each phase interact with the stress on each of the phases across the interface is described and two additional sets of conditions on tractions are developed which contain an adjustable parameter. However, Sahay (2009, private communications) has shown that these can be recast in a form in which the adjustable parameter is no longer present, as well as the conservation of total energy, which is not explicitly addressed in the original formulation, holds true.

The exhaustive and complete work on the boundary value problem on plane wave reflection and transmission from a plane interface using Deresiewicz and Skalak (1963) boundary conditions is due to Dutta and Odé(1982). However, there is no rigorous published work on reflection and transmission coefficients with de la Cruz and Spanos

(1989) boundary conditions. The lone paper on this topic is by the authors of these boundary conditions themselves (de la Cruz and Spanos, 1993). In it, some numerical results, without showing analytical developments, are reported. These results appear to be drastically different from Deresiewicz and Skalak boundary conditions based results, however, no direct comparison of the two is shown. The lack of details of the analytical development makes it impossible to verify the results. Nevertheless, in the view of Sahay (2009, private communications), one has to rework the reflection and transmission boundary value problem with the (modified) de la Cruz and Spanos (1989) boundary conditions.

Furthermore, a consistent framework of the Biot theory (Biot, 1956) must include fluid viscous stress term into its constitutive equations, therefore, a reworking of the reflection and transmission boundary value problems with both, the Deresiewicz and Skalak (1963) and the de la Cruz and Spanos (1989), boundary conditions are warranted. The details about this extension of the Biot theory are given in Sahay (2008) and the resulting framework is known as viscosity-extended Biot theory. This framework has been included in the 2009 edition of "The Rock Physics Hand Book" (G. Mavko et al.), therefore, it may be taken as firmly established. Because of the missing fluid strain-rate term, the classical Biot theory contains a shear wave process whose velocity is zero. From the outset of the development of the Biot framework, because of its non-propagating nature, it was not taken into consideration and the existence of only two compressional (fast and slow) waves and a (fast) shear wave was assumed. In the viscosity-extended Biot framework the second or slow shear is no longer non-propagating, it appears akin to a viscous wave in fluid. In the seismic frequency band, the fast compressional and shear waves are essentially in-phase motion of constituent

phases and they are observed as the seismic P- and S- waves, respectively.

It is shown in Sahay (1996) that for dynamical purposes, the centre-of-mass and internal fields (mass weighted vector sum and vector difference of solid and fluid displacement fields, respectively) may be more appropriate. It is because the center-of-mass field, which is associated with total linear momentum flux, describes the transport of translational kinetic energy; therefore, it represents three translational degrees of freedom of material points. Geophones register translational degrees of freedom and measure the field associated with total linear momentum, indeed they track the center-of-mass field. The internal field is associated with spin (angular momentum about center-of-mass) flux, it describes transport of rotational kinetic energy; therefore, it represents three rotational degrees of freedom of material points. While the internal field is not detected directly, its value can be ascertained from the registered center-of-mass field. Thus, the viscosity-extended Biot theory stated in terms the centre-of-mass and internal fields has to be taken for the purposes of wave propagation studies. A straightforward linear transformation reformulates the description of the viscosity-extended theory stated in terms of average solid and fluid displacements fields to the framework of the centre-of-mass and internal fields. It turns out that the mathematical analysis also gets simplified in this framework.

I.3 Objectives of the thesis and its outline

In the view of the above, boundary value problems for reflection and transmission of (i) a fast compressional plane wave and (ii) a fast shear plane wave incident at a planar welded contact of two fluid saturated porous half-spaces which is subjected to (a)

Deresiewicz and Skalak (1963) boundary conditions and (b) de la Cruz and Spanos (1989) boundary conditions need to be worked out within the framework of viscosity-extended Biot theory. I have carried out precisely that in this thesis. For consistency, I have taken the Deresiewicz and Skalak (1963) boundary conditions that are amended to include fluid viscous stress part and the reformulated de la Cruz and Spanos (1989) boundary conditions that are conserving total energy flux explicitly. Hereafter, these modified boundary conditions shall be referred as DS09 and dCS09 boundary conditions, respectively.

In chapter II, boundary value problems for a plane fast compressional wave and a plane fast shear wave incident at a welded planar contact of two poroelastic half-spaces subjected to (a) DS09 and (b) dCS09 boundary conditions are worked out. Since there are four reflected and four transmitted waves, a system of 8 equations is setup which is solved numerically to yield the reflection and transmission coefficients as a function of the angle of incidence and the frequency. A compact notation is employed that allows mathematical expressions to have the appearance as of the linear elasticity. It also provides an ease in the analytical developments and numerical computations. This chapter is complemented by the list of symbols presented in Appendix A, a review of the viscosity-extended Biot equations of motion presented in Appendix B and a critical overview of the DS09 and dCS09 boundary conditions presented in Appendix C.

In chapter III, some numerical results for reflection and transmission coefficients are presented. For normal incident fast compressional wave, I observe that the reflection and transmission coefficients for both boundary conditions are similar to each other. In the low frequency regime (defined by the Biot critical frequencies of the two media),

they are akin to those for the equivalent visco-elastic framework. In the high frequency regime, they predict below the response of the equivalent visco-elastic framework. For non-normal incident case, the predicted trends for both boundary conditions are different from each other.

In chapter IV, I present remarks about the scope of this work. Based upon numerical simulations that I have carried out, I have proposed a set of laboratory experiments to run validity check on the two sets of boundary conditions.

Chapter II

PLANE WAVE REFLECTION AND TRANSMISSION IN POROELASTICITY

In this chapter the boundary value problems for reflection and transmission of a fast compressional plane wave, as well as, a fast shear plane wave across a planar interface of two fluid saturated porous half-spaces that is subjected to (i) modified Deresiewicz and Skalak (1963) boundary conditions and (ii) modified de la Cruz and Spanos (1989) boundary conditions are stated and their solutions are developed. The details about the boundary conditions are presented in Appendix C. The cartesian coordinate system is the natural framework here.

II.1 Statement of the problems

Let there be two porous half-spaces in welded contact such that the boundary is marked by the plane $z = 0$. Let the regions $z \leq 0$ and $z \geq 0$ are occupied by the half-spaces labeled as "a" and "b", respectively. The positive z-axes is taken pointing downwards (see Figure 1), so "a" and "b" are the upper and the lower half-spaces, respectively. Henceforth, (a) and (b) shall label the half-spaces as superscripts on field quantities and as subscripts on material properties.

Let a monochromatic plane wave, which may be fast compressional or fast shear, incident at the boundary from the upper half-space.

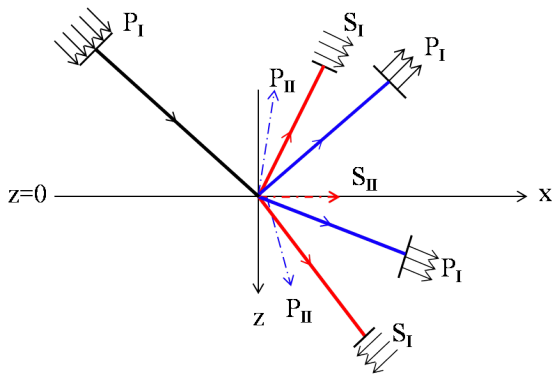

Figure 1. Geometry and the incident and scattered wave fields. The solid black line is the incident fast compressional $(\mathrm{P_I})$ wave (that can be fast shear $(\mathrm{S_I})$ wave also). The solid and dash-dot blue line denote the scattered fast $(\mathrm{P_I})$ and slow $(\mathrm{P_{II}})$ compressional waves, respectively. The solid and dash-dot red line correspond to fast $(\mathrm{S_I})$ and slow $(\mathrm{S_{II}})$ shear waves, respectively.

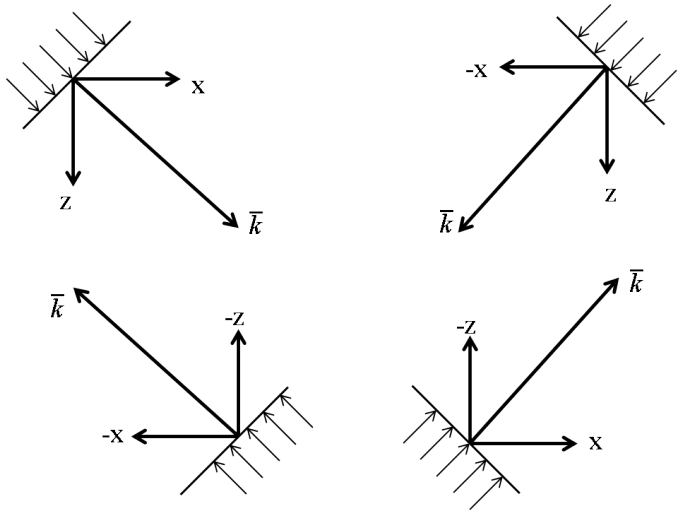

Figure 2. Wave vector with respecto to the direction of propagation.

Let $\mathbf{u}^{(a)} = \left(\mathbf{u}^{\mathrm{m}(a)} \;\; \mathbf{u}^{\mathrm{i}(a)}\right)^{\mathrm{T}}$ and $\mathbf{u}^{(b)} = (\mathbf{u}^{\mathrm{m}(b)} \;\; \mathbf{u}^{\mathrm{i}(b)})^{\mathrm{T}}$, where $^{\mathrm{T}}$ stands for transpose, be the fields in the upper and the lower half-spaces, respectively. Here $\mathbf{u}^{\mathrm{m}}$'s and $\mathbf{u}^{\mathrm{i}}$'s stand for centre-of-mass and internal fields, respectively, which are the mass weighted vector sum and the vector difference of the average displacement field of the solid and the fluid phases.

The governing equations of motion for fields , in the framework of viscosity-extended Biot theory (Sahay 2008) of poroelasticity, in the frequency domain read (see Appendix B for additional details):

$$\boldsymbol{\alpha}_{(a)} \nabla(\nabla \cdot \mathbf{u}^{(a)}) - \boldsymbol{\beta}_{(a)} \nabla \times \nabla \times \mathbf{u}^{(a)} + \omega^2 \mathbf{u}^{(a)} = 0 \quad \text{for } z \leq 0, \tag{1}$$

and

$$\boldsymbol{\alpha}_{(b)} \nabla(\nabla \cdot \mathbf{u}^{(b)}) - \boldsymbol{\beta}_{(b)} \nabla \times \nabla \times \mathbf{u}^{(b)} + \omega^2 \mathbf{u}^{(b)} = 0 \quad \text{for } z \geq 0. \tag{2}$$

$\boldsymbol{\alpha}$'s and $\boldsymbol{\beta}$'s are 2×2 matrices associated with P- and S-motions, respectively. The elements of these matrices have dimensions of velocity squared and their explicit expressions, in terms of constituents' material properties and frequency, are given by equations (184) through (187), (199), and (200). The constitutive equations corresponding to the two regions read:

$$\boldsymbol{\tau}^{(a)}_{jk} \;=\; \boldsymbol{\Omega}_{(a)} \boldsymbol{\rho}_{(a)} \left\{ \left(\boldsymbol{\alpha}_{(a)} - 2\boldsymbol{\beta}_{(a)} \right) \mathbf{u}^{(a)}_{ll} \delta_{jk} + 2\boldsymbol{\beta}_{(a)} \; \breve{\mathbf{u}}^{(a)}_{jk} \right\} \quad \text{for } z \leq 0, \tag{3}$$

and

$$\boldsymbol{\tau}^{(b)}_{jk} \;=\; \boldsymbol{\Omega}_{(b)} \boldsymbol{\rho}_{(b)} \left\{ \left(\boldsymbol{\alpha}_{(b)} - 2\boldsymbol{\beta}_{(b)} \right) \mathbf{u}^{(b)}_{ll} \delta_{jk} + 2\boldsymbol{\beta}_{(b)} \; \breve{\mathbf{u}}^{(b)}_{jk} \right\} \quad \text{for } z \geq 0. \tag{4}$$

Here, $\boldsymbol{\tau}_{jk} = \left(\tau^{\mathrm{m}}_{jk} \;\; \tau^{\mathrm{i}}_{jk}\right)^{\mathrm{T}}$ and τ^{m}_{jk} is the centre-of-mass or total stress and τ^{i}_{jk} is the internal stress. $\mathbf{u}_{jk} = \left(\mathrm{u}^{\mathrm{m}}_{jk} \;\; \mathrm{u}^{\mathrm{i}}_{jk}\right)$ where $\mathrm{u}^{\mathrm{m}}_{jk}$ and $\mathrm{u}^{\mathrm{i}}_{jk}$ are the strain field associated with centre-of-mass and internal fields, respectively ($\breve{}$ on strain field denotes its deviatoric

part). $\boldsymbol{\Omega}$'s and $\boldsymbol{\rho}$'s are 2×2 diagonal matrices. $\boldsymbol{\Omega}$'s are dimensionless matrices that contain the Biot relaxation frequency (Ω_{i}) and there are defined by equation (201). $\boldsymbol{\rho}$'s are density matrices and there are defined by (172).

For the first set of two problems, corresponding to incident fast compressional and shear waves, the fields satisfy the boundary conditions due to Deresiewicz and Skakal (1963) generalized for fluid viscosity (see Appendix C.1.4), which are expressed as follows

$$\left\langle \mathbf{T}^{-1}\dot{\mathbf{u}} \right\rangle = \mathbf{0} \tag{5}$$

$$\left\langle \mathbf{T}^{\mathrm{T}}\boldsymbol{\tau}_{jk}\hat{n}_j - \mathbf{D}\dot{\mathbf{u}} \right\rangle = \mathbf{0}. \tag{6}$$

Henceforth, the bra-ket symbol, $\langle\ \rangle$, represents the jump in the quantity within its argument. The matrix $\mathbf{T}$ is defined in terms of constituents' properties in equation (230).

For the second set of two problems, corresponding to incident fast compressional and shear waves, the fields satisfy de la Cruz and Spanos (1989) boundary conditions reformulated by Sahay (2009, personal communications) (see Appendix C.2.2) which are expressed as follows

$$\langle \mathbf{G}\ \mathbf{u} \rangle = \mathbf{0}, \tag{7}$$

$$\langle \mathbf{H}\ \boldsymbol{\tau}_{jk}\hat{n}_j \rangle = \mathbf{0}, \tag{8}$$

where the matrices $\mathbf{G}$ and $\mathbf{H}$ are defined in terms of constituents' physical properties in equations (261) and (262), respectively.

II.2 The solution

At first, the general solutions for equations of motion (1) and (2) are developed in terms of a complete set of orthonormal basis functions. Thereafter, those solutions are plugged into the boundary conditions to solved for arbitrary constants which are the desired reflection and transmission coefficients.

Equations of motion (1) and (2) are a 6×6 system of coupled 2nd order partial differential equation. For plane wave problems under consideration, field quantities can be taken independent of one of the coordinates. That still leaves them to be a 4×4 system of coupled 2nd order PDE. In order to solve them, the vector decomposition of wave fields in terms of curl-free and divergence-free parts is carried out. Thereby, a 2×2 matrix Helmholtz equations for each potential set are obtained. By employing a normal co-ordinate transformation, the each matrix Helmholtz equations are decoupled into two scalar Helmholtz equations. For those a solution is seeked in terms a complete set of orthonomal harmonic exponential functions, which are also viewed as plane waves.

The analysis in the subsections II.2.1 through II.2.4 pertain equally to the both equations of motion (1) and (2). For the clarity of notation, the subscript and the superscripts (*a*) and (*b*) labeling the half-spaces are dropped.

II.2.1 Decoupling of equations of motion

For 2D case, say, independent of y coordinate, the vector decomposition

$$\mathbf{u} \;=\; \nabla\mathbf{\Phi} + \nabla \times (\hat{y}\mathbf{\Psi}) \tag{9}$$

is introduced where potentials are

$$\mathbf{\Phi} = \left(\Phi^{\mathrm{m}}, \Phi^{\mathrm{i}}\right)^{\mathrm{T}}$$

and

$$\mathbf{\Psi} = \left(\Psi^{\mathrm{m}}, \Psi^{\mathrm{i}}\right)^{\mathrm{T}}.$$

It uncouples equations of motion (1) and (2) into curl-free (compression) and divergence-free (shear) parts by rendering a 2×2 matrix Helmholtz equation for each set of potentials

$$\boldsymbol{\alpha}\nabla^2\mathbf{\Phi} + \omega^2\mathbf{\Phi} = 0, \tag{10}$$

$$\boldsymbol{\beta}\nabla^2\mathbf{\Psi} + \omega^2\mathbf{\Psi} = 0. \tag{11}$$

II.2.2 Decoupling of the matrix Helmholtz equation for potentials

P Potentials

The matrix Helmoltz equations for P potentials are

$$\left(\boldsymbol{\alpha}\nabla^2 + \omega^2\mathbf{I}\right)\mathbf{\Phi} = \mathbf{0} \tag{12}$$

The above equations is diagonalized by introducing the transformation

$$\mathbf{\Phi} = \mathbf{R}_\alpha\boldsymbol{\phi} \quad \text{where} \quad \boldsymbol{\phi} = (\phi^{\mathrm{I}}, \phi^{\mathrm{II}})^{\mathrm{T}}, \tag{13}$$

$$\mathbf{R}_\alpha = \left(\mathbf{r}_{\alpha_{\mathrm{I}}}, \mathbf{r}_{\alpha_{\mathrm{II}}}\right) \text{ and } \mathbf{L}_\alpha = \left(\mathbf{l}_{\alpha_{\mathrm{I}}}, \mathbf{l}_{\alpha_{\mathrm{II}}}\right), \tag{14}$$

where $\mathbf{R}_\alpha$ and $\mathbf{L}_\alpha$ are the right- and left- eigenvector matrices of the non-symmetric second order $\boldsymbol{\alpha}$ matrix such that they are orthonormal to each other,

$$\mathbf{L}_\alpha^{\mathrm{T}}\,\mathbf{R}_\alpha = \mathbf{I}, \tag{15}$$

and diagonalize the $\boldsymbol{\alpha}$ matrix,

$$\mathbf{L}_{\alpha}^{\mathrm{T}}\ \boldsymbol{\alpha}\ \mathbf{R}_{\alpha} = \boldsymbol{\Lambda}_{\alpha} \equiv \begin{pmatrix} \alpha_{\mathrm{I}}^2 & 0 \\ 0 & \alpha_{\mathrm{II}}^2 \end{pmatrix}. \tag{16}$$

The pair $(\alpha_{\mathrm{I}}^2, \alpha_{\mathrm{II}}^2)$ are the eigenvalues of the $\boldsymbol{\alpha}$ matrix, given by

$$\alpha_{\mathrm{I}}^2, \alpha_{\mathrm{II}}^2 = \frac{\mathrm{Tr}_{\alpha} \pm \sqrt{\mathrm{Tr}_{\alpha}^2 - 4\Delta_{\alpha}}}{2} = \frac{\mathrm{Tr}_{\alpha}}{2}\left(1 \pm \sqrt{1 - 4\frac{\Delta_{\alpha}}{\mathrm{Tr}_{\alpha}^2}}\right). \tag{17}$$

Here Tr_{α} and Δ_{α} stand for the trace and the determinant of the $\boldsymbol{\alpha}$ matrix, respectively. This normal coordinate transformation of equation (12) is obtained by substituting equation (13) into it, followed by the application of $\mathbf{L}_{\alpha}^{\mathrm{T}}$ upon it from the left, and using the identities (15) and (16). This yields the following set of two decoupled scalar Helmholtz equations for the transformed field $\boldsymbol{\phi}$

$$\left(\boldsymbol{\Lambda}_{\boldsymbol{\alpha}}\nabla^2 + \omega^2\mathbf{I}\right)\boldsymbol{\phi} = \mathbf{0}, \quad \text{i. e.,} \quad \begin{pmatrix} \alpha_{\mathrm{I}}^2 & 0 \\ 0 & \alpha_{\mathrm{II}}^2 \end{pmatrix} \nabla^2 \begin{pmatrix} \phi^{\mathrm{I}} \\ \phi^{\mathrm{II}} \end{pmatrix} + \omega^2 \begin{pmatrix} \phi^{\mathrm{I}} \\ \phi^{\mathrm{II}} \end{pmatrix} = \begin{pmatrix} 0 \\ 0 \end{pmatrix}. \tag{18}$$

The decoupled potential fields ϕ^{I} (fast P) and ϕ^{II} (slow P) propagate with complex velocities α_{I} and α_{II}, respectively. The wave field vectors corresponding to these are the right eigenvectors of the $\boldsymbol{\alpha}$ matrix

$$\mathbf{r}_{\alpha_{\mathrm{I}}} = \frac{1}{\mathrm{N}_{\alpha_{\mathrm{I}}}} \begin{pmatrix} 1 \\ \\ \gamma_{\alpha_{\mathrm{I}}} \end{pmatrix} \tag{19}$$

and

$$\mathbf{r}_{\alpha_{\mathrm{II}}} = \frac{1}{\mathrm{N}_{\alpha_{\mathrm{II}}}} \begin{pmatrix} \gamma_{\alpha_{\mathrm{II}}} \\ \\ 1 \end{pmatrix}, \tag{20}$$

where $\gamma_{\alpha_{\mathrm{I}}} = (\alpha_{\mathrm{I}}^2 - \alpha_{\mathrm{mm}})/\alpha_{\mathrm{mi}}$ and $\gamma_{\alpha_{\mathrm{II}}} = \alpha_{\mathrm{mi}}/(\alpha_{\mathrm{II}}^2 - \alpha_{\mathrm{mm}})$. $\mathrm{N}_{\alpha_{\mathrm{I}}} = \left(1 + \gamma_{\alpha_{\mathrm{I}}}^2\alpha_{\mathrm{mi}}/\alpha_{\mathrm{im}}\right)^{1/2}$ and $\mathrm{N}_{\alpha_{\mathrm{II}}} = \left(1 + \gamma_{\alpha_{\mathrm{II}}}^2\alpha_{\mathrm{im}}/\alpha_{\mathrm{mi}}\right)^{1/2}$ are the normalizations constants. $\boldsymbol{\phi} = \mathbf{L}_{\alpha}^{\mathrm{T}}\boldsymbol{\Phi}$ expresses

how the center-of-mass and internal fields contribute to these two waves, where the left eigenvectors of the $\boldsymbol{\alpha}$ matrix are

$$\mathbf{l}_{\alpha_{\mathrm{I}}} = \frac{1}{\mathrm{N}_{\alpha_{\mathrm{I}}}} \begin{pmatrix} 1 \\ \\ \gamma_{\alpha_{\mathrm{I}}} \frac{\alpha_{\mathrm{mi}}}{\alpha_{\mathrm{im}}} \end{pmatrix} \tag{21}$$

and

$$\mathbf{l}_{\alpha_{\mathrm{II}}} = \frac{1}{\mathrm{N}_{\alpha_{\mathrm{II}}}} \begin{pmatrix} \gamma_{\alpha_{\mathrm{II}}} \frac{\alpha_{\mathrm{im}}}{\alpha_{\mathrm{mi}}} \\ \\ 1 \end{pmatrix}. \tag{22}$$

S Potentials

The matrix Helmoltz equation for the shear potentials pair

$$\left(\boldsymbol{\beta}\nabla^2 + \omega^2 \mathbf{I}\right) \boldsymbol{\Psi} = \mathbf{0} \tag{23}$$

can be diagonalized by introducing the transformation

$$\boldsymbol{\Psi} = \mathbf{R}_\beta \, \boldsymbol{\psi} \quad \text{where} \quad \boldsymbol{\psi} = (\psi^{\mathrm{I}} \;\; \psi^{\mathrm{II}})^{\mathrm{T}}, \tag{24}$$

and

$$\mathbf{R}_\beta = \left(\mathbf{r}_{\beta_{\mathrm{I}}}, \mathbf{r}_{\beta_{\mathrm{II}}}\right) \tag{25}$$

and

$$\mathbf{L}_{\boldsymbol{\beta}} = \left(\mathbf{l}_{\beta_{\mathrm{I}}}, \mathbf{l}_{\beta_{\mathrm{II}}}\right) \tag{26}$$

are, respectively, right- and left- eigenvector matrices of the non-symmetric second order $\boldsymbol{\beta}$ matrix such that they are orthonormal to each other,

$$\mathbf{L}_\beta^{\mathrm{T}} \, \mathbf{R}_\beta = \mathbf{I}, \tag{27}$$

and diagonalize the $\boldsymbol{\beta}$ matrix,

$$\mathbf{L}_\beta^{\mathrm{T}} \, \boldsymbol{\beta} \, \mathbf{R}_\beta = \boldsymbol{\Lambda}_\beta \equiv \begin{pmatrix} \beta_{\mathrm{I}}^2 & 0 \\ \\ 0 & \beta_{\mathrm{II}}^2 \end{pmatrix}. \tag{28}$$

The pair $(\beta_{\text{I}}{}^2, \beta_{\text{II}}{}^2)$ are the eigenvalues of the $\boldsymbol{\beta}$ matrix, given by

$$\beta_{\text{I}}{}^2, \beta_{\text{II}}{}^2 = \frac{\text{Tr}_\beta \pm \sqrt{\text{Tr}_\beta^2 - 4\Delta_\beta}}{2} = \frac{\text{Tr}_\beta}{2}\left(1 \pm \sqrt{1 - 4\frac{\Delta_\beta}{\text{Tr}_\beta^2}}\right). \tag{29}$$

Here Tr_β and Δ_β stand for the trace and the determinant of the $\boldsymbol{\beta}$ matrix, respectively. This normal coordinate transformation of equation (23) is obtained by substituting equation (24) into it, followed by the application of $\mathbf{L}_\beta^{\text{T}}$ upon it from the left, and using the identities (28) and (29). This yields the following set of two decoupled scalar Helmholtz equations for the transformed field $\boldsymbol{\psi}$

$$\left(\boldsymbol{\Lambda}_\beta \nabla^2 + \omega^2 \mathbf{I}\right)\boldsymbol{\psi} = \mathbf{0}, \quad \text{i. e.,} \quad \begin{pmatrix} \beta_{\text{I}}^2 & 0 \\ 0 & \beta_{\text{II}}^2 \end{pmatrix} \nabla^2 \begin{pmatrix} \psi^{\text{I}} \\ \psi^{\text{II}} \end{pmatrix} + \omega^2 \begin{pmatrix} \psi^{\text{I}} \\ \psi^{\text{II}} \end{pmatrix} = \begin{pmatrix} 0 \\ 0 \end{pmatrix}. \tag{30}$$

The decoupled potential fields ψ^{I} (fast S) and ψ^{II} (slow S) propagate with complex velocities β_{I} and β_{II}, respectively. The wave field vectors corresponding to these are the right eigenvectors of the $\boldsymbol{\beta}$ matrix

$$\mathbf{r}_{\beta_{\text{I}}} = \frac{1}{\text{N}_{\beta_{\text{I}}}} \begin{pmatrix} 1 \\ \\ \gamma_{\beta_{\text{I}}} \end{pmatrix} \quad \text{and} \quad \mathbf{r}_{\beta_{\text{II}}} = \frac{1}{\text{N}_{\beta_{\text{II}}}} \begin{pmatrix} \gamma_{\beta_{\text{II}}} \\ \\ 1 \end{pmatrix}, \tag{31}$$

where $\gamma_{\beta_{\text{I}}} = (\beta_{\text{I}}^2 - \beta_{\text{mm}})/\beta_{\text{mi}}$ and $\gamma_{\beta_{\text{II}}} = \beta_{\text{mi}}/(\beta_{\text{II}}^2 - \beta_{\text{mm}})$. $\text{N}_{\beta_{\text{I}}} = \left(1 + \gamma^{\beta_{\text{I}}{}^2}\beta_{\text{mi}}/\beta_{\text{im}}\right)^{1/2}$ and $\text{N}_{\beta_{\text{II}}} = \left(1 + \gamma_{\beta_{\text{II}}}{}^2\beta_{\text{im}}/\beta_{\text{mi}}\right)^{1/2}$ are the normalizations constants. $\boldsymbol{\psi} = \mathbf{L}^{\boldsymbol{\beta}^{\text{T}}}\boldsymbol{\Psi}$ expresses how the center-of-mass and internal fields contribute to these two waves, where the left eigenvectors of the $\boldsymbol{\beta}$ matrix are

$$\mathbf{l}_{\beta_{\text{I}}} = \frac{1}{\text{N}_{\beta_{\text{I}}}} \begin{pmatrix} 1 \\ \\ \gamma_{\beta_{\text{I}}} \frac{\beta_{\text{mi}}}{\beta_{\text{im}}} \end{pmatrix} \tag{32}$$

and

$$\mathbf{l}_{\beta_{\text{II}}} = \frac{1}{\text{N}_{\beta_{\text{II}}}} \begin{pmatrix} \gamma_{\beta_{\text{II}}} \frac{\beta_{\text{im}}}{\beta_{\text{mi}}} \\ \\ 1 \end{pmatrix}. \tag{33}$$

II.2.3 Plane wave solution for decoupled potentials

The horizontal slownesses are taken to be the free parameters. The appropriate plane wave solution for scalar Helmholtz equation pairs (18) and (30) thus read

$$\begin{aligned} \boldsymbol{\phi}^{\pm} = \begin{pmatrix} \phi^{\mathrm{I}\pm} \\ \phi^{\mathrm{II}\pm} \end{pmatrix} &= e^{i\omega px} \begin{pmatrix} e^{\pm i\omega q_{\alpha_{\mathrm{I}}} z} & 0 \\ 0 & e^{\pm i\omega q_{\alpha_{\mathrm{II}}} z} \end{pmatrix} \begin{pmatrix} a_{\mathrm{I}}^{\pm} \\ a_{\mathrm{II}}^{\pm} \end{pmatrix} \\ &= e^{i\omega(px\ \mathbf{I}\ \pm\ \boldsymbol{Q}_{\alpha}\ z)} \mathbf{a}^{\pm}, \end{aligned} \tag{34}$$

and

$$\begin{aligned} \boldsymbol{\psi}^{\pm} = \begin{pmatrix} \psi^{\mathrm{I}\pm} \\ \psi^{\mathrm{II}\pm} \end{pmatrix} &= e^{i\omega px} \begin{pmatrix} e^{\pm i\omega q_{\alpha_{\mathrm{I}}} z} & 0 \\ 0 & e^{\pm i\omega q_{\alpha_{\mathrm{II}}} z} \end{pmatrix} \begin{pmatrix} b_{\mathrm{I}}^{\pm} \\ b_{\mathrm{II}}^{\pm} \end{pmatrix} \\ &= e^{i\omega\left(p\mathbf{I}\pm\ \boldsymbol{Q}_{\beta}\ z\right)} \mathbf{b}^{\pm}. \end{aligned} \tag{35}$$

$\mathbf{I}$ is 2×2 identity matrix. The ± signs label the upgoing and the downgoing wave fields, respectively. The associated vertical slownesses are defined by

$$q_{\alpha_{\mathrm{I}}}^2 = \frac{1}{\alpha_{\mathrm{I}}^2} - p^2, \qquad q_{\alpha_{\mathrm{II}}}^2 = \frac{1}{\alpha_{\mathrm{II}}^2} - p^2, \tag{36}$$

and

$$q_{\beta_{\mathrm{I}}}^2 = \frac{1}{\beta_{\mathrm{I}}^2} - p^2, \qquad q_{\beta_{\mathrm{II}}}^2 = \frac{1}{\alpha_{\mathrm{II}}^2} - p^2. \tag{37}$$

$a_{\mathrm{I}}^{\pm}$, $a_{\mathrm{II}}^{\pm}$, $b_{\mathrm{I}}^{\pm}$, and $b_{\mathrm{II}}^{\pm}$ are arbitrary constants,

$$\mathbf{Q}_{\alpha} = \begin{pmatrix} q_{\alpha_{\mathrm{I}}} & 0 \\ 0 & q_{\alpha_{\mathrm{II}}} \end{pmatrix}, \quad \mathbf{Q}_{\beta} = \begin{pmatrix} q_{\beta_{\mathrm{I}}} & 0 \\ 0 & q_{\beta_{\mathrm{II}}} \end{pmatrix}, \tag{38}$$

and

$$\mathbf{Q}_{\alpha}^2 = (\boldsymbol{\Lambda}_{\alpha})^{-1} - p^2\mathbf{I}, \quad \mathbf{Q}_{\beta}^2 = (\boldsymbol{\Lambda}_{\beta})^{-1} - p^2\mathbf{I}. \tag{39}$$

It should be noted that in (34) and (35) solutions for each potentials are decoupled. It is written in vectorial form for mathematical convenience later.

II.2.4 Expressions of displacements and stresses in terms of decouple potentials

From equations (12) and (3 or 4) the tangential and vertical components of displacements and stresses are

$$\mathbf{u}_x = \partial_x \mathbf{\Phi} - \partial_z \mathbf{\Psi} \tag{40}$$

$$\mathbf{u}_z = \partial_z \mathbf{\Phi} + \partial_x \mathbf{\Psi} \tag{41}$$

$$\boldsymbol{\tau}_{xx} = \mathbf{\Omega}\boldsymbol{\rho}\left[\left(\boldsymbol{\alpha}\nabla^2 - 2\boldsymbol{\beta}\partial_z^2\right)\mathbf{\Phi} - 2\boldsymbol{\beta}\partial_{xz}\mathbf{\Psi}\right] \tag{42}$$

$$\boldsymbol{\tau}_{xz} = \mathbf{\Omega}\boldsymbol{\rho}\left[2\boldsymbol{\beta}\partial_{xz}\mathbf{\Phi} + \boldsymbol{\beta}\left(\nabla^2 - 2\partial_z^2\right)\mathbf{\Psi}\right] \tag{43}$$

$$\boldsymbol{\tau}_{zz} = \mathbf{\Omega}\boldsymbol{\rho}\left[\left(\boldsymbol{\alpha}\nabla^2 - 2\boldsymbol{\beta}\partial_x^2\right)\mathbf{\Phi} + 2\boldsymbol{\beta}\partial_{xz}\mathbf{\Psi}\right] \tag{44}$$

Using identities $\mathbf{\Phi} = \mathbf{R}^{\alpha}\boldsymbol{\phi}$ and $\mathbf{\Psi} = \mathbf{R}^{\beta}\boldsymbol{\psi}$ (see equations 14 and 24, respectively), the above equations are rewritten in terms of decoupled potentials $\boldsymbol{\phi}$ and $\boldsymbol{\psi}$ as

$$\mathbf{u}_x = \mathbf{R}^{\alpha}\partial_x\boldsymbol{\phi} - \mathbf{R}^{\beta}\partial_z\boldsymbol{\psi} \tag{45}$$

$$\mathbf{u}_z = \mathbf{R}^{\alpha}\partial_z\boldsymbol{\phi} + \mathbf{R}^{\beta}\partial_x\boldsymbol{\psi} \tag{46}$$

$$\boldsymbol{\tau}_{xx} = \mathbf{\Omega}\boldsymbol{\rho}\left[\left(\boldsymbol{\alpha}\mathbf{R}^{\alpha}\nabla^2 - 2\boldsymbol{\beta}\mathbf{R}^{\alpha}\partial_z^2\right)\boldsymbol{\phi} - 2\boldsymbol{\beta}\mathbf{R}^{\beta}\partial_{xz}\boldsymbol{\psi}\right] \tag{47}$$

$$\boldsymbol{\tau}_{xz} = \mathbf{\Omega}\boldsymbol{\rho}\left[2\boldsymbol{\beta}\mathbf{R}^{\alpha}\partial_{xz}\boldsymbol{\phi} + \boldsymbol{\beta}\mathbf{R}^{\beta}\left(\nabla^2 - 2\partial_z^2\right)\boldsymbol{\psi}\right] \tag{48}$$

$$\boldsymbol{\tau}_{zz} = \mathbf{\Omega}\boldsymbol{\rho}\left[\left(\boldsymbol{\alpha}\mathbf{R}^{\alpha}\nabla^2 - 2\boldsymbol{\beta}\mathbf{R}^{\alpha}\partial_x^2\right)\boldsymbol{\phi} + 2\boldsymbol{\beta}\mathbf{R}^{\beta}\partial_{xz}\boldsymbol{\psi}\right] \tag{49}$$

Plugging in the elemental solutions (34) and (35) for potentials, the expressions of displacements and stresses are obtained as below

$$\mathbf{u}_x = i\omega p\mathbf{R}^\alpha\boldsymbol{\phi}^\pm \mp i\omega\mathbf{R}^\beta\mathbf{Q}_\beta\boldsymbol{\psi}^\pm \tag{50}$$

$$\mathbf{u}_z = \pm i\omega\mathbf{R}^\alpha\mathbf{Q}_\alpha\boldsymbol{\phi}^\pm + i\omega p\mathbf{R}^\beta\boldsymbol{\psi}^\pm \tag{51}$$

$$\begin{aligned}
\boldsymbol{\tau}_{xx} &= -\omega^2\boldsymbol{\Omega}\boldsymbol{\rho}[(\boldsymbol{\alpha}\mathbf{R}^\alpha(\boldsymbol{\Lambda}^\alpha)^{-1} - \boldsymbol{\beta}\mathbf{R}^\alpha\mathbf{Q}_\alpha^2)\boldsymbol{\phi}^\pm \mp 2p\boldsymbol{\beta}\mathbf{R}^\beta\mathbf{Q}_\beta\boldsymbol{\psi}^\pm] \\
&= -\omega^2\boldsymbol{\Omega}\boldsymbol{\rho}\left[\left(\mathbf{R}^\alpha\boldsymbol{\Lambda}^\alpha(\boldsymbol{\Lambda}^\alpha)^{-1} - \boldsymbol{\beta}\mathbf{R}^\alpha\left((\boldsymbol{\Lambda}^\alpha)^{-1} - p^2\mathbf{I}\right)\right)\boldsymbol{\phi}^\pm \mp 2p\mathbf{R}^\beta\boldsymbol{\Lambda}^\beta\mathbf{Q}_\beta\boldsymbol{\psi}^\pm\right] \\
&= -\omega^2\boldsymbol{\Omega}\boldsymbol{\rho}\left[\left(\mathbf{R}^\alpha\boldsymbol{\Lambda}^\alpha(\boldsymbol{\Lambda}^\alpha)^{-1} - \boldsymbol{\beta}\mathbf{R}^\alpha\left(\mathbf{L}^{\alpha^{\mathrm{T}}}\boldsymbol{\alpha}^{-\mathbf{1}}\,\mathbf{R}^\alpha - p^2\mathbf{I}\right)\right)\boldsymbol{\phi}^\pm \mp 2p\mathbf{R}^\beta\boldsymbol{\Lambda}^\beta\mathbf{Q}_\beta\boldsymbol{\psi}^\pm\right] \\
&= -\omega^2\boldsymbol{\Omega}\boldsymbol{\rho}\left[\left(\mathbf{I} - \boldsymbol{\beta}\boldsymbol{\alpha}^{-\mathbf{1}} - p^2\boldsymbol{\beta}\right)\mathbf{R}^\alpha\boldsymbol{\phi}^\pm \mp 2p\mathbf{R}^\beta\boldsymbol{\Lambda}^\beta\mathbf{Q}_\beta\boldsymbol{\psi}^\pm\right] \qquad (52) \\
&= -\omega^2\boldsymbol{\Omega}\boldsymbol{\rho}[((\boldsymbol{\alpha} - 2\boldsymbol{\beta})\mathbf{R}^\alpha\mathbf{Q}_\alpha^2 + p^2\boldsymbol{\alpha}\mathbf{R}^\alpha)\boldsymbol{\phi}^\pm \mp 2p\boldsymbol{\beta}\mathbf{R}^\beta\mathbf{Q}_\beta\boldsymbol{\psi}^\pm]
\end{aligned}$$

$$\begin{aligned}
\boldsymbol{\tau}_{xz} &= -\omega^2\boldsymbol{\Omega}\boldsymbol{\rho}[\pm 2p\boldsymbol{\beta}\mathbf{R}^\alpha\mathbf{Q}_\alpha\boldsymbol{\phi}^\pm + \boldsymbol{\beta}\mathbf{R}^\beta\left((\boldsymbol{\Lambda}^\beta)^{-1} - 2\mathbf{Q}_\beta^2\right)\boldsymbol{\psi}^\pm] \\
&= -\omega^2\boldsymbol{\Omega}\boldsymbol{\rho}[\pm 2p\boldsymbol{\beta}\mathbf{R}^\alpha\mathbf{Q}_\alpha\boldsymbol{\phi}^\pm - \boldsymbol{\beta}\mathbf{R}^\beta\left((\boldsymbol{\Lambda}^\beta)^{-1} - 2p^2\right)\boldsymbol{\psi}^\pm] \\
&= -\omega^2\boldsymbol{\Omega}\boldsymbol{\rho}[\pm 2p\boldsymbol{\beta}\mathbf{R}^\alpha\mathbf{Q}_\alpha\boldsymbol{\phi}^\pm - \left(\mathbf{I} - 2p^2\boldsymbol{\beta}\right)\mathbf{R}^\beta\boldsymbol{\psi}^\pm] \qquad (53) \\
&= \omega^2\boldsymbol{\Omega}\boldsymbol{\rho}\boldsymbol{\beta}[\mp 2p\mathbf{R}^\alpha\mathbf{Q}_\alpha\boldsymbol{\phi}^\pm + \mathbf{R}^\beta(\mathbf{Q}_\beta^2 - p^2)\boldsymbol{\psi}^\pm]
\end{aligned}$$

$$\begin{aligned}
\boldsymbol{\tau}_{zz} &= -\omega^2\boldsymbol{\Omega}\boldsymbol{\rho}\left[\left(\boldsymbol{\alpha}\mathbf{R}^\alpha(\boldsymbol{\Lambda}^\alpha)^{-1} - 2\boldsymbol{\beta}\mathbf{R}^\alpha p^2\right)\boldsymbol{\phi}^\pm \pm 2p\boldsymbol{\beta}\mathbf{R}^\beta\mathbf{Q}_\beta\boldsymbol{\psi}^\pm\right] \\
&= -\omega^2\boldsymbol{\Omega}\boldsymbol{\rho}\left[\left(\mathbf{I} - 2p^2\boldsymbol{\beta}\right)\mathbf{R}^\alpha\boldsymbol{\phi}^\pm \pm 2p\boldsymbol{\beta}\mathbf{R}^\beta\mathbf{Q}_\beta\boldsymbol{\psi}^\pm\right] \qquad (54) \\
&= \omega^2\boldsymbol{\Omega}\boldsymbol{\rho}\left[\left(-p^2\boldsymbol{\alpha}\mathbf{R}^\alpha + 2p^2\boldsymbol{\beta}\mathbf{R}^\alpha - \boldsymbol{\alpha}\mathbf{R}^\alpha\mathbf{Q}_\alpha^2\right)\boldsymbol{\phi}^\pm \mp 2p\boldsymbol{\beta}\mathbf{R}^\beta\mathbf{Q}_\beta\boldsymbol{\psi}^\pm\right]
\end{aligned}$$

where the superscript $\pm$ in potentials $\boldsymbol{\phi}$ and $\boldsymbol{\psi}$ denotes the upgoing or downgoing wave direction as illustrated in Figure 2. Based on the above results, for each mode the

associated expressions of displacements and stresses are listed in tabular form below.

	Fast P	Slow P
	$\phi^{\mathrm{I}\pm}$	$\phi^{\mathrm{II}\pm}$
$\mathbf{u}_x$	$i\omega p\ \mathbf{r}^{\alpha_{\mathrm{I}}}$	$i\omega p\ \mathbf{r}^{\alpha_{\mathrm{II}}}$
$\mathbf{u}_z$	$\pm i\omega\ q_{\alpha_{\mathrm{I}}}\mathbf{r}^{\alpha_{\mathrm{I}}}$	$\pm i\omega\ q_{\alpha_{\mathrm{II}}}\mathbf{r}^{\alpha_{\mathrm{II}}}$
$\boldsymbol{\tau}_{xx}$	$-\omega^2\boldsymbol{\Omega\rho}\left(\mathbf{I}-\boldsymbol{\beta\alpha}^{-1}-p^2\boldsymbol{\beta}\right)\mathbf{r}^{\alpha_{\mathrm{I}}}$	$-\omega^2\boldsymbol{\Omega\rho}\left(\mathbf{I}-\boldsymbol{\beta\alpha}^{-1}-p^2\boldsymbol{\beta}\right)\mathbf{r}^{\alpha_{\mathrm{II}}}$
$\boldsymbol{\tau}_{xz}$	$\mp 2\omega^2 p\ q_{\alpha_{\mathrm{I}}}\boldsymbol{\Omega\rho\beta}\ \mathbf{r}^{\alpha_{\mathrm{I}}}$	$\mp 2\omega^2 p\ q_{\alpha_{\mathrm{II}}}\boldsymbol{\Omega\rho\beta}\ \mathbf{r}^{\alpha_{\mathrm{II}}}$
$\boldsymbol{\tau}_{zz}$	$-\omega^2\boldsymbol{\Omega\rho}\left(\mathbf{I}-2p^2\boldsymbol{\beta}\right)\ \mathbf{r}^{\alpha_{\mathrm{I}}}$	$-\omega^2\boldsymbol{\Omega\rho}\left(\mathbf{I}-2p^2\boldsymbol{\beta}\right)\ \mathbf{r}^{\alpha_{\mathrm{II}}}$

(55)

	Fast S	Slow S
	$\psi^{\mathrm{I}\pm}$	$\psi^{\mathrm{II}\pm}$
	$\mp i\omega\ q_{\beta_{\mathrm{I}}}\mathbf{r}^{\beta_{\mathrm{I}}}$	$\mp i\omega\ q_{\beta_{\mathrm{II}}}\mathbf{r}^{\beta_{\mathrm{II}}}$
	$i\omega p\ \mathbf{r}^{\beta_{\mathrm{I}}}$	$i\omega p\ \mathbf{r}^{\beta_{\mathrm{II}}}$
	$\pm 2\omega^2 p\beta_{\mathrm{I}}^2 q_{\beta_{\mathrm{I}}}\boldsymbol{\Omega\rho}\ \mathbf{r}^{\beta_{\mathrm{I}}}$	$\pm 2\omega^2 p\beta_{\mathrm{II}}^2 q_{\beta_{\mathrm{II}}}\boldsymbol{\Omega\rho}\ \mathbf{r}^{\beta_{\mathrm{II}}}$
	$\omega^2\boldsymbol{\Omega\rho}\left(\mathbf{I}-2p^2\boldsymbol{\beta}\right)\ \mathbf{r}^{\beta_{\mathrm{I}}}$	$\omega^2\boldsymbol{\Omega\rho}\left(\mathbf{I}-2p^2\boldsymbol{\beta}\right)\ \mathbf{r}^{\beta_{\mathrm{II}}}$
	$\mp 2\omega^2 pq_{\beta_{\mathrm{I}}}\boldsymbol{\Omega\rho\beta}\ \mathbf{r}^{\beta_{\mathrm{I}}}$	$\mp 2\omega^2 pq_{\beta_{\mathrm{II}}}\boldsymbol{\Omega\rho\beta}\ \mathbf{r}^{\beta_{\mathrm{II}}}$

These are utilized in writing down the explicit expressions for displacement and stresses associated with both incident cases, which are development in the next two sections. For clarity, notations for the amplitude of reflection and transmission potential are explained in table I. The first and second subscripts stand for the nature of incident and scattered wave fields, respectively. The symbol w stands for $\mathrm{P_I}$, $\mathrm{P_{II}}$, $\mathrm{S_I}$ or $\mathrm{S_{II}}$.

Table I. Notations for amplitudes of reflection and transmission potentials.

Reflection coefficients	Transmission coefficients
$\mathbf{r}_{\mathrm{wP}} = \begin{pmatrix} \mathrm{r}_{\mathrm{wP_I}} \\ \mathrm{r}_{\mathrm{wP_{II}}} \end{pmatrix}$	$\mathbf{t}_{\mathrm{wS}} = \begin{pmatrix} \mathrm{t}_{\mathrm{wS_I}} \\ \mathrm{t}_{\mathrm{wS_{II}}} \end{pmatrix}$
$\mathbf{r}_{\mathrm{wS}} = \begin{pmatrix} \mathrm{r}_{\mathrm{wS_I}} \\ \mathrm{r}_{\mathrm{wS_{II}}} \end{pmatrix}$	$\mathbf{t}_{\mathrm{wP}} = \begin{pmatrix} \mathrm{t}_{\mathrm{wP_I}} \\ \mathrm{t}_{\mathrm{wP_{II}}} \end{pmatrix}$

II.2.5 Displacements and stresses associated with an incident down-going $\mathrm{P_I}$-wave for both media

$\mathbf{I}^{\mathrm{in}}_{\mathrm{P_I}}$ is the amplitude vector $(1 \;\; 0)^{\mathrm{T}}$ associated with the incident down-going fast compressional wave in the medium "a". With the aid of expressions of displacements and stresses for modes given in (55) and using the notations for reflection and transmission amplitude given in table I, for top medium "a"

$$\begin{aligned}
\mathbf{u}^{(a)}_x &= i\omega p \mathbf{R}^{\alpha}_{(a)} e^{i\omega(p\mathbf{I}x + \boldsymbol{Q}_{\alpha_{(a)}} z)} \mathbf{I}^{\mathrm{in}}_{\mathrm{P_I}} + i\omega p \mathbf{R}^{\alpha}_{(a)} e^{i\omega(p\mathbf{I}x - \boldsymbol{Q}_{\alpha_{(a)}} z)} \mathbf{r}_{\mathrm{P_IP}} \\
&\quad + i\omega \mathbf{R}^{\beta}_{(a)} \boldsymbol{Q}_{\beta_{(a)}} e^{i\omega(p\mathbf{I}x - \boldsymbol{Q}_{\beta_{(a)}} z)} \mathbf{r}_{\mathrm{P_IS}} \qquad \text{for } z \leq 0, \qquad (56) \\
\mathbf{u}^{(a)}_z &= i\omega \mathbf{R}^{\alpha}_{(a)} \boldsymbol{Q}_{\alpha_{(a)}} e^{i\omega(p\mathbf{I}x + \boldsymbol{Q}_{\alpha_{(a)}} z)} \mathbf{I}^{\mathrm{in}}_{\mathrm{P_I}} - i\omega \mathbf{R}^{\alpha}_{(a)} \boldsymbol{Q}_{\alpha_{(a)}} e^{i\omega(p\mathbf{I}x - \boldsymbol{Q}_{\alpha_{(a)}} z)} \mathbf{r}_{\mathrm{P_IP}} \\
&\quad + i\omega p \mathbf{R}^{\beta}_{(a)} e^{i\omega(p\mathbf{I}x - \boldsymbol{Q}_{\beta_{(a)}} z)} \mathbf{r}_{\mathrm{P_IS}} \qquad \text{for } z \leq 0, \qquad (57)
\end{aligned}$$

$$\begin{aligned}
\boldsymbol{\tau}^{(a)}_{xz} &= -\omega^2 \boldsymbol{\Omega}_{(a)} \boldsymbol{\rho}_{(a)} \Big[2p\boldsymbol{\beta}_{(a)} \mathbf{R}^{\alpha}_{(a)} \boldsymbol{Q}_{\alpha_{(a)}} e^{i\omega(p\mathbf{I}x + \boldsymbol{Q}_{\alpha_{(a)}} z)} \mathbf{I}^{\text{in}}_{\text{P}_\text{I}} \\
&\quad -2p\boldsymbol{\beta}_{(a)} \mathbf{R}^{\alpha}_{(a)} \boldsymbol{Q}_{\alpha_{(a)}} e^{i\omega(p\mathbf{I}x - \boldsymbol{Q}_{\alpha_{(a)}} z)} \mathbf{r}_{\text{P}_\text{I}\text{S}} \\
&\quad -\left(\mathbf{I} - 2p^2\boldsymbol{\beta}_{(a)}\right) \mathbf{R}^{\beta}_{(a)} e^{i\omega(p\mathbf{I}x - \boldsymbol{Q}_{\beta_{(a)}} z)} \mathbf{r}_{\text{P}_\text{I}\text{S}} \Big] \qquad \text{for } z \le 0, \qquad (58) \\
\boldsymbol{\tau}^{(a)}_{zz} &= -\omega^2 \boldsymbol{\Omega}_{(a)} \boldsymbol{\rho}_{(a)} \Big[\left(\mathbf{I} - 2p^2\boldsymbol{\beta}_{(a)}\right) \mathbf{R}^{\alpha}_{(a)} e^{i\omega(p\mathbf{I}x + \boldsymbol{Q}_{\alpha_{(a)}} z)} \mathbf{I}^{\text{in}}_{\text{P}_\text{I}} \\
&\quad + \left(\mathbf{I} - 2p^2\boldsymbol{\beta}_{(a)}\right) \mathbf{R}^{\alpha}_{(a)} e^{i\omega(p\mathbf{I}x - \boldsymbol{Q}_{\alpha_{(a)}} z)} \mathbf{r}_{\text{P}_\text{I}\text{P}} \\
&\quad -2p\boldsymbol{\beta}_{(a)} \mathbf{R}^{\beta}_{(a)} \boldsymbol{Q}_{\beta_{(a)}} e^{i\omega(p\mathbf{I}x - \boldsymbol{Q}_{\beta_{(a)}} z)} \mathbf{r}_{\text{P}_\text{I}\text{S}} \Big] \qquad \text{for } z \le 0. \qquad (59)
\end{aligned}$$

For medium "b"

$$\begin{aligned}
\mathbf{u}^{(b)}_{x} &= i\omega p \mathbf{R}^{\alpha}_{(b)} e^{i\omega(p\mathbf{I}x + \boldsymbol{Q}_{\alpha_{(b)}} z)} \mathbf{t}_{\text{P}_\text{I}\text{P}} \\
&\quad -i\omega \mathbf{R}^{\beta}_{(b)} \boldsymbol{Q}_{\beta_{(b)}} e^{i\omega(p\mathbf{I}x + \boldsymbol{Q}_{\beta_{(b)}} z)} \mathbf{t}_{\text{P}_\text{I}\text{S}} \qquad \text{for } z \ge 0, \qquad (60) \\
\mathbf{u}^{(b)}_{z} &= i\omega \mathbf{R}^{\alpha}_{(b)} \boldsymbol{Q}_{\alpha_{(b)}} e^{i\omega(p\mathbf{I}x + \boldsymbol{Q}_{\alpha_{(b)}} z)} \mathbf{t}_{\text{P}_\text{I}\text{P}} \\
&\quad +i\omega p \mathbf{R}^{\beta}_{(b)} e^{i\omega(p\mathbf{I}x + \boldsymbol{Q}_{\beta_{(b)}} z)} \mathbf{t}_{\text{P}_\text{I}\text{S}} \qquad \text{for } z \ge 0, \qquad (61) \\
\boldsymbol{\tau}^{(b)}_{xz} &= -\omega^2 \boldsymbol{\Omega}_{(b)} \boldsymbol{\rho}_{(b)} \Big[2p\boldsymbol{\beta}_{(b)} \mathbf{R}^{\alpha}_{(b)} \boldsymbol{Q}_{\alpha_{(b)}} e^{i\omega(p\mathbf{I}x + \boldsymbol{Q}_{\alpha_{(b)}} z)} \mathbf{t}_{\text{P}_\text{I}\text{P}} \\
&\quad -\left(\mathbf{I} - 2p^2\boldsymbol{\beta}_{(b)}\right) \mathbf{R}^{\beta}_{(b)} e^{i\omega(p\mathbf{I}x + \boldsymbol{Q}_{\beta_{(b)}} z)} \mathbf{t}_{\text{P}_\text{I}\text{S}} \Big] \qquad \text{for } z \ge 0, \qquad (62) \\
\boldsymbol{\tau}^{(b)}_{zz} &= -\omega^2 \boldsymbol{\Omega}_{(b)} \boldsymbol{\rho}_{(b)} \Big[\left(\mathbf{I} - 2p^2\boldsymbol{\beta}_{(b)}\right) \mathbf{R}^{\alpha}_{(b)} e^{i\omega(p\mathbf{I}x + \boldsymbol{Q}_{\alpha_{(b)}} z)} \mathbf{t}_{\text{P}_\text{I}\text{P}} \\
&\quad +2p\boldsymbol{\beta}_{(b)} \mathbf{R}^{\beta}_{(b)} \boldsymbol{Q}_{\beta_{(b)}} e^{i\omega(p\mathbf{I}x + \boldsymbol{Q}_{\beta_{(b)}} z)} \mathbf{t}_{\text{P}_\text{I}\text{S}} \Big] \qquad \text{for } z \ge 0. \qquad (63)
\end{aligned}$$

II.2.6 Displacements and stresses associated with an incident down-going S_I-wave for both media

$\mathbf{I}^{\text{in}}_{S_I} = (1 \;\; 0)^{\text{T}}$ is the amplitude of the incident fast shear wave. For top medium "a"

$$\begin{aligned}
\mathbf{u}^{(a)}_x &= -i\omega \mathbf{R}^{\beta}_{(a)} \boldsymbol{Q}_{\beta_{(a)}} e^{i\omega(p\mathbf{I}x + \boldsymbol{Q}_{\beta_{(a)}} z)} \mathbf{I}^{\text{in}}_{S_I} + i\omega \mathbf{R}^{\beta}_{(a)} \boldsymbol{Q}_{\beta_{(a)}} e^{i\omega(p\mathbf{I}x - \boldsymbol{Q}_{\beta_{(a)}} z)} \mathbf{r}_{S_I S} \\
&\quad + i\omega p \mathbf{R}^{\alpha}_{(a)} e^{i\omega(p\mathbf{I}x - \boldsymbol{Q}_{\alpha_{(a)}} z)} \mathbf{r}_{S_I P} \qquad \text{for } z \le 0, \qquad (64) \\
\mathbf{u}^{(a)}_z &= i\omega p \mathbf{R}^{\beta}_{(a)} e^{i\omega(p\mathbf{I}x + \boldsymbol{Q}_{\beta_{(a)}} z)} \mathbf{I}^{\text{in}}_{S_I} + i\omega p \mathbf{R}^{\beta}_{(a)} e^{i\omega(p\mathbf{I}x - \boldsymbol{Q}_{\beta_{(a)}} z)} \mathbf{r}_{S_I S} \\
&\quad - i\omega \mathbf{R}^{\alpha}_{(a)} \boldsymbol{Q}_{\alpha_{(a)}} e^{i\omega(p\mathbf{I}x - \boldsymbol{Q}_{\alpha_{(a)}} z)} \mathbf{r}_{S_I P} \qquad \text{for } z \le 0, \qquad (65) \\
\boldsymbol{\tau}^{(a)}_{xz} &= -\omega^2 \boldsymbol{\Omega}_{(a)} \boldsymbol{\rho}_{(a)} \Big[-\left(\mathbf{I} - 2p^2 \boldsymbol{\beta}_{(a)}\right) \mathbf{R}^{\beta}_{(a)} e^{i\omega(p\mathbf{I}x + \boldsymbol{Q}_{\beta_{(a)}} z)} \mathbf{I}^{\text{in}}_{S_I} \\
&\quad - \left(\mathbf{I} - 2p^2 \boldsymbol{\beta}_{(a)}\right) \mathbf{R}^{\beta}_{(a)} e^{i\omega(p\mathbf{I}x - \boldsymbol{Q}_{\beta_{(a)}} z)} \mathbf{r}_{S_I S} \\
&\quad - 2p \boldsymbol{\beta}_{(a)} \mathbf{R}^{\alpha}_{(a)} \boldsymbol{Q}_{\alpha_{(a)}} e^{i\omega(p\mathbf{I}x - \boldsymbol{Q}_{\alpha_{(a)}} z)} \mathbf{r}_{S_I P} \Big] \qquad \text{for } z \le 0, \qquad (66) \\
\boldsymbol{\tau}^{(a)}_{zz} &= -\omega^2 \boldsymbol{\Omega}_{(a)} \boldsymbol{\rho}_{(a)} \Big[2p \boldsymbol{\beta}_{(a)} \mathbf{R}^{\beta}_{(a)} \boldsymbol{Q}_{\beta_{(a)}} e^{i\omega(p\mathbf{I}x + \boldsymbol{Q}_{\beta_{(a)}} z)} \mathbf{I}^{\text{in}}_{S_I} \\
&\quad - 2p \boldsymbol{\beta}_{(a)} \mathbf{R}^{\beta}_{(a)} \boldsymbol{Q}_{\beta_{(a)}} e^{i\omega(p\mathbf{I}x - \boldsymbol{Q}_{\beta_{(a)}} z)} \mathbf{r}_{S_I S} \\
&\quad + \left(\mathbf{I} - 2p^2 \boldsymbol{\beta}_{(a)}\right) \mathbf{R}^{\alpha}_{(a)} e^{i\omega(p\mathbf{I}x - \boldsymbol{Q}_{\alpha_{(a)}} z)} \mathbf{r}_{S_I P} \Big] \qquad \text{for } z \le 0. \qquad (67)
\end{aligned}$$

For medium "b"

$$\begin{aligned}
\mathbf{u}^{(b)}_x &= -i\omega \mathbf{R}^{\beta}_{(b)} \boldsymbol{Q}_{\beta_{(b)}} e^{i\omega(p\mathbf{I}x + \boldsymbol{Q}_{\beta_{(b)}} z)} \mathbf{t}_{S_I S} \\
&\quad + i\omega p \mathbf{R}^{\alpha}_{(b)} e^{i\omega(p\mathbf{I}x + \boldsymbol{Q}_{\alpha_{(b)}} z)} \mathbf{t}_{S_I P} \qquad \text{for } z \ge 0, \qquad (68) \\
\mathbf{u}^{(b)}_z &= i\omega p \mathbf{R}^{\beta}_{(b)} e^{i\omega(p\mathbf{I}x + \boldsymbol{Q}_{\beta_{(b)}} z)} \mathbf{t}_{S_I S} \\
&\quad + i\omega \mathbf{R}^{\alpha}_{(b)} \boldsymbol{Q}_{\alpha_{(b)}} e^{i\omega(p\mathbf{I}x + \boldsymbol{Q}_{\alpha_{(b)}} z)} \mathbf{t}_{S_I P} \qquad \text{for } z \ge 0 \qquad (69) \\
\boldsymbol{\tau}^{(b)}_{xz} &= -\omega^2 \boldsymbol{\Omega}_{(b)} \boldsymbol{\rho}_{(b)} \Big[-\left(\mathbf{I} - 2p^2 \boldsymbol{\beta}_{(b)}\right) \mathbf{R}^{\beta}_{(b)} e^{i\omega(p\mathbf{I}x + \boldsymbol{Q}_{\beta_{(b)}} z)} \mathbf{t}_{S_I S} \\
&\quad + 2p \boldsymbol{\beta}_{(b)} \mathbf{R}^{\alpha}_{(b)} \boldsymbol{Q}_{\alpha_{(b)}} e^{i\omega(p\mathbf{I}x + \boldsymbol{Q}_{\alpha_{(b)}} z)} \mathbf{t}_{S_I P} \Big] \qquad \text{for } z \ge 0, \qquad (70) \\
\boldsymbol{\tau}^{(b)}_{zz} &= -\omega^2 \boldsymbol{\Omega}_{(b)} \boldsymbol{\rho}_{(b)} \Big[2p \boldsymbol{\beta}_{(b)} \mathbf{R}^{\beta}_{(b)} \boldsymbol{Q}_{\beta_{(b)}} e^{i\omega(p\mathbf{I}x + \boldsymbol{Q}_{\beta_{(b)}} z)} \mathbf{t}_{S_I S} \\
&\quad + \left(\mathbf{I} - 2p^2 \boldsymbol{\beta}_{(b)}\right) \mathbf{R}^{\alpha}_{(b)} e^{i\omega(p\mathbf{I}x + \boldsymbol{Q}_{\alpha_{(b)}} z)} \mathbf{t}_{S_I P} \Big] \qquad \text{for } z \ge 0. \qquad (71)
\end{aligned}$$

II.2.7 Some Notations

In order to simplify algebraic manipulation and computation, I define the following notations which have been used henceforth. These quantities are 2×2 matrices and its elements have dimensions of acoustic impedance.

$$\boldsymbol{\mathcal{K}} = 2p\boldsymbol{\Omega\rho\beta}\mathbf{R}^{\alpha}\boldsymbol{Q}_{\alpha} \tag{72}$$

$$\boldsymbol{\mathcal{M}} = \boldsymbol{\Omega\rho}\left(\mathbf{I}-2p^2\boldsymbol{\beta}\right)\mathbf{R}^{\beta} \tag{73}$$

$$\boldsymbol{\mathcal{N}} = \boldsymbol{\Omega\rho}\left(\mathbf{I}-2p^2\boldsymbol{\beta}\right)\mathbf{R}^{\alpha} \tag{74}$$

$$\boldsymbol{\mathcal{J}} = 2p\boldsymbol{\Omega\rho\beta}\mathbf{R}^{\alpha}\boldsymbol{Q}_{\alpha} \tag{75}$$

$$\boldsymbol{\mathcal{L}} = \boldsymbol{\Omega\rho}\left(\mathbf{I}-2p^2\boldsymbol{\beta}\right)\mathbf{R}^{\beta} \tag{76}$$

$$\boldsymbol{\mathcal{S}} = \boldsymbol{\Omega\rho}\left(\mathbf{I}-2p^2\boldsymbol{\beta}\right)\mathbf{R}^{\alpha} \tag{77}$$

$$\boldsymbol{Z}^{\alpha} = \boldsymbol{\Omega\rho\alpha}\mathbf{R}^{\alpha}\boldsymbol{Q}_{\alpha} \tag{78}$$

$$\boldsymbol{Z}^{\beta} = \boldsymbol{\Omega\rho\beta}\mathbf{R}^{\beta}\boldsymbol{Q}_{\beta} \tag{79}$$

In the following, the system of equations for reflection and transmission coefficients are set up for the four cases, namely, DS09 and dCS09 subjected to incident $\mathrm{P_I}$ and $\mathrm{S_I}$. In each case, the set of the eight equations are rearranged into a matricidal form to have the following general structure,

$$\begin{bmatrix} \boldsymbol{\mathcal{A}} & \boldsymbol{\mathcal{B}} \\ \\ \boldsymbol{\mathcal{C}} & \boldsymbol{\mathcal{D}} \end{bmatrix} \begin{bmatrix} \mathbf{r} \\ \\ \mathbf{t} \end{bmatrix} = \begin{bmatrix} \mathbf{p} \\ \\ \mathbf{q} \end{bmatrix} \tag{80}$$

where $\mathbf{r} = \left(\mathbf{r}_{\mathrm{wP}} \;\; \mathbf{r}_{\mathrm{wS}}\right)^{\mathrm{T}}$ and $\mathbf{t} = \left(\mathbf{t}_{\mathrm{wP}} \;\; \mathbf{t}_{\mathrm{wS}}\right)^{\mathrm{T}}$ are the reflection and transmission coefficients vectors to be determined. Both $\mathbf{r}$ and $\mathbf{t}$ contain four elements (further notations are explained in table I). The $\boldsymbol{\mathcal{A}}, \boldsymbol{\mathcal{B}}, \boldsymbol{\mathcal{C}}$, and $\boldsymbol{\mathcal{D}}$ are 4×4 matrices, and, $\mathbf{p}$ and $\mathbf{q}$ are four element vectors that depend on the incident field. For completeness, the modified

Deresiewicz and Skalak (1963) boundary conditions (5) and (6) are expressed, for 2D problem under considerations, as follows

$$\mathbf{u}_x^{(a)} = \mathbf{T}_{(a)}\mathbf{T}_{(b)}^{-1}\mathbf{u}_x^{(b)} \tag{81}$$

$$\mathbf{u}_z^{(a)} = \mathbf{T}_{(a)}\mathbf{T}_{(b)}^{-1}\mathbf{u}_z^{(b)} \tag{82}$$

$$\mathbf{T}_{(a)}^T\boldsymbol{\tau}_{xz}^{(a)} + \mathbf{D}_{(a)}\mathbf{u}_x^{(a)} = \mathbf{T}_{(b)}^T\boldsymbol{\tau}_{xz}^{(b)} + \mathbf{D}_{(b)}\mathbf{u}_x^{(b)} \tag{83}$$

$$\mathbf{T}_{(a)}^T\boldsymbol{\tau}_{zz}^{(a)} + \mathbf{D}_{(a)}\mathbf{u}_z^{(a)} = \mathbf{T}_{(b)}^T\boldsymbol{\tau}_{zz}^{(b)} + \mathbf{D}_{(b)}\mathbf{u}_z^{(b)}. \tag{84}$$

For 2D problem under considerations, the modified de la Cruz and Spanos (1989) boundary conditions (7) and (8) are expressed as follows

$$\mathbf{u}_x^{(a)} = \mathbf{G}_{(a)}^{-1}\mathbf{G}_{(b)}\mathbf{u}_x^{(b)}, \tag{85}$$

$$\mathbf{u}_z^{(a)} = \mathbf{G}_{(a)}^{-1}\mathbf{G}_{(b)}\mathbf{u}_z^{(b)}, \tag{86}$$

$$\boldsymbol{\tau}_{xz}^{(a)} = \mathbf{H}_{(a)}^{-1}\mathbf{H}_{(b)}\boldsymbol{\tau}_{xz}^{(b)}, \tag{87}$$

$$\boldsymbol{\tau}_{zz}^{(a)} = \mathbf{H}_{(a)}^{-1}\mathbf{H}_{(b)}\boldsymbol{\tau}_{zz}^{(b)}. \tag{88}$$

II.2.8 8×8 system of equations for the DS09 boundary conditions: Incident fast P-wave

In equations (81) through (84), using the formulas developed in §II.2.5 and evaluating at $z = 0$, followed by some rearrangements, the resulting system of equations is

$$\begin{bmatrix} -p\mathbf{R}_{(a)}^{\alpha} & -\mathbf{R}_{(a)}^{\beta}\boldsymbol{Q}_{\beta_{(a)}} & p\mathbf{T}_{(a)}\mathbf{T}_{(b)}^{-1}\mathbf{R}_{(b)}^{\alpha} & -\mathbf{T}_{(a)}\mathbf{T}_{(b)}^{-1}\mathbf{R}_{(b)}^{\beta}\boldsymbol{Q}_{\beta_{(b)}} \\ \mathbf{R}_{(a)}^{\alpha}\boldsymbol{Q}_{\alpha_{(a)}} & -p\mathbf{R}_{(a)}^{\beta} & \mathbf{T}_{(a)}\mathbf{T}_{(b)}^{-1}\mathbf{R}_{(b)}^{\alpha}\boldsymbol{Q}_{\alpha_{(b)}} & p\mathbf{T}_{(a)}\mathbf{T}_{(b)}^{-1}\mathbf{R}_{(b)}^{\beta} \\ \left(\mathbf{T}_{(a)}^T\boldsymbol{\mathcal{K}}_{(a)} - p\mathbf{D}_{(a)}\mathbf{R}_{(a)}^{\alpha}\right) & \left(\mathbf{T}_{(a)}^T\boldsymbol{\mathcal{M}}_{(a)} - \mathbf{D}_{(a)}\mathbf{R}_{(a)}^{\beta}\boldsymbol{Q}_{\beta_{(a)}}\right) & \left(\mathbf{T}_{(b)}^T\boldsymbol{\mathcal{K}}_{(b)} + p\mathbf{D}_{(b)}\mathbf{R}_{(b)}^{\alpha}\right) & -\left(\mathbf{T}_{(b)}^T\boldsymbol{\mathcal{M}}_{(b)} + \mathbf{D}_{(b)}\mathbf{R}_{(b)}^{\beta}\boldsymbol{Q}_{\beta_{(b)}}\right) \\ \left(\mathbf{D}_{(a)}\mathbf{R}_{(a)}^{\alpha}\boldsymbol{Q}_{\alpha_{(a)}} - \mathbf{T}_{(a)}^T\boldsymbol{\mathcal{N}}_{(a)}\right) & \left(2p\mathbf{T}_{(a)}^T\mathbf{Z}_{(a)}^{\beta} - p\mathbf{D}_{(a)}\mathbf{R}_{(a)}^{\beta}\right) & \left(\mathbf{T}_{(b)}^T\boldsymbol{\mathcal{N}}_{(b)} + \mathbf{D}_{(b)}\mathbf{R}_{(b)}^{\alpha}\boldsymbol{Q}_{\alpha_{(b)}}\right) & \left(2p\mathbf{T}_{(b)}^T\mathbf{Z}_{(b)}^{\beta} + p\mathbf{D}_{(b)}\mathbf{R}_{(b)}^{\beta}\right) \end{bmatrix} \begin{bmatrix} \mathrm{r}_{\mathrm{P_I P}} \\ \mathrm{r}_{\mathrm{P_I S}} \\ \mathrm{t}_{\mathrm{P_I P}} \\ \mathrm{t}_{\mathrm{P_I S}} \end{bmatrix}$$

$$= \begin{bmatrix} p\mathbf{R}^{\alpha}_{(a)}\mathbf{I}^{\text{in}}_{\text{P}_\text{I}} \\ \\ \mathbf{R}^{\alpha}_{(a)}\boldsymbol{Q}_{\alpha_{(a)}}\mathbf{I}^{\text{in}}_{\text{P}_\text{I}} \\ \\ \mathbf{T}^{T}_{(a)}\boldsymbol{\mathcal{K}}_{(a)} + p\mathbf{D}_{(a)}\mathbf{R}^{\alpha}_{(a)}\mathbf{I}^{\text{in}}_{\text{P}_\text{I}} \\ \\ \mathbf{T}^{T}_{(a)}\boldsymbol{\mathcal{N}}_{(a)} + \mathbf{D}_{(a)}\mathbf{R}^{\alpha}_{(a)}\boldsymbol{Q}_{\alpha_{(a)}}\mathbf{I}^{\text{in}}_{\text{P}_\text{I}} \end{bmatrix} \tag{89}$$

From the above, the terms of the block matrix representation (eqn 80) are read as

$$\boldsymbol{\mathcal{A}} = \begin{bmatrix} -p\mathbf{R}^{\alpha}_{(a)} & -\mathbf{R}^{\beta}_{(a)}\boldsymbol{Q}_{\beta_{(a)}} \\ \\ \mathbf{R}^{\alpha}_{(a)}\boldsymbol{Q}_{\alpha_{(a)}} & -p\mathbf{R}^{\beta}_{(a)} \end{bmatrix} \tag{90}$$

$$\boldsymbol{\mathcal{B}} = \begin{bmatrix} p\mathbf{T}_{(a)}\mathbf{T}^{-1}_{(b)}\mathbf{R}^{\alpha}_{(b)} & -\mathbf{T}_{(a)}\mathbf{T}^{-1}_{(b)}\mathbf{R}^{\beta}_{(b)}\boldsymbol{Q}_{\beta_{(b)}} \\ \\ \mathbf{T}_{(a)}\mathbf{T}^{-1}_{(b)}\mathbf{R}^{\alpha}_{(b)}\boldsymbol{Q}_{\alpha_{(b)}} & p\mathbf{T}_{(a)}\mathbf{T}^{-1}_{(b)}\mathbf{R}^{\beta}_{(b)} \end{bmatrix} \tag{91}$$

(92)

$$\boldsymbol{\mathcal{C}} = \begin{bmatrix} \left(\mathbf{T}^{T}_{(a)}\boldsymbol{\mathcal{K}}_{(a)} - p\mathbf{D}_{(a)}\mathbf{R}^{\alpha}_{(a)}\right) & \left(\mathbf{T}^{T}_{(a)}\boldsymbol{\mathcal{M}}_{(a)} - \mathbf{D}_{(a)}\mathbf{R}^{\beta}_{(a)}\boldsymbol{Q}_{\beta_{(a)}}\right) \\ \\ \left(\mathbf{D}_{(a)}\mathbf{R}^{\alpha}_{(a)}\boldsymbol{Q}_{\alpha_{(a)}} - \mathbf{T}^{T}_{(a)}\boldsymbol{\mathcal{N}}_{(a)}\right) & \left(2p\mathbf{T}^{T}_{(a)}\mathbf{Z}^{\beta}_{(a)} - p\mathbf{D}_{(a)}\mathbf{R}^{\beta}_{(a)}\right) \end{bmatrix} \tag{93}$$

$$\boldsymbol{\mathcal{D}} = \begin{bmatrix} \left(\mathbf{T}^{T}_{(b)}\boldsymbol{\mathcal{K}}_{(b)} + p\mathbf{D}_{(b)}\mathbf{R}^{\alpha}_{(b)}\right) & -\left(\mathbf{T}^{T}_{(b)}\boldsymbol{\mathcal{M}}_{(b)} + \mathbf{D}_{(b)}\mathbf{R}^{\beta}_{(b)}\boldsymbol{Q}_{\beta_{(b)}}\right) \\ \\ \left(\mathbf{T}^{T}_{(b)}\boldsymbol{\mathcal{N}}_{(b)} + \mathbf{D}_{(b)}\mathbf{R}^{\alpha}_{(b)}\boldsymbol{Q}_{\alpha_{(b)}}\right) & \left(2p\mathbf{T}^{T}_{(b)}\mathbf{Z}^{\beta}_{(b)} + p\mathbf{D}_{(b)}\mathbf{R}^{\beta}_{(b)}\right) \end{bmatrix} \tag{94}$$

$$\mathbf{p} = \begin{bmatrix} p\mathbf{R}^{\alpha}_{(a)}\mathbf{I}^{\text{in}}_{\text{P}_\text{I}} \\ \\ \mathbf{R}^{\alpha}_{(a)}\boldsymbol{Q}_{\alpha_{(a)}}\mathbf{I}^{\text{in}}_{\text{P}_\text{I}} \end{bmatrix} \tag{95}$$

$$\mathbf{q} = \begin{bmatrix} \mathbf{T}^T_{(a)}\boldsymbol{\mathcal{K}}_{(a)} + p\mathbf{D}_{(a)}\mathbf{R}^{\alpha}_{(a)}\mathbf{I}^{\text{in}}_{\text{P}_\text{I}} \\ \\ \mathbf{T}^T_{(a)}\boldsymbol{\mathcal{N}}_{(a)} + \mathbf{D}_{(a)}\mathbf{R}^{\alpha}_{(a)}\boldsymbol{Q}_{\alpha_{(a)}}\mathbf{I}^{\text{in}}_{\text{P}_\text{I}} \end{bmatrix} \tag{96}$$

II.2.9 8×8 system of equations for the DS09 boundary conditions: Incident fast S-wave

In equations (81) through (84), using the formulas developed in §II.2.6 and evaluating at $z = 0$, followed by some rearrangements, the resulting system of equations is

$$\begin{bmatrix} \mathbf{R}^{\beta}_{(a)}\boldsymbol{Q}_{\beta_{(a)}} & p\mathbf{R}^{\alpha}_{(a)} & \mathbf{T}_{(a)}\mathbf{T}^{-1}_{(b)}\mathbf{R}^{\beta}_{(b)}\boldsymbol{Q}_{\beta_{(b)}} & -p\mathbf{T}_{(a)}\mathbf{T}^{-1}_{(b)}\mathbf{R}^{\alpha}_{(b)} \\ -p\mathbf{R}^{\beta}_{(a)} & \mathbf{R}^{\alpha}_{(a)}\boldsymbol{Q}_{\alpha_{(a)}} & p\mathbf{T}_{(a)}\mathbf{T}^{-1}_{(b)}\mathbf{R}^{\beta}_{(b)} & \mathbf{T}_{(a)}\mathbf{T}^{-1}_{(b)}\mathbf{R}^{\alpha}_{(b)}\boldsymbol{Q}_{\alpha_{(b)}} \\ \left(\mathbf{D}_{(a)}\mathbf{R}^{\beta}_{(a)}\boldsymbol{Q}_{\beta_{(a)}} - \mathbf{T}^T_{(a)}\boldsymbol{\mathcal{M}}_{(a)}\right) & \left(p\mathbf{D}_{(a)}\mathbf{R}^{\alpha}_{(a)} - \mathbf{T}^T_{(a)}\boldsymbol{\mathcal{K}}_{(a)}\right) & \left(\mathbf{D}_{(b)}\mathbf{R}^{\beta}_{(b)}\boldsymbol{Q}_{\beta_{(b)}} + \mathbf{T}^T_{(b)}\boldsymbol{\mathcal{M}}_{(b)}\right) & -(p\mathbf{D}_{(b)}\mathbf{R}^{\alpha}_{(b)} + \mathbf{T}^T_{(b)}\boldsymbol{\mathcal{K}}_{(b)}) \\ (2p\mathbf{T}^T_{(a)}\mathbf{Z}^{\beta}_{(a)} - p\mathbf{D}_{(a)}\mathbf{R}^{\beta}_{(a)}) & (\mathbf{D}_{(a)}\mathbf{R}^{\alpha}_{(a)}\boldsymbol{Q}_{\alpha_{(a)}} - \mathbf{T}^T_{(a)}\boldsymbol{\mathcal{N}}_{(a)}) & (p\mathbf{D}_{(b)}\mathbf{R}^{\beta}_{(b)} + 2p\mathbf{T}^T_{(b)}\mathbf{Z}^{\beta}_{(b)}) & (\mathbf{D}_{(b)}\mathbf{R}^{\alpha}_{(b)}\boldsymbol{Q}_{\alpha_{(b)}} + \mathbf{T}^T_{(b)}\boldsymbol{\mathcal{N}}_{(b)}) \end{bmatrix} \begin{bmatrix} \mathrm{r}_{\mathrm{S_I S}} \\ \mathrm{r}_{\mathrm{S_I P}} \\ \mathrm{t}_{\mathrm{S_I S}} \\ \mathrm{t}_{\mathrm{S_I P}} \end{bmatrix}$$

$$= \begin{bmatrix} \mathbf{R}^{\beta}_{(a)}\boldsymbol{Q}_{\beta_{(a)}}\mathbf{I}^{\text{in}}_{\text{S}_\text{I}} \\ \\ p\mathbf{R}^{\beta}_{(a)}\mathbf{I}^{\text{in}}_{\text{S}_\text{I}} \\ \\ (\mathbf{D}_{(a)}\mathbf{R}^{\beta}_{(a)}\boldsymbol{Q}_{\beta_{(a)}} + \mathbf{T}^T_{(a)}\boldsymbol{\mathcal{M}}_{(a)})\mathbf{I}^{\text{in}}_{\text{S}_\text{I}} \\ \\ (p\mathbf{D}_{(a)}\mathbf{R}^{\beta}_{(a)} + 2p\mathbf{T}^T_{(a)}\mathbf{Z}^{\beta}_{(a)})\mathbf{I}^{\text{in}}_{\text{S}_\text{I}} \end{bmatrix} \tag{97}$$

where the terms for the block matrix (equations 80) are given by

$$\boldsymbol{\mathcal{A}} = \begin{bmatrix} \mathbf{R}^{\beta}_{(a)}\boldsymbol{Q}_{\beta_{(a)}} & p\mathbf{R}^{\alpha}_{(a)} \\ \\ -p\mathbf{R}^{\beta}_{(a)} & \mathbf{R}^{\alpha}_{(a)}\boldsymbol{Q}_{\alpha_{(a)}} \end{bmatrix} \tag{98}$$

$$\boldsymbol{\mathcal{B}} = \begin{bmatrix} \mathbf{T}_{(a)}\mathbf{T}^{-1}_{(b)}\mathbf{R}^{\beta}_{(b)}\boldsymbol{Q}_{\beta_{(b)}} & -p\mathbf{T}_{(a)}\mathbf{T}^{-1}_{(b)}\mathbf{R}^{\alpha}_{(b)} \\ \\ p\mathbf{T}_{(a)}\mathbf{T}^{-1}_{(b)}\mathbf{R}^{\beta}_{(b)} & \mathbf{T}_{(a)}\mathbf{T}^{-1}_{(b)}\mathbf{R}^{\alpha}_{(b)}\boldsymbol{Q}_{\alpha_{(b)}} \end{bmatrix} \tag{99}$$

$$\boldsymbol{\mathcal{C}} = \begin{bmatrix} \left(\mathbf{D}_{(a)}\mathbf{R}^{\beta}_{(a)}\boldsymbol{Q}_{\beta_{(a)}} - \mathbf{T}^{T}_{(a)}\boldsymbol{\mathcal{M}}_{(a)}\right) & \left(p\mathbf{D}_{(a)}\mathbf{R}^{\alpha}_{(a)} - \mathbf{T}^{T}_{(a)}\boldsymbol{\mathcal{K}}_{(a)}\right) \\ \left(2p\mathbf{T}^{T}_{(a)}\mathbf{Z}^{\beta}_{(a)} - p\mathbf{D}_{(a)}\mathbf{R}^{\beta}_{(a)}\right) & \left(\mathbf{D}_{(a)}\mathbf{R}^{\alpha}_{(a)}\boldsymbol{Q}_{\alpha_{(a)}} - \mathbf{T}^{T}_{(a)}\boldsymbol{\mathcal{N}}_{(a)}\right) \end{bmatrix} \tag{100}$$

$$\boldsymbol{\mathcal{D}} = \begin{bmatrix} \left(\mathbf{D}_{(b)}\mathbf{R}^{\beta}_{(b)}\boldsymbol{Q}_{\beta_{(b)}} + \mathbf{T}^{T}_{(b)}\boldsymbol{\mathcal{M}}_{(b)}\right) & -\left(p\mathbf{D}_{(b)}\mathbf{R}^{\alpha}_{(b)} + \mathbf{T}^{T}_{(b)}\boldsymbol{\mathcal{K}}_{(b)}\right) \\ \left(p\mathbf{D}_{(b)}\mathbf{R}^{\beta}_{(b)} + 2p\mathbf{T}^{T}_{(b)}\mathbf{Z}^{\beta}_{(b)}\right) & \left(\mathbf{D}_{(b)}\mathbf{R}^{\alpha}_{(b)}\boldsymbol{Q}_{\alpha_{(b)}} + \mathbf{T}^{T}_{(b)}\boldsymbol{\mathcal{N}}_{(b)}\right) \end{bmatrix} \tag{101}$$

$$\mathbf{p} = \begin{bmatrix} \mathbf{R}^{\beta}_{(a)}\boldsymbol{Q}_{\beta_{(a)}}\mathbf{I}^{\text{in}}_{\text{S}_\text{I}} \\ p\mathbf{R}^{\beta}_{(a)}\mathbf{I}^{\text{in}}_{\text{S}_\text{I}} \end{bmatrix} \tag{102}$$

$$\mathbf{q} = \begin{bmatrix} (\mathbf{D}_{(a)}\mathbf{R}^{\beta}_{(a)}\boldsymbol{Q}_{\beta_{(a)}} + \mathbf{T}^{T}_{(a)}\boldsymbol{\mathcal{M}}_{(a)})\mathbf{I}^{\text{in}}_{\text{S}_\text{I}} \\ (p\mathbf{D}_{(a)}\mathbf{R}^{\beta}_{(a)} + 2p\mathbf{T}^{T}_{(a)}\mathbf{Z}^{\beta}_{(a)})\mathbf{I}^{\text{in}}_{\text{S}_\text{I}} \end{bmatrix} \tag{103}$$

II.2.10 8×8 system of equations for the dCS09 boundary conditions: Incident fast P-wave

In equations (85) through (88), using the formulas developed in §II.2.5 and evaluating at $z = 0$, followed by some rearrangements, the resulting system of equations is

$$\begin{bmatrix} -p\mathbf{R}^{\alpha}_{(a)} & -\mathbf{R}^{\beta}_{(a)}\boldsymbol{Q}_{\beta_{(a)}} & p\mathbf{G}^{-1}_{(a)}\mathbf{G}_{(b)}\mathbf{R}^{\alpha}_{(b)} & -\mathbf{G}^{-1}_{(a)}\mathbf{G}_{(b)}\mathbf{R}^{\beta}_{(b)}\boldsymbol{Q}_{\beta_{(b)}} \\ \mathbf{R}^{\alpha}_{(a)}\boldsymbol{Q}_{\alpha_{(a)}} & -p\mathbf{R}^{\beta}_{(a)} & \mathbf{G}^{-1}_{(a)}\mathbf{G}_{(b)}\mathbf{R}^{\alpha}_{(b)}\boldsymbol{Q}_{\alpha_{(b)}} & p\mathbf{G}^{-1}_{(a)}\mathbf{G}_{(b)}\mathbf{R}^{\beta}_{(b)} \\ \boldsymbol{\mathcal{J}}_{(a)} & \boldsymbol{\mathcal{L}}_{(a)} & \mathbf{H}^{-1}_{(a)}\mathbf{H}_{(b)}\boldsymbol{\mathcal{J}}_{(b)} & -\mathbf{H}^{-1}_{(a)}\mathbf{H}_{(b)}\boldsymbol{\mathcal{L}}_{(b)} \\ -\boldsymbol{\mathcal{S}}_{(a)} & 2p\boldsymbol{Z}^{\beta}_{(a)} & \mathbf{H}^{-1}_{(a)}\mathbf{H}_{(b)}\boldsymbol{\mathcal{S}}_{(b)} & 2p\mathbf{H}^{-1}_{(a)}\mathbf{H}_{(b)}\boldsymbol{Z}^{\beta}_{(b)} \end{bmatrix} \begin{bmatrix} \mathrm{r}_{\mathrm{P_I P}} \\ \mathrm{r}_{\mathrm{P_I S}} \\ \mathrm{t}_{\mathrm{P_I P}} \\ \mathrm{t}_{\mathrm{P_I S}} \end{bmatrix} = \begin{bmatrix} p\mathbf{R}^{\alpha}_{(a)}\mathbf{I}^{\text{in}}_{\text{P}_\text{I}} \\ \mathbf{R}^{\alpha}_{(a)}\boldsymbol{Q}_{\alpha_{(a)}}\mathbf{I}^{\text{in}}_{\text{P}_\text{I}} \\ \boldsymbol{\mathcal{J}}_{(a)}\mathbf{I}^{\text{in}}_{\text{P}_\text{I}} \\ \boldsymbol{\mathcal{S}}_{(a)}\mathbf{I}^{\text{in}}_{\text{P}_\text{I}} \end{bmatrix} \tag{104}$$

where the terms for the block matrix representation (equation 80) are given by

$$\mathcal{A} = \begin{bmatrix} -p\mathbf{R}^{\alpha}_{(a)} & -\mathbf{R}^{\beta}_{(a)}\boldsymbol{Q}_{\beta_{(a)}} \\ \\ \mathbf{R}^{\alpha}_{(a)}\boldsymbol{Q}_{\alpha_{(a)}} & -p\mathbf{R}^{\beta}_{(a)} \end{bmatrix} \tag{105}$$

$$\mathcal{B} = \begin{bmatrix} p\mathbf{G}^{-1}_{(a)}\mathbf{G}_{(b)}\mathbf{R}^{\alpha}_{(b)} & -\mathbf{G}^{-1}_{(a)}\mathbf{G}_{(b)}\mathbf{R}^{\beta}_{(b)}\boldsymbol{Q}_{\beta_{(b)}} \\ \\ \mathbf{G}^{-1}_{(a)}\mathbf{G}_{(b)}\mathbf{R}^{\alpha}_{(b)}\boldsymbol{Q}_{\alpha_{(b)}} & p\mathbf{G}^{-1}_{(a)}\mathbf{G}_{(b)}\mathbf{R}^{\beta}_{(b)} \end{bmatrix} \tag{106}$$

$$\mathcal{C} = \begin{bmatrix} \boldsymbol{\mathcal{J}}_{(a)} & \boldsymbol{\mathcal{L}}_{(a)} \\ \\ -\boldsymbol{\mathcal{S}}_{(a)} & 2p\boldsymbol{Z}^{\beta}_{(a)} \end{bmatrix} \tag{107}$$

$$\mathcal{D} = \begin{bmatrix} \mathbf{H}^{-1}_{(a)}\mathbf{H}_{(b)}\boldsymbol{\mathcal{J}}_{(b)} & -\mathbf{H}^{-1}_{(a)}\mathbf{H}_{(b)}\boldsymbol{\mathcal{L}}_{(b)} \\ \\ \mathbf{H}^{-1}_{(a)}\mathbf{H}_{(b)}\boldsymbol{\mathcal{S}}_{(b)} & 2p\mathbf{H}^{-1}_{(a)}\mathbf{H}_{(b)}\boldsymbol{Z}^{\beta}_{(b)} \end{bmatrix} \tag{108}$$

$$\mathbf{p} = \begin{bmatrix} p\mathbf{R}^{\alpha}_{(a)}\mathbf{I}^{\text{in}}_{\text{P}_\text{I}} \\ \\ \mathbf{R}^{\alpha}_{(a)}\boldsymbol{Q}_{\alpha_{(a)}}\mathbf{I}^{\text{in}}_{\text{P}_\text{I}} \end{bmatrix} \tag{109}$$

$$\mathbf{q} = \begin{bmatrix} \boldsymbol{\mathcal{J}}_{(a)}\mathbf{I}^{\text{in}}_{\text{P}_\text{I}} \\ \\ \boldsymbol{\mathcal{S}}_{(a)}\mathbf{I}^{\text{in}}_{\text{P}_\text{I}} \end{bmatrix} \tag{110}$$

II.2.11 8×8 system of equations for the dCS09 boundary conditions: Incident fast S-wave

In equations (85) through (88), using the formulas developed in §II.2.6 and evaluating at $z = 0$, followed by some rearrangements, the resulting system of equations is

$$\begin{bmatrix} \mathbf{R}^{\beta}_{(a)}\boldsymbol{Q}_{\beta_{(a)}} & p\mathbf{R}^{\alpha}_{(a)} & \mathbf{G}^{-1}_{(a)}\mathbf{G}_{(b)}\mathbf{R}^{\beta}_{(b)}\boldsymbol{Q}_{\beta_{(b)}} & -p\mathbf{G}^{-1}_{(a)}\mathbf{G}_{(b)}\mathbf{R}^{\alpha}_{(b)} \\ -p\mathbf{R}^{\beta}_{(a)} & \mathbf{R}^{\alpha}_{(a)}\boldsymbol{Q}_{\alpha_{(a)}} & p\mathbf{G}^{-1}_{(a)}\mathbf{G}_{(b)}\mathbf{R}^{\beta}_{(b)} & \mathbf{G}^{-1}_{(a)}\mathbf{G}_{(b)}\mathbf{R}^{\alpha}_{(b)}\boldsymbol{Q}_{\alpha_{(b)}} \\ -\boldsymbol{\mathcal{L}}_{(a)} & -\boldsymbol{\mathcal{J}}_{(a)} & \mathbf{H}^{-1}_{(a)}\mathbf{H}_{(b)}\boldsymbol{\mathcal{L}}_{(b)} & -\mathbf{H}^{-1}_{(a)}\mathbf{H}_{(b)}\boldsymbol{\mathcal{J}}_{(b)} \\ 2p\mathbf{Z}^{\beta}_{(a)} & -\boldsymbol{\mathcal{S}}_{(a)} & 2p\mathbf{H}^{-1}_{(a)}\mathbf{H}_{(b)}\mathbf{Z}^{\beta}_{(b)} & \mathbf{H}^{-1}_{(a)}\mathbf{H}_{(b)}\boldsymbol{\mathcal{S}}_{(b)} \end{bmatrix} \begin{bmatrix} \mathrm{r}_{\mathrm{S_I S}} \\ \mathrm{r}_{\mathrm{S_I P}} \\ \mathrm{t}_{\mathrm{S_I S}} \\ \mathrm{t}_{\mathrm{S_I P}} \end{bmatrix} = \begin{bmatrix} \mathbf{R}^{\beta}_{(a)}\boldsymbol{Q}_{\beta_{(a)}}\mathbf{I}^{\mathrm{in}}_{\mathrm{S_I}} \\ p\mathbf{R}^{\beta}_{(a)}\mathbf{I}^{\mathrm{in}}_{\mathrm{S_I}} \\ \boldsymbol{\mathcal{L}}_{(a)}\mathbf{I}^{\mathrm{in}}_{\mathrm{S_I}} \\ 2p\mathbf{Z}^{\beta}_{(a)}\mathbf{I}^{\mathrm{in}}_{\mathrm{S_I}} \end{bmatrix}$$

where the terms for the block matrix representation (equation 80) are given by

$$\mathcal{A} = \begin{bmatrix} \mathbf{R}^{\beta}_{(a)}\boldsymbol{Q}_{\beta_{(a)}} & p\mathbf{R}^{\alpha}_{(a)} \\ -p\mathbf{R}^{\beta}_{(a)} & \mathbf{R}^{\alpha}_{(a)}\boldsymbol{Q}_{\alpha_{(a)}} \end{bmatrix} \tag{111}$$

$$\mathcal{B} = \begin{bmatrix} \mathbf{G}^{-1}_{(a)}\mathbf{G}_{(b)}\mathbf{R}^{\beta}_{(b)}\boldsymbol{Q}_{\beta_{(b)}} & -p\mathbf{G}^{-1}_{(a)}\mathbf{G}_{(b)}\mathbf{R}^{\alpha}_{(b)} \\ p\mathbf{G}^{-1}_{(a)}\mathbf{G}_{(b)}\mathbf{R}^{\beta}_{(b)} & \mathbf{G}^{-1}_{(a)}\mathbf{G}_{(b)}\mathbf{R}^{\alpha}_{(b)}\boldsymbol{Q}_{\alpha_{(b)}} \end{bmatrix} \tag{112}$$

$$\mathcal{C} = \begin{bmatrix} -\boldsymbol{\mathcal{L}}_{(a)} & -\boldsymbol{\mathcal{J}}_{(a)} \\ 2p\mathbf{Z}^{\beta}_{(a)} & -\boldsymbol{\mathcal{S}}_{(a)} \end{bmatrix} \tag{113}$$

$$\mathcal{D} = \begin{bmatrix} \mathbf{H}_{(a)}^{-1}\mathbf{H}_{(b)}\boldsymbol{\mathcal{L}}_{(b)} & -\mathbf{H}_{(a)}^{-1}\mathbf{H}_{(b)}\boldsymbol{\mathcal{J}}_{(b)} \\ 2p\mathbf{H}_{(a)}^{-1}\mathbf{H}_{(b)}\mathbf{Z}_{(b)}^{\beta} & \mathbf{H}_{(a)}^{-1}\mathbf{H}_{(b)}\boldsymbol{\mathcal{S}}_{(b)} \end{bmatrix} \tag{114}$$

(115)

$$\mathbf{p} = \begin{bmatrix} \mathbf{R}_{(a)}^{\beta}\boldsymbol{Q}_{\beta_{(a)}}\mathbf{I}_{\mathrm{S_I}}^{\mathrm{in}} \\ p\mathbf{R}_{(a)}^{\beta}\mathbf{I}_{\mathrm{S_I}}^{\mathrm{in}} \end{bmatrix} \tag{116}$$

$$\mathbf{q} = \begin{bmatrix} \boldsymbol{\mathcal{L}}_{(a)}\mathbf{I}_{\mathrm{S_I}}^{\mathrm{in}} \\ 2p\mathbf{Z}_{(a)}^{\beta}\mathbf{I}_{\mathrm{S_I}}^{\mathrm{in}} \end{bmatrix} \tag{117}$$

II.2.12 Reflection and transmission coefficients for potentials

For all four cases under considerations, the algebraic equations for reflection and transmission coefficients for potentials have the form stated in (80). In (80), by eliminating the transmission coefficients from equations, the reflection coefficients are obtained as below.

$$\begin{aligned} \mathcal{B}^{-1}\mathcal{A}\,\mathbf{r} + \mathbf{t} &= \mathcal{B}^{-1}\mathbf{p} \\ \mathcal{D}^{-1}\mathcal{C}\,\mathbf{r} + \mathbf{t} &= \mathcal{D}^{-1}\mathbf{q} \\ \mathbf{r} &= (\mathcal{B}^{-1}\mathcal{A} - \mathcal{D}^{-1}\mathcal{C})^{-1}(\mathcal{B}^{-1}\mathbf{p} - \mathcal{D}^{-1}\mathbf{q}) \end{aligned} \tag{118}$$

Likewise, the transmission coefficients are

$$\begin{aligned} \mathbf{r} + \mathcal{A}^{-1}\mathcal{B}\,\mathbf{t} &= \mathcal{A}^{-1}\mathbf{p} \\ \mathbf{r} + \mathcal{C}^{-1}\mathcal{D}\,\mathbf{t} &= \mathcal{C}^{-1}\mathbf{q} \\ \mathbf{t} &= (\mathcal{A}^{-1}\mathcal{B} - \mathcal{C}^{-1}\mathcal{D})^{-1}(\mathcal{A}^{-1}\mathbf{p} - \mathcal{C}^{-1}\mathbf{q}) \end{aligned} \tag{119}$$

The expressions (118) and (119) are used to compute the reflection and transmission coefficients.

II.2.13 Displacement potential

The analyzed solutions for the coefficient amplitudes described in the previous subsections are related to potential. In practice, we are interested in coefficient amplitudes related to displacement and velocity particle-motion . The displacement amplitudes are obtained when the particle displacements are measured with respect to the direction of the wave vector, they have the following expressions:

Table II. Displacement amplitude

Potential Amplitude	Displacement Amplitude
r_{wP_I}	$r_{wP_I}\frac{V_{P_I}}{V_w}$
$r_{wP_{II}}$	$r_{wP_{II}}\frac{V_{P_{II}}}{V_w}$
r_{wS_I}	$r_{wS_I}\frac{V_{S_I}}{V_w}$
$r_{wS_{II}}$	$r_{wS_{II}}\frac{V_{S_{II}}}{V_w}$
t_{wP_I}	$r_{wP_I}\frac{V_{P_I}}{V_w}$
$t_{wP_{II}}$	$r_{wP_{II}}\frac{V_{P_{II}}}{V_w}$
t_{wS_I}	$r_{wS_I}\frac{V_{S_I}}{V_w}$
$t_{wS_{II}}$	$r_{w\ S_{II}}\frac{VS_{II}}{V_w}$

where V stands for velocities and $w = P_I, P_{II}, S_I$ or S_{II}

II.2.14 Energy flux

Utilizing results of §II.2.4, for each mode, the associated expressions of velocities and stresses are listed below.

	Fast P	Slow P
	$\phi^{\mathrm{I}\pm}$	$\phi^{\mathrm{II}\pm}$
	$e^{i\omega(px\pm q_{\alpha_{\mathrm{I}}} z)}\phi_0^{\mathrm{I}}$	$e^{i\omega(px\pm q_{\alpha_{\mathrm{II}}} z)}\phi_0^{\mathrm{II}}$
$\mathbf{v}_x$	$\omega^2 p\ \mathbf{r}^{\alpha_{\mathrm{I}}}$	$\omega^2 p\ \mathbf{r}^{\alpha_{\mathrm{II}}}$
$\mathbf{v}_z$	$\pm\omega^2\ q_{\alpha_{\mathrm{I}}}\mathbf{r}^{\alpha_{\mathrm{I}}}$	$\pm\omega^2\ q_{\alpha_{\mathrm{II}}}\mathbf{r}^{\alpha_{\mathrm{II}}}$
$\boldsymbol{\tau}_{xx}$	$-\omega^2\boldsymbol{\Omega\rho}\left(\mathbf{I}-\boldsymbol{\beta\alpha}^{-1}-p^2\boldsymbol{\beta}\right)\mathbf{r}^{\alpha_{\mathrm{I}}}$	$-\omega^2\boldsymbol{\Omega\rho}\left(\mathbf{I}-\boldsymbol{\beta\alpha}^{-1}-p^2\boldsymbol{\beta}\right)\mathbf{r}^{\alpha_{\mathrm{II}}}$
$\boldsymbol{\tau}_{xz}$	$\mp 2\omega^2 p\ q_{\alpha_{\mathrm{I}}}\boldsymbol{\Omega\rho\beta}\ \mathbf{r}^{\alpha_{\mathrm{I}}}$	$\mp 2\omega^2 p\ q_{\alpha_{\mathrm{II}}}\boldsymbol{\Omega\rho\beta}\ \mathbf{r}^{\alpha_{\mathrm{II}}}$
$\boldsymbol{\tau}_{zz}$	$-\omega^2\boldsymbol{\Omega\rho}\left(\mathbf{I}-2p^2\boldsymbol{\beta}\right)\ \mathbf{r}^{\alpha_{\mathrm{I}}}$	$-\omega^2\boldsymbol{\Omega\rho}\left(\mathbf{I}-2p^2\boldsymbol{\beta}\right)\ \mathbf{r}^{\alpha_{\mathrm{II}}}$

	Fast S	Slow S
	$\psi^{\mathrm{I}\pm}$	$\psi^{\mathrm{II}\pm}$
	$e^{i\omega(px\pm q_{\beta_{\mathrm{I}}} z)}\psi_0^{\mathrm{I}}$	$e^{i\omega(px\pm q_{\beta_{\mathrm{II}}} z)}\psi_0^{\mathrm{II}}$
	$\mp\omega^2\ q_{\beta_{\mathrm{I}}}\mathbf{r}^{\beta_{\mathrm{I}}}$	$\mp\omega^2\ q_{\beta_{\mathrm{II}}}\mathbf{r}^{\beta_{\mathrm{II}}}$
	$\omega^2 p\ \mathbf{r}^{\beta_{\mathrm{I}}}$	$\omega^2 p\ \mathbf{r}^{\beta_{\mathrm{II}}}$
	$\pm 2\omega^2 p\beta_{\mathrm{I}}^2 q_{\beta_{\mathrm{I}}}\boldsymbol{\Omega\rho}\ \mathbf{r}^{\beta_{\mathrm{I}}}$	$\pm 2\omega^2 p\beta_{\mathrm{II}}^2 q_{\beta_{\mathrm{II}}}\boldsymbol{\Omega\rho}\ \mathbf{r}^{\beta_{\mathrm{II}}}$
	$\omega^2\boldsymbol{\Omega\rho}\left(\mathbf{I}-2p^2\boldsymbol{\beta}\right)\ \mathbf{r}^{\beta_{\mathrm{I}}}$	$\omega^2\boldsymbol{\Omega\rho}\left(\mathbf{I}-2p^2\boldsymbol{\beta}\right)\ \mathbf{r}^{\beta_{\mathrm{II}}}$
	$\mp 2\omega^2 p q_{\beta_{\mathrm{I}}}\boldsymbol{\Omega\rho\beta}\ \mathbf{r}^{\beta_{\mathrm{I}}}$	$\mp 2\omega^2 p q_{\beta_{\mathrm{II}}}\boldsymbol{\Omega\rho\beta}\ \mathbf{r}^{\beta_{\mathrm{II}}}$

For the energy flux associated with the center of mass field, we need the quantities that are associated with that field only. This can be achieved by applying the projection vector $\mathcal{P}^{\mathrm{T}} = (1 \;\; 0)$, from left, on the quantities listed above ($^{\mathrm{T}}$ stands for transposed). For a down-going fast P-wave, with slowness vector $\mathbf{S} = (p, q_{\alpha_I})$ and amplitude ϕ_0, they take the form

$$\begin{aligned}
\mathrm{v}_x^{\mathrm{m}} &= \omega^2 \, \Gamma_x^{\mathrm{m}} \, e^{i\omega(\mathbf{S}\cdot\mathbf{x}-t)} \, \phi_0, \\
\mathrm{v}_z^{\mathrm{m}} &= \omega^2 \, \Gamma_z^{\mathrm{m}} \, e^{i\omega(\mathbf{S}\cdot\mathbf{x}-t)} \, \phi_0, \\
\tau_{xx}^{\mathrm{m}} &= -\omega^2 \, \Lambda_{xx}^{\mathrm{m}} \, e^{i\omega(\mathbf{S}\cdot\mathbf{x}-t)} \, \phi_0, \\
\tau_{xz}^{\mathrm{m}} &= -\omega^2 \, \Lambda_{xz}^{\mathrm{m}} \, e^{i\omega(\mathbf{S}\cdot\mathbf{x}-t)} \, \phi_0, \\
\tau_{zz}^{\mathrm{m}} &= -\omega^2 \, \Lambda_{zz}^{\mathrm{m}} \, e^{i\omega(\mathbf{S}\cdot\mathbf{x}-t)} \, \phi_0.
\end{aligned} \tag{120}$$

In the above, for clarity, the following notations have been utilized

$$\begin{aligned}
\mathcal{P}^{\mathrm{T}} \;\; p \, \mathbf{r}^{\alpha_{\mathrm{I}}} &\equiv \Gamma_x^{\mathrm{m}}, \\
\mathcal{P}^{\mathrm{T}} \;\; q_{\alpha_{\mathrm{I}}} \mathbf{r}^{\alpha_{\mathrm{I}}} &\equiv \Gamma_z^{\mathrm{m}}, \\
\mathcal{P}^{\mathrm{T}} \;\; \boldsymbol{\Omega\rho}\left(\mathbf{I} - \boldsymbol{\beta\alpha^{-1}} - p^2\boldsymbol{\beta}\right) \mathbf{r}^{\alpha_{\mathrm{I}}} &\equiv \Lambda_{xx}^{\mathrm{m}}, \\
\mathcal{P}^{\mathrm{T}} \;\; 2p \, q_{\alpha_{\mathrm{I}}} \boldsymbol{\Omega\rho\beta} \, \mathbf{r}^{\alpha_{\mathrm{I}}} &\equiv \Lambda_{xz}^{\mathrm{m}}, \\
\mathcal{P}^{\mathrm{T}} \;\; \boldsymbol{\Omega\rho}\left(\mathbf{I} - 2p^2\boldsymbol{\beta}\right) \, \mathbf{r}^{\alpha_{\mathrm{I}}} &\equiv \Lambda_{zz}^{\mathrm{m}}.
\end{aligned} \tag{121}$$

The corresponding energy flux is

$$\begin{aligned}
J_k^{\mathrm{m}} &= -\Re\left(\tau_{jk}^{\mathrm{m}} \mathrm{v}_j^{\mathrm{m}}\right) \\
&= \frac{\omega^4}{4}\left(\Lambda_{jk}^{\mathrm{m}} e^{i\omega(\mathbf{S}\cdot\mathbf{x}-t)} \, \phi_0^{\mathrm{m}} + \Lambda_{jk}^{\mathrm{m}*} e^{-i\omega(\mathbf{S}^*\cdot\mathbf{x}-t)} \, \phi_0^{\mathrm{m}*}\right) \\
&\quad \left(\Gamma_k^{\mathrm{m}} e^{i\omega(\mathbf{S}\cdot\mathbf{x}-t)} \, \phi_0^{\mathrm{m}} + \Gamma_k^{*} e^{-i\omega(\mathbf{S}^*\cdot\mathbf{x}-t)} \, \phi_0^{\mathrm{m}*}\right).
\end{aligned} \tag{122}$$

The mean of the energy flux vector $\bar{J}_k$ is

$$\bar{J}_k = \frac{\omega}{2\pi}\int_0^{\frac{2\pi}{\omega}} J_k \mathrm{d}t, \tag{123}$$

which leads to

$$\bar{J}_k \;=\; \frac{\omega^4}{4}\phi_0^{\mathrm{m}}\phi_0^{\mathrm{m}*}\left(\Lambda_{jk}^{\mathrm{m}}\Gamma_k^{\mathrm{m}*}+\Lambda_{jk}^{\mathrm{m}*}\Gamma_k^{\mathrm{m}}\right)e^{i\omega(\mathbf{S}-\mathbf{S}^*)\cdot\mathbf{x}}. \tag{124}$$

For completeness, Γ^{m}'s and Λ^{m}'s associated with other wave fields are listed as follows.

	Up-going Fast P
	ϕ^{I^-}
Γ_x^{m}	$\mathcal{P}^{\mathrm{T}} \quad p\mathbf{r}^{\alpha_{\mathrm{II}}}$
Γ_z^{m}	$-\mathcal{P}^{\mathrm{T}} \quad q_{\alpha_{\mathrm{I}}}\mathbf{r}^{\alpha_{\mathrm{II}}}$
$\Lambda_{xx}^{\mathrm{m}}$	$-\mathcal{P}^{\mathrm{T}} \quad \boldsymbol{\Omega\rho}\left(\mathbf{I}-\boldsymbol{\beta\alpha}^{-\mathbf{1}}-p^2\boldsymbol{\beta}\right)\mathbf{r}^{\alpha_{\mathrm{II}}}$
$\Lambda_{xz}^{\mathrm{m}}$	$\mathcal{P}^{\mathrm{T}} \quad 2p\; q_{\alpha_{\mathrm{I}}}\boldsymbol{\Omega\rho\beta}\;\mathbf{r}^{\alpha_{\mathrm{II}}}$
$\Lambda_{zz}^{\mathrm{m}}$	$-\mathcal{P}^{\mathrm{T}} \quad \boldsymbol{\Omega\rho}\left(\mathbf{I}-2p^2\boldsymbol{\beta}\right)\;\mathbf{r}^{\alpha_{\mathrm{II}}}$

	Down-going Slow P	Up-going Slow P
	ϕ^{II^+}	ϕ^{II^-}
	$\mathcal{P}^{\mathrm{T}} \quad p\mathbf{r}^{\alpha_{\mathrm{II}}}$	$\mathcal{P}^{\mathrm{T}} \quad p\mathbf{r}^{\alpha_{\mathrm{II}}}$
	$\mathcal{P}^{\mathrm{T}} \quad q_{\alpha_{\mathrm{II}}}\mathbf{r}^{\alpha_{\mathrm{II}}}$	$-\mathcal{P}^{\mathrm{T}} \quad q_{\alpha_{\mathrm{II}}}\mathbf{r}^{\alpha_{\mathrm{II}}}$
	$-\mathcal{P}^{\mathrm{T}} \quad \boldsymbol{\Omega\rho}\left(\mathbf{I}-\boldsymbol{\beta\alpha}^{-\mathbf{1}}-p^2\boldsymbol{\beta}\right)\mathbf{r}^{\alpha_{\mathrm{II}}}$	$-\mathcal{P}^{\mathrm{T}} \quad \boldsymbol{\Omega\rho}\left(\mathbf{I}-\boldsymbol{\beta\alpha}^{-\mathbf{1}}-p^2\boldsymbol{\beta}\right)\mathbf{r}^{\alpha_{\mathrm{II}}}$
	$-\mathcal{P}^{\mathrm{T}} \quad 2p\; q_{\alpha_{\mathrm{II}}}\boldsymbol{\Omega\rho\beta}\;\mathbf{r}^{\alpha_{\mathrm{II}}}$	$\mathcal{P}^{\mathrm{T}} \quad 2p\; q_{\alpha_{\mathrm{II}}}\boldsymbol{\Omega\rho\beta}\;\mathbf{r}^{\alpha_{\mathrm{II}}}$
	$-\mathcal{P}^{\mathrm{T}} \quad \boldsymbol{\Omega\rho}\left(\mathbf{I}-2p^2\boldsymbol{\beta}\right)\;\mathbf{r}^{\alpha_{\mathrm{II}}}$	$-\mathcal{P}^{\mathrm{T}} \quad \boldsymbol{\Omega\rho}\left(\mathbf{I}-2p^2\boldsymbol{\beta}\right)\;\mathbf{r}^{\alpha_{\mathrm{II}}}$

	Down-going Fast S	Up-going Fast S
	ψ^{I^+}	ψ^{I^-}
Γ^{m}_{x}	$-\mathcal{P}^{\mathrm{T}}\ q_{\beta_{\mathrm{I}}}\mathbf{r}^{\beta_{\mathrm{I}}}$	$\mathcal{P}^{\mathrm{T}}\ q_{\beta_{\mathrm{I}}}\mathbf{r}^{\beta_{\mathrm{I}}}$
Γ^{m}_{z}	$\mathcal{P}^{\mathrm{T}}\ \ p\ \mathbf{r}^{\beta_{\mathrm{I}}}$	$\mathcal{P}^{\mathrm{T}}\ \ p\ \mathbf{r}^{\beta_{\mathrm{I}}}$
$\Lambda^{\mathrm{m}}_{xx}$	$\mathcal{P}^{\mathrm{T}}\ \ 2p\beta^2_{\mathrm{I}}q_{\beta_{\mathrm{I}}}\boldsymbol{\Omega\rho}\ \mathbf{r}^{\beta_{\mathrm{I}}}$	$-\mathcal{P}^{\mathrm{T}}\ \ 2p\beta^2_{\mathrm{I}}q_{\beta_{\mathrm{I}}}\boldsymbol{\Omega\rho}\ \mathbf{r}^{\beta_{\mathrm{I}}}$
$\Lambda^{\mathrm{m}}_{xz}$	$\mathcal{P}^{\mathrm{T}}\ \ \boldsymbol{\Omega\rho}\left(\mathbf{I}-2p^2\boldsymbol{\beta}\right)\ \mathbf{r}^{\beta_{\mathrm{I}}}$	$\mathcal{P}^{\mathrm{T}}\ \ \boldsymbol{\Omega\rho}\left(\mathbf{I}-2p^2\boldsymbol{\beta}\right)\ \mathbf{r}^{\beta_{\mathrm{I}}}$
$\Lambda^{\mathrm{m}}_{zz}$	$-\mathcal{P}^{\mathrm{T}}\ \ 2pq_{\beta_{\mathrm{I}}}\boldsymbol{\Omega\rho\beta}\ \mathbf{r}^{\beta_{\mathrm{I}}}$	$\mathcal{P}^{\mathrm{T}}\ \ 2pq_{\beta_{\mathrm{I}}}\boldsymbol{\Omega\rho\beta}\ \mathbf{r}^{\beta_{\mathrm{I}}}$
	Down-going Slow S	Up-going Slow S
	ψ^{II^+}	ψ^{II^-}
	$-\mathcal{P}^{\mathrm{T}}\ q_{\beta_{\mathrm{II}}}\mathbf{r}^{\beta_{\mathrm{II}}}$	$\mathcal{P}^{\mathrm{T}}\ q_{\beta_{\mathrm{II}}}\mathbf{r}^{\beta_{\mathrm{II}}}$
	$\mathcal{P}^{\mathrm{T}}\ \ p\ \mathbf{r}^{\beta_{\mathrm{II}}}$	$\mathcal{P}^{\mathrm{T}}\ \ p\ \mathbf{r}^{\beta_{\mathrm{II}}}$
	$\mathcal{P}^{\mathrm{T}}\ \ 2p\beta^2_{\mathrm{II}}q_{\beta_{\mathrm{II}}}\boldsymbol{\Omega\rho}\ \mathbf{r}^{\beta_{\mathrm{II}}}$	$-\mathcal{P}^{\mathrm{T}}\ \ 2p\beta^2_{\mathrm{II}}q_{\beta_{\mathrm{II}}}\boldsymbol{\Omega\rho}\ \mathbf{r}^{\beta_{\mathrm{II}}}$
	$\mathcal{P}^{\mathrm{T}}\ \ \boldsymbol{\Omega\rho}\left(\mathbf{I}-2p^2\boldsymbol{\beta}\right)\ \mathbf{r}^{\beta_{\mathrm{II}}}$	$\mathcal{P}^{\mathrm{T}}\ \ \boldsymbol{\Omega\rho}\left(\mathbf{I}-2p^2\boldsymbol{\beta}\right)\ \mathbf{r}^{\beta_{\mathrm{II}}}$
	$-\mathcal{P}^{\mathrm{T}}\ \ 2pq_{\beta_{\mathrm{II}}}\boldsymbol{\Omega\rho\beta}\ \mathbf{r}^{\beta_{\mathrm{II}}}$	$\mathcal{P}^{\mathrm{T}}\ \ 2pq_{\beta_{\mathrm{II}}}\boldsymbol{\Omega\rho\beta}\ \mathbf{r}^{\beta_{\mathrm{II}}}$

Chapter III

SOME NUMERICAL RESULTS

In this chapter, results of a set of numerical computations for reflection and transmission coefficients are reported. They highlight some of the implicit features of the DS09 and dCS09 boundary conditions.

For display purposes, the reflection and transmission coefficients are presented in terms of normal energy flux associated with the centre-of-mass and internal components of the wave fields. The preference for normal energy flux over displacement potential has been made for ease in presentation. The choice of the centre-of-mass component of the wave field is because it is the field that is recorded by the sensors. To show relative motion of fluid with respect to solid frame, normal energy flux of the internal component of the wave fields are also plotted.

To cover the entire frequency spectrum of interest in exploration seismology (see table I), the results are displayed for 1 Hz to 100 MHz band. The Biot critical frequency, which marks the transition from viscous coupling regime to inertial coupling regime, is indicated on the frequency axes as a red and blue triangles for top and bottom half-spaces, respectively.

Table III. Spectrum for seismic methods

Method	Frequency band
Surface-seismic	1 Hz -10^2 Hz
Tomography /VPS	10^2 Hz - 10^3 Hz
Well logging	10^3 Hz - 10^4 Hz
Ultrasonic (Laboratory)	10^5 Hz - 10^7 Hz

At first, I present an intriguing paradox about energy conservation exhibited by boundary conditions. Thereafter, I present the results that show that for a non-normal incidence the response of two boundary conditions are quite different, although, for normal incidence they show similar responses. Finally, I show the results of numerical experiment for angle-dependence.

III.1 Paradox on normal energy flux of the centre-of-mass component of the wave fields

I take the case of a porous frame whose top and bottom halves are saturated with oil and water, respectively. This is the case of two porous half-spaces with identical frame properties in perfect contact, i.e., porosities on both sides are same and pores of two sides are completely aligned at the interface. In the terminology of Deresiewicz and Skalak (1963) framework, it is the open pore case. The interface permeability for this case is to be taken as infinity. For computation purposes, I have assigned a value of $k_s = 10^{20}$. The frame and fluid properties are listed in Appendix A.

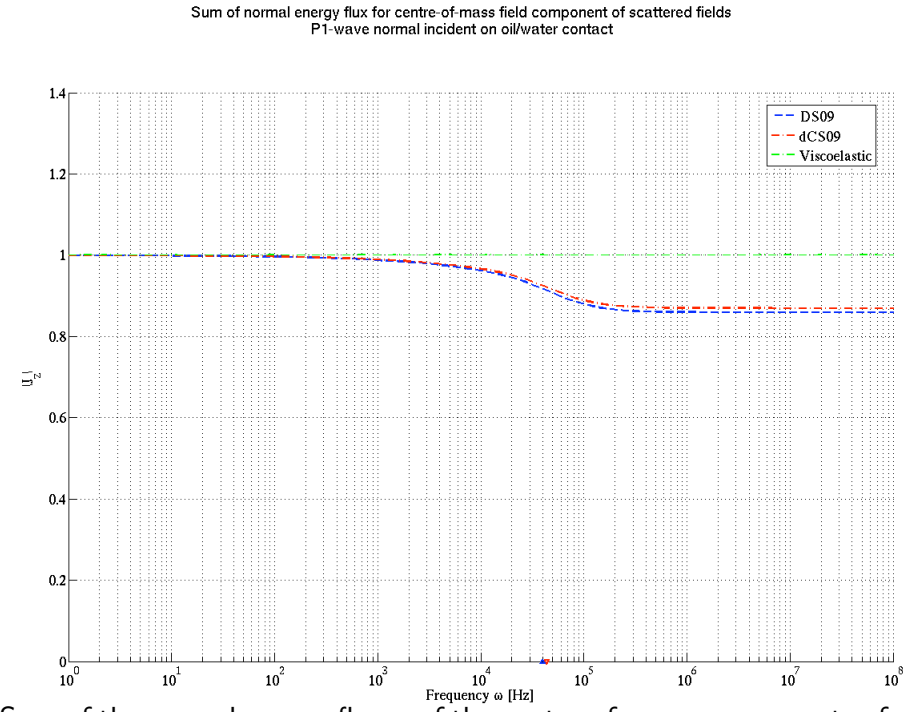

Figure 3. Sum of the normal energy fluxes of the centre-of-mass components of all scattered fields. The dashed blue line and dashed-dot red line correspond to the DS09 and dCS09 boundary conditions respectively. The values are scaled by the normal energy flux for the incident wave. The energy is conserved at low frequencies but not at high frequencies by both boundary conditions. The transition is around the Biot critical frequencies (plotted as red and blue triangles for top and bottom half-spaces respectively).

In figure 3, the sum of normal energy flux associated with the centre-of-mass component of all reflected and transmitted waves for a normal incident fast compressional wave is presented. For comparison purposes, the responses of the equivalent viscoelastic half-spaces in welded contact is also presented in dashed-dot green line. The properties of equivalent visco-elastic half-space were worked out according to the formulas presented in Appendix B.

The Figure 3 shows that, for both DS09 and dCS09 boundary conditions, the normal energy fluxes for all scattered fields added up to unity only in low frequency band. As one approaches the Biot critical frequencies, both curves start shooting down from the expected unity value. Ultimately, in the frequency band beyond the Biot critical frequencies, they stabilize to a constant value which is less than unity. However, the corresponding viscoelastic curve has always an unity value.

What has been displayed in the figure 3 is exactly what a sensor would track as seismic response. It seems paradoxical that the registered seismic responses in the seismic frequency band would be conservative, whereas in the ultrasonic band it would not be. If properties corresponding to a weak frame is taken, the Biot critical frequency may migrate to the lower frequency regime, and thus non conservation of energy may appear even in regular seismic data.

A validity check

In order to test the validity of the code, in the above example, I replaced the saturating fluid oil in the upper half-space by water. Thus, in a real sense, there is no a longer physical boundary.

For both DS09 and dCS09 boundary conditions, the incident fast compressional wave is expected to appear entirely as transmitted compressional P-wave, without suffering any conversions to other kind of wave fields. Figure 4 precisely shows that.

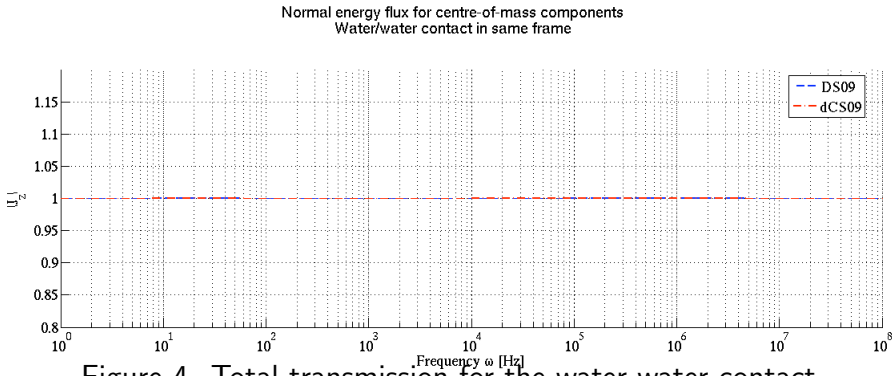

Figure 4. Total transmission for the water water contact.

In view of the above, the paradox on normal energy flux of the centre-of-mass component of the field is not a numerical error of the code; if the poroelastic framework is true, then one is expected to observe such a paradox in the register seismic data.

In Figure 5 the normal components of total energy flux, centre-of-mass part of energy flux, and internal part of energy flux, sum over all reflected and transmitted wave fields are plotted for both, DS09 and dCS09, boundary conditions. It shows that, indeed internal part of energy is involve in the total balance of energy. The right bottom panel of the Figure 7 clearly shows that the deficit in the energy flux of the centre-of-mass component is correlated to the increment of the energy flux of the internal part of the transmitted slow compressional wave. The energy flux for centre-of-mass part that are undershooting from the unity. Upon including the internal part contributions,

the deficit is wiped out. In fact, the total energy curve are slightly overshooting over the unity. This overshoot may be numerical because of the use of homogeneous plane wave decomposition in this work. The internal field part is highly attenuating, so for properly accounting it one may have to use in-homogeneous plane wave decomposition.

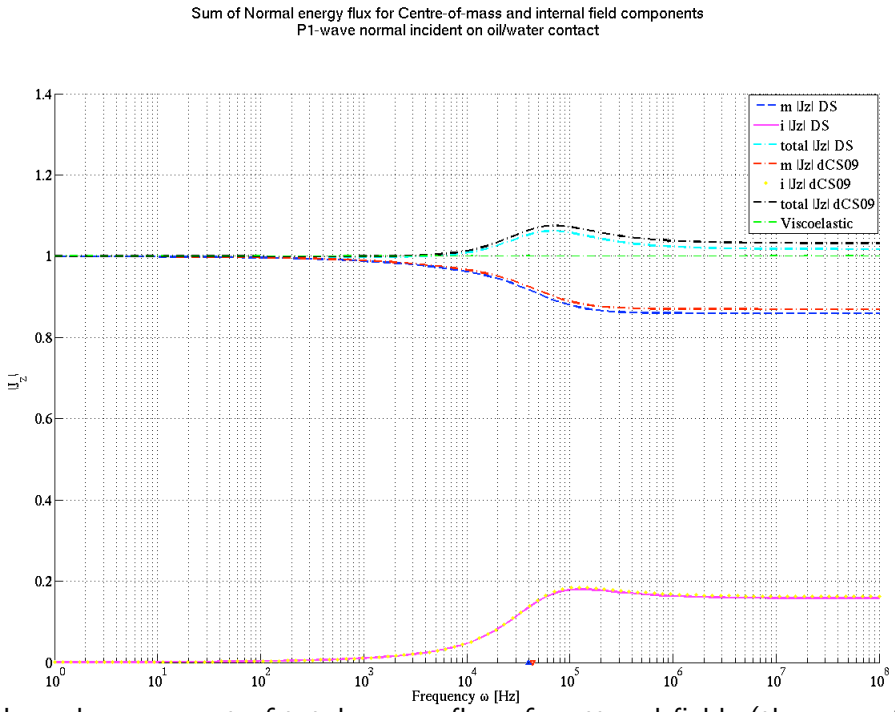

Figure 5. Normal component of total energy flux of scattered fields (the sum of centre-of-mass and internal fluxes all reflected and transmitted waves) as the function of frequency showing how Deresiewicz and Skalak (1963), and de la Cruz and Spanos (1989) boundary conditions stand up to the principle of energy conservation. The centre-of-mass, internal component and total energy fluxes corresponding to DS09 are plotted as dashed blue line, dotted magenta line and dashdot green line, respectively. The centre-of-mass, internal component and total energy flux corresponding to dCS09 are plotted as dashdot red line, dotted yellow line and dashdot black line, respectively. The equivalent visco-elastic case is in dashdot green line.

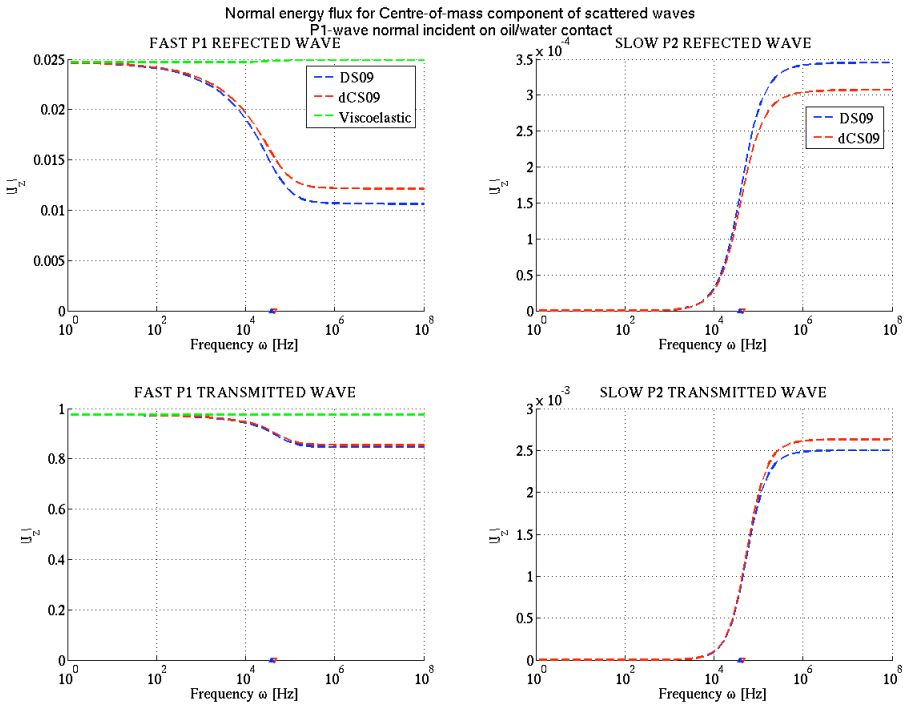

Figure 6. Normal component of the centre-of-mass part of the energy fluxes for scattered fields. Top and bottom panels on left-hand side correspond to the reflected and transmitted fast P-wave, while the top and bottom right-hand side panels correspond to the reflected and transmitted slow P-wave. It should be observed that as the energy fluxes of slow-wave processes are increasing, the energy fluxes in the fast-waves are decreasing as function of frequency.

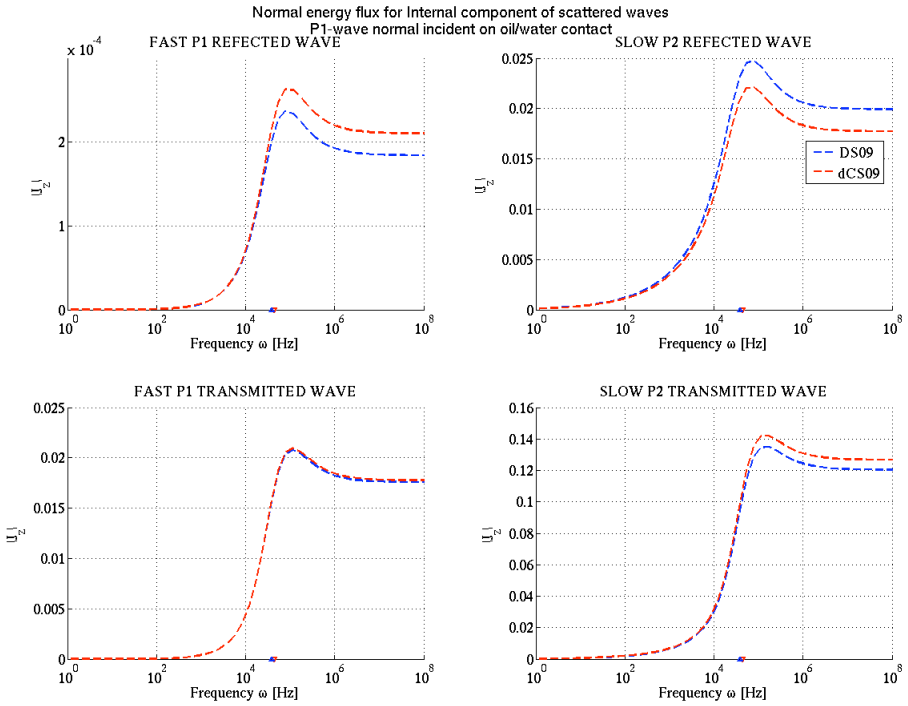

Figure 7. Normal component of the internal parts of the energy fluxes for scattered fields. Top and bottom panels on left-hand side correspond to the reflected and transmitted fast P-wave, while the top and bottom right-hand side panels correspond to the reflected and transmitted slow P-wave. It should be observed that as the energy in the centre-of-mass part of fast waves (Figure 6, left hand-side panels) is decreasing as function of frequency, the internal energy part of slow-wave processes is increasing (right hand-side panels of this figure).

III.1.1 Normal incident fast shear wave

Commonly it is belived that a shear wave is not affected by fluids. So if the solid-frames of the two sides of the interface are the same, no boundary is expected for S-waves, no matter what are the saturating fluids. In our set-up frame properties on the two sides are the same, therefore a complete transmission is expected.

For the fast-wave plotted in the figure 8, the DS09 shows the expected results. The dCS09 framework predicts a strong reflection according a less transmission in low frequency regime. However, at high frequencies, the effect of fluid disappears, such as observed in the below figure.

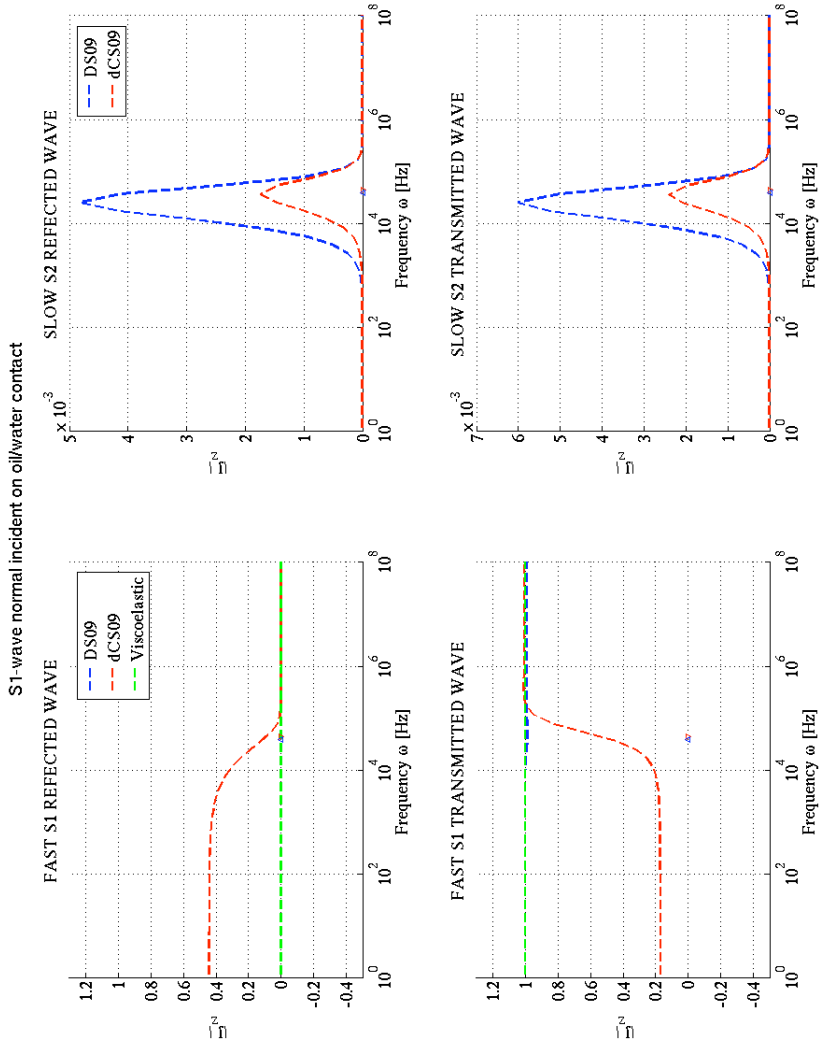

Figure 8. Energy flux for scattered S-wave.

III.2 Non-normal incidence case

In this subsection I report results about non-normal incidence fast waves. For demostration purposes, I take the incident angle to be $\theta = 20$. The set up of porous half-spaces is the same as previous section.

III.2.1 Incident fast compressional wave

The two left-hand panels in the top of Figure 9 show that for low frequencies the dCS09 has weaker transmission and stronger reflection compared to DS09, and DS09 response is akin to the equivalent visco-elastic case. For high frequencies the DS09 and dCS09 response tends to be similar and below the visco-elastic curve. The two left-hand panels in the bottom show the presence of converted shear waves for the dCS09 whereas for DS09 they are not present.

III.2.2 Incident fast shear wave

For the case of an inicident fast shear wave at non-normal incidence, the dCS09 plotted in figure 10, shows a similar behavior as the normal incidence case in the subsection III.2.1.

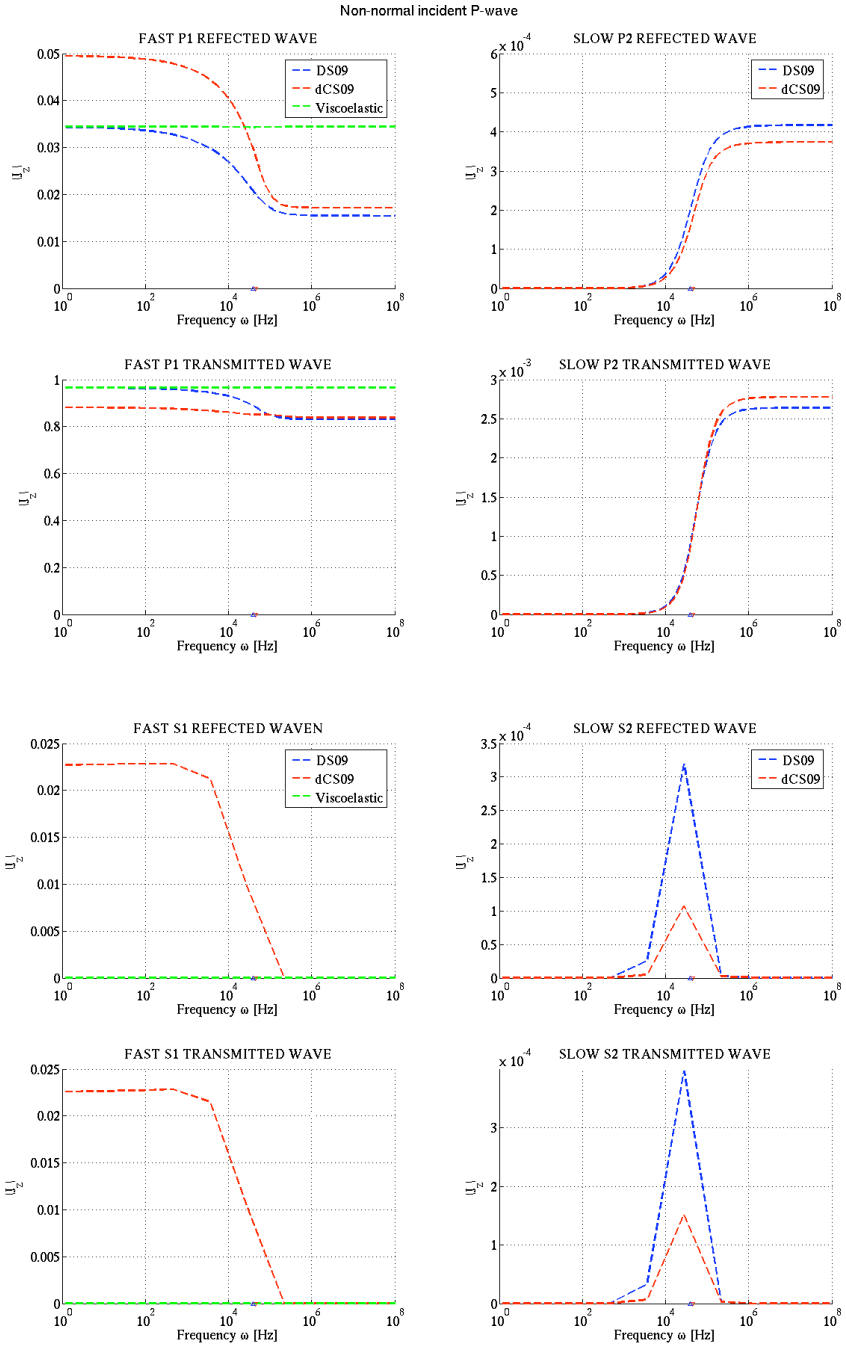

Figure 9. In the four top panels, the energy flux corresponding to the centre-of-mass component for scattered P-wave, while in the four bottom panels the energy flux corresponding to the centre-of-mass component for an incident to scattered S-wave are shown.

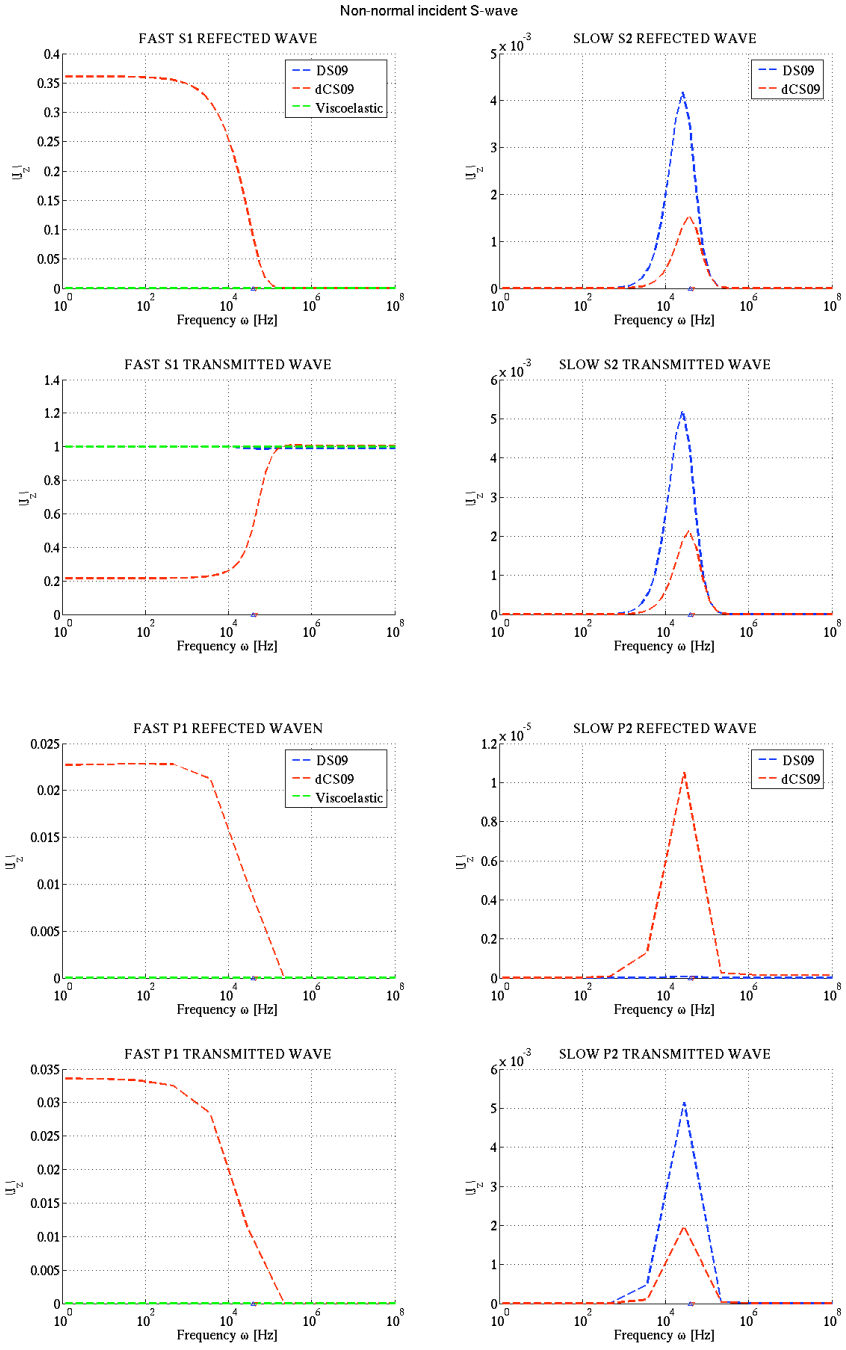

Figure 10. In the top four panels the energy flux corresponding to the centre-of-mass component for scattered S-wave are presented, while in the bottom four panels the energy flux corresponding to the centre-of-mass component for scattered P-wave are shown.

Likewise, the converted fast P-wave in the two left-hand side panels in the bottom of Figure 10 predicts conversions of energy from S-waves into P-waves for dCS09 case. The results for DS09 (and visco-elastic framework) show no conversion.

III.2.3 Amplitude analysis angle-dependence

A new methodology to determine physical properties of media at low frequencies is called AVO (Amplitude vs Offset), or more properly AVA (Amplitude vs Angle of incidence). It is a method that uses the pre-stack data to detect the presence of hydrocarbons in the resorvoir. Forward modeling of AVA is the best way to validate data and interpret results.

This subsection introduce an analysis of the displacement amplitude for an incident fast P-wave with respect to angle of incidence for a given frequency. For comparison, the previous case of the oil/water contact is analyzed. At first, I fixed the frequency at 20 Hz (see Figures 11 through 14) which is a regular seismic frequency employed in exploration. In here, it can be observed that the DS09 and the visco-elastic case tends to be similar, such as observed in previous example. At second, I fixed the frequency at 500 KHz (see Figures 15 through 18) which is a frequency used in laboratory studies. This results are comparable with the high frequencies regime in Figure 7, where the DS09 and dCS09 curve tends to be similar and they are different with respect to the visco-elastic case.

The left-hand sides plots in the next figures correspond to the displacement amplitude, while the right-hand side plots are its corresponding phases.

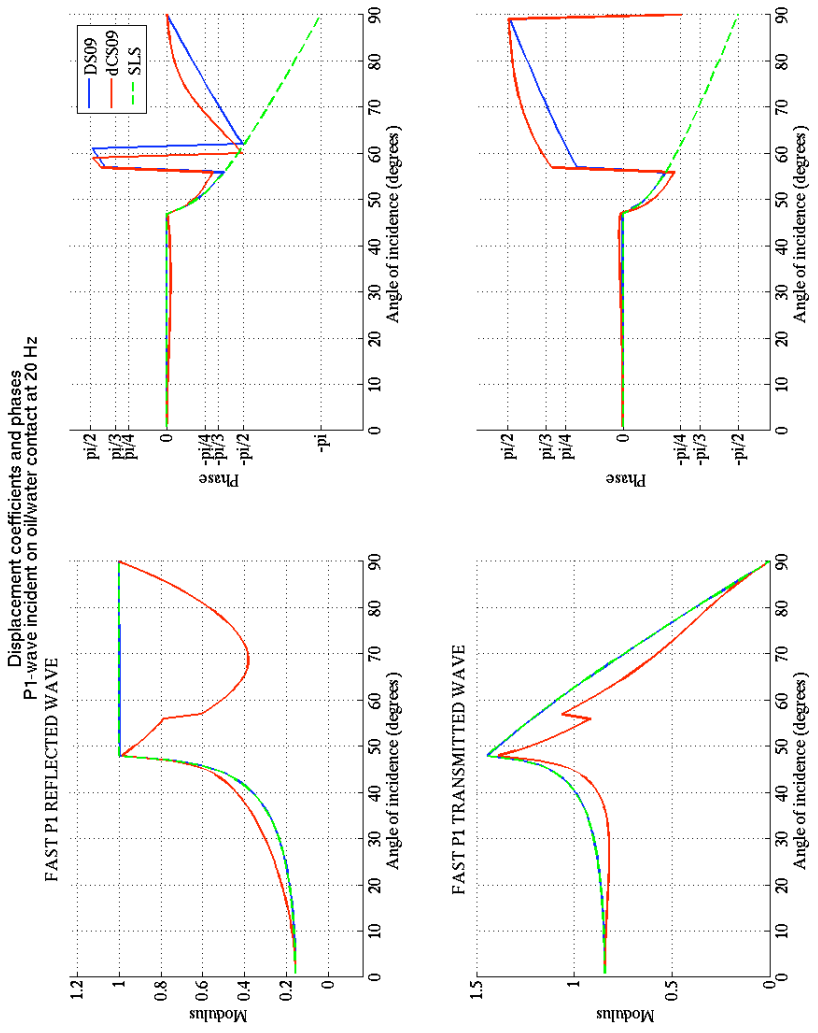

Figure 11. Displacement amplitude and phases for scattered fast P-wave at 20 Hz.

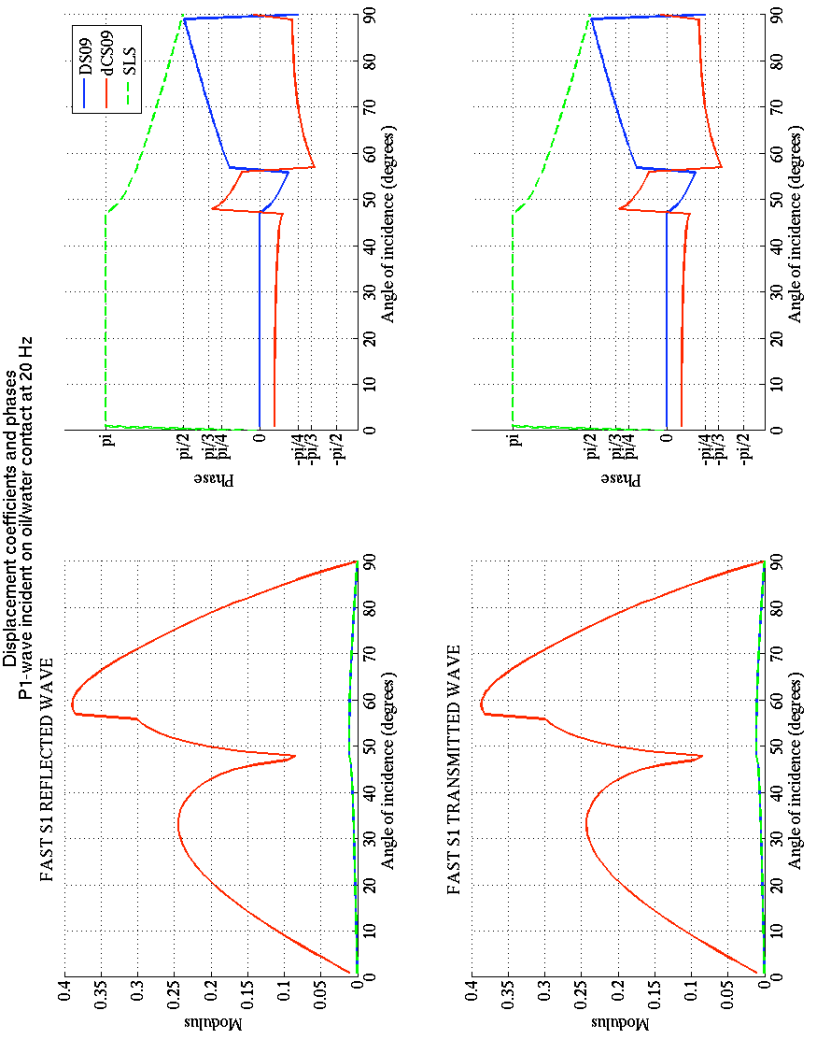

Figure 12. Displacement amplitude and phases for scattered fast S-wave at 20 Hz.

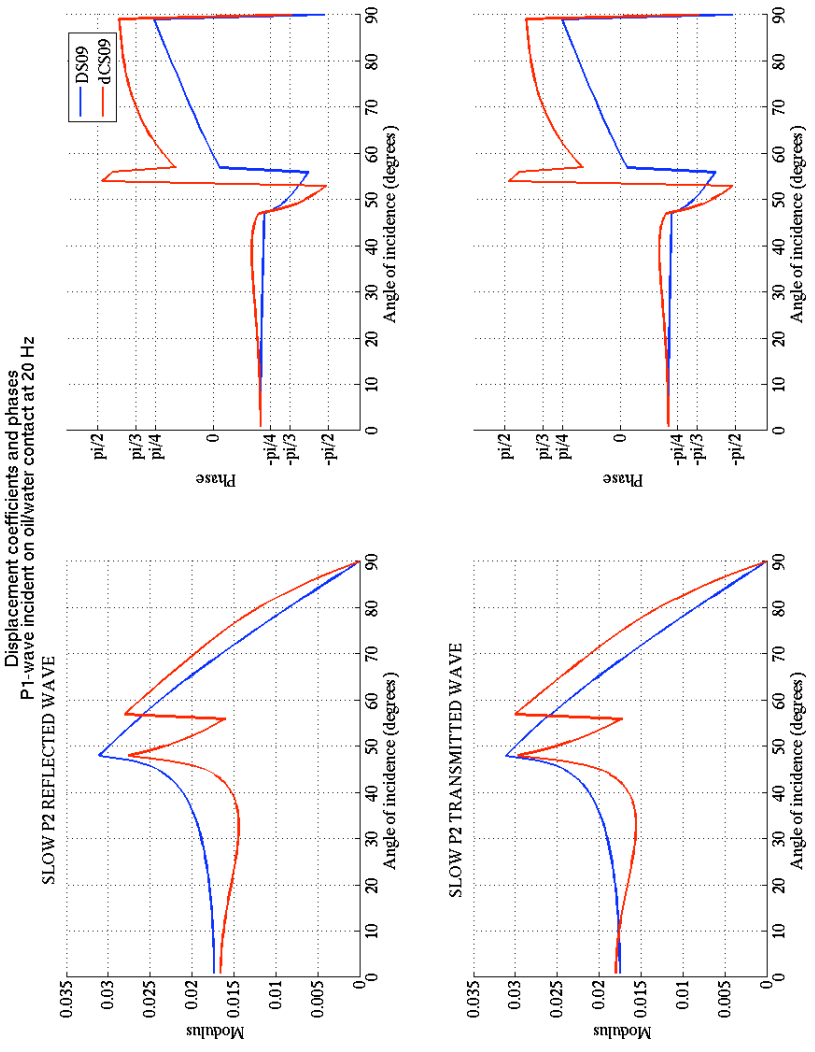

Figure 13. Displacement amplitude and phases for scattered slow P-wave at 20 Hz.

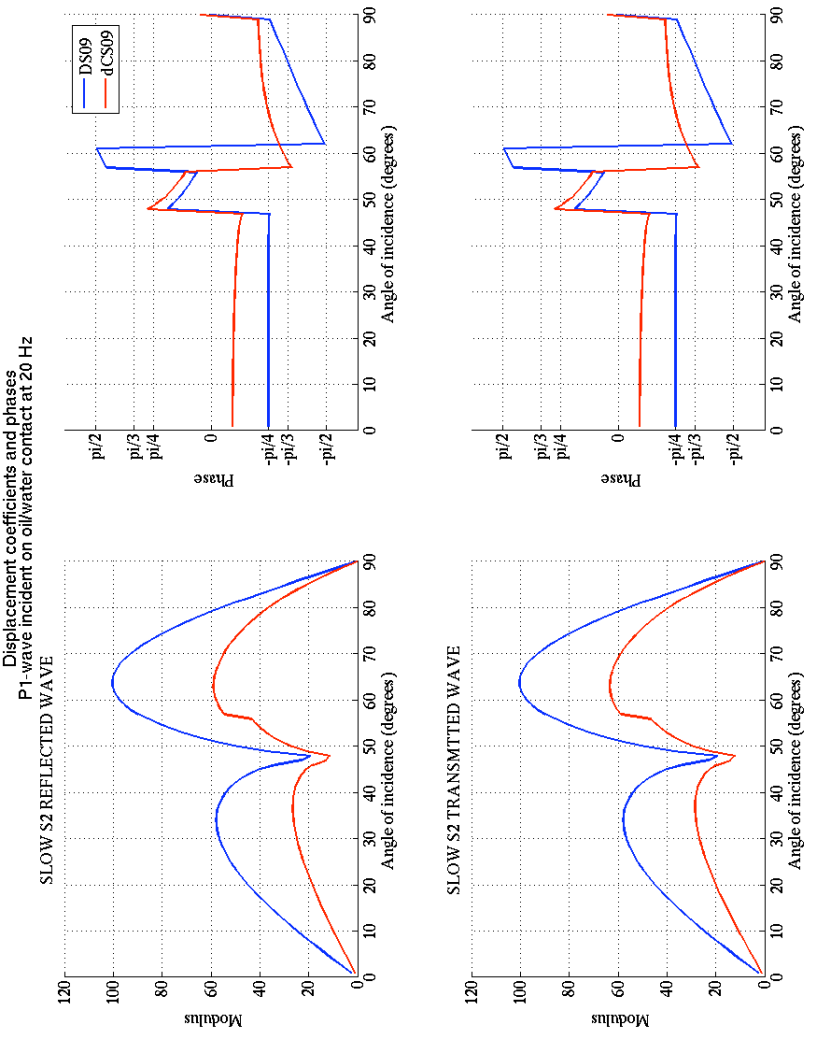

Figure 14. Displacement amplitude and phases for scattered slow S-wave at 20 Hz.

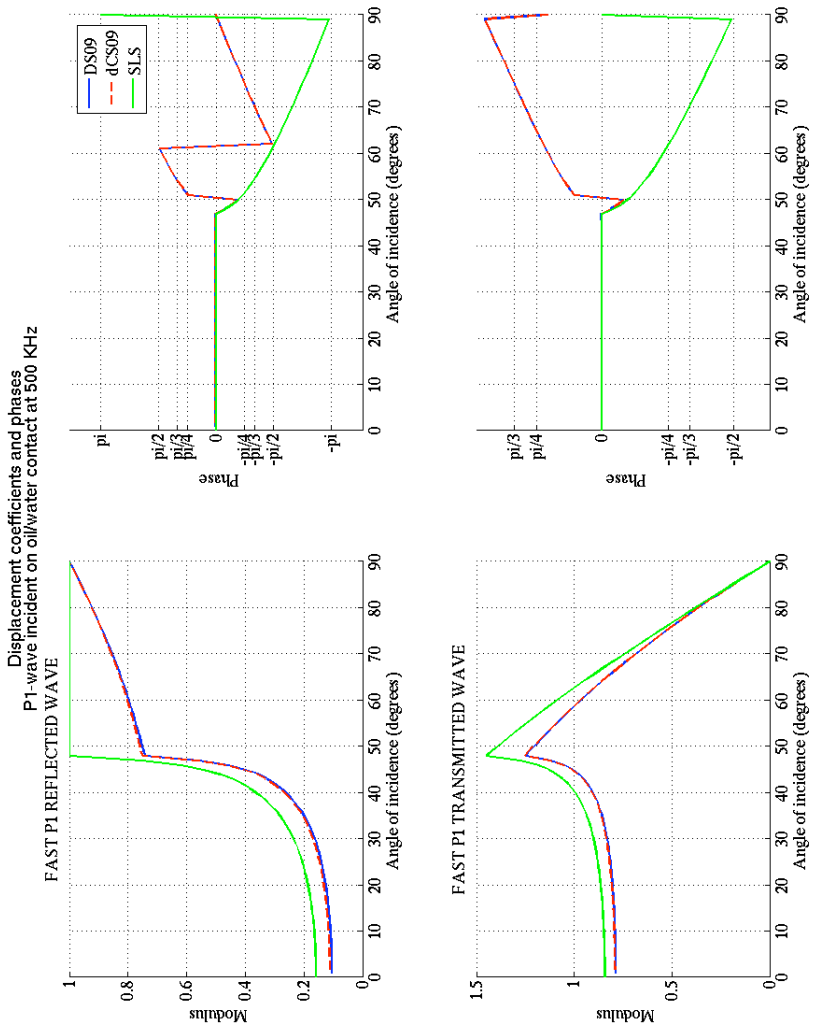

Figure 15. Displacement amplitude and phases for scattered fast P-wave at 500 K Hz.

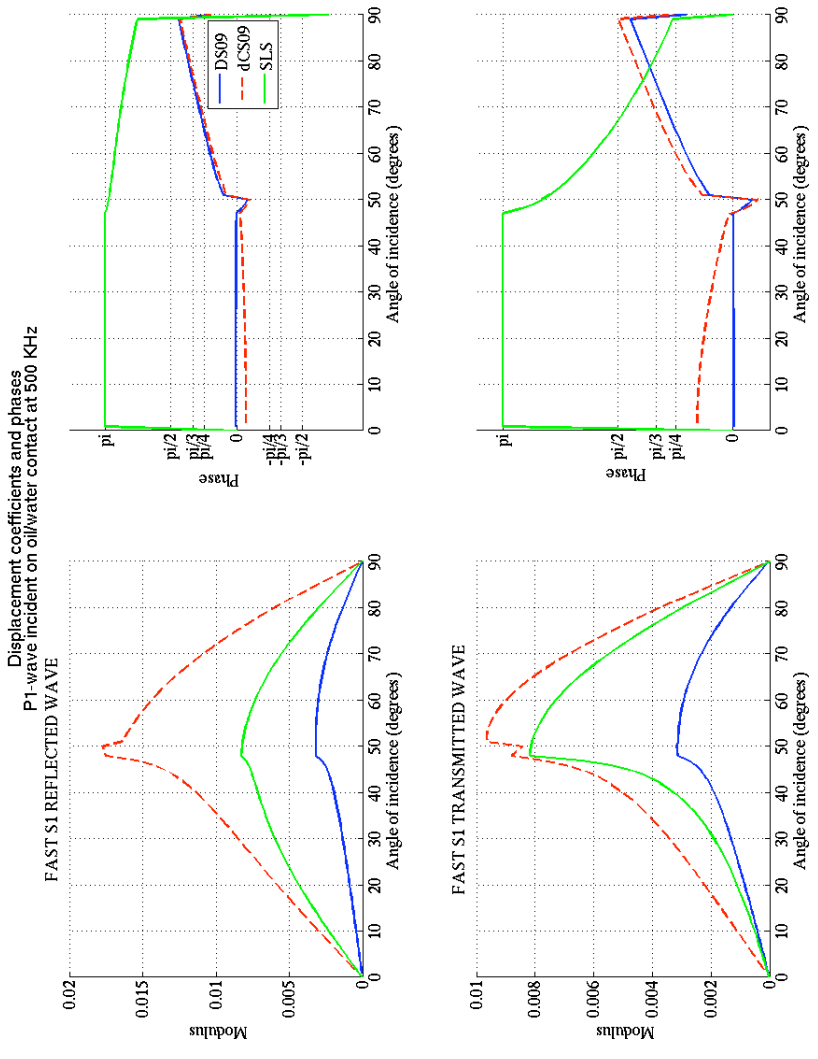

Figure 16. Displacement amplitude and phases for scattered fast S-wave at 500 K Hz.

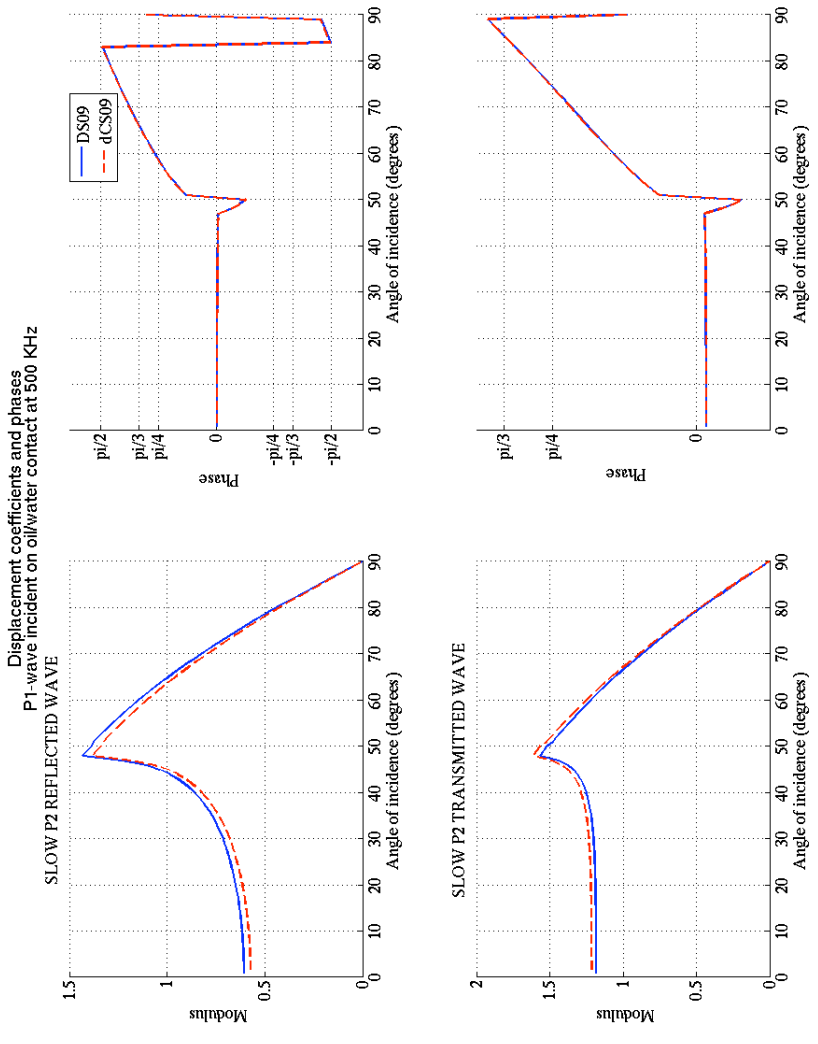

Figure 17. Displacement amplitude and phases for scattered slow P-wave at 500 K Hz.

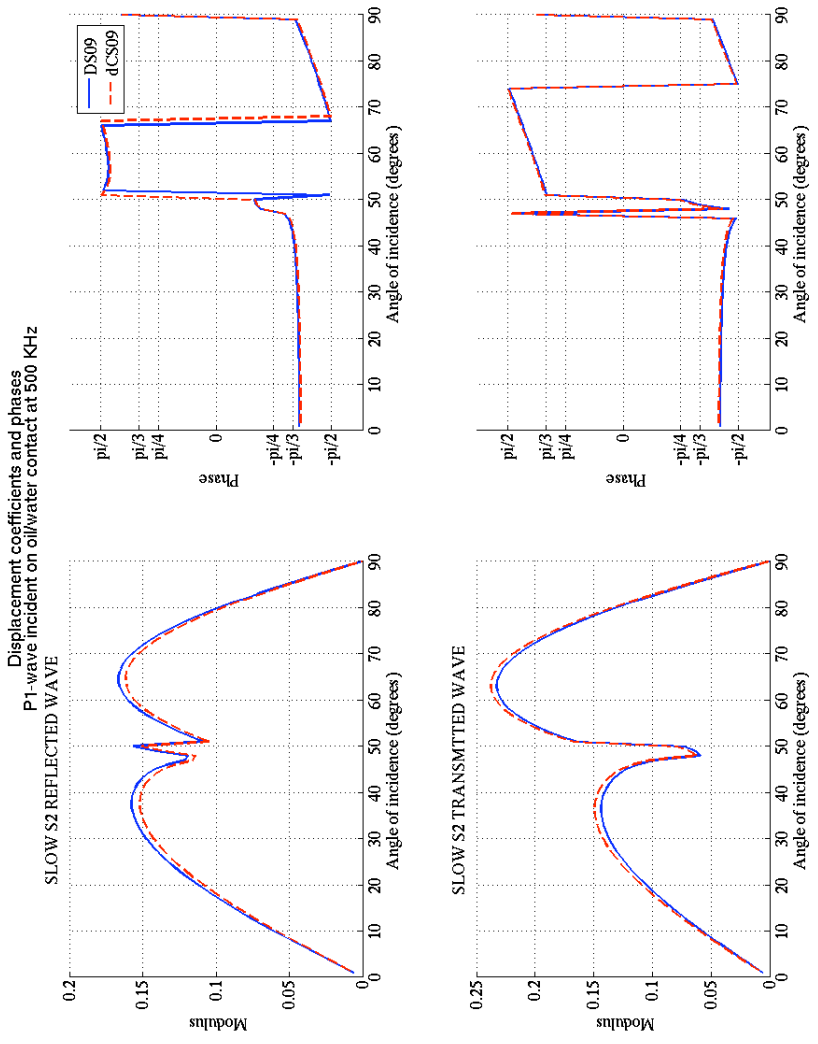

Figure 18. Displacement amplitude and phases for scattered slow S-wave at 500 K Hz.

Chapter IV

CONCLUSIONS

In this chapter, I shall summarize the main accomplishments of this work and present recommendations for future works.

Based upon the analytical solutions and numerical computations for reflection and transmission boundary value problems associated with incident fast compressional and shear plane waves for (a) modified Deresiewicz and Skalak (1963) boundary conditions (DS09) and (b) modified de la Cruz and Spanos (1989) boundary conditions (dCS09) that I have carried out in the preceding chapters, I conclude the following:

I. In the low frequency regime (defined by the Biot critical frequencies of the two media), a loss is observed for the sum of energy flux for centre-of-mass components, no matter which boundary conditions is chosen. However, when the energy of the internal components is also taken into the account, the total energy flux is conserved for all frequencies. In spite of that there is energy conservation one is likely to observe an apparent loss in real data, since a sensor tracks only the centre-of-mass field.

II. For normal incident fast compressional wave, the reflection and transmission coefficients for both boundary conditions are similar. In the low frequency regime, they are akin to those for the equivalent visco-elastic framework. In the high frequency regime, they are below the response of the equivalent visco-elastic framework.

III. For a fast P incident wave at non-normal incidence at low frequencies, the DS09 is closely similar to the visco-elastic case, while the dCS09 framework shows the strong reflection. For high frequencies, the reflection coefficients with DS09 and dCS09 tend to be similar, but these are less than in the visco-elastic case.

IV. In the case for normal as well as non-normal incident fast S-wave, there are distinct differences between the two sets of boundary conditions. In low frequency band, dCS09 predicts a strong reflection for a fast shear wave incident upon a fluid/fluid contact in a porous medium, whereas DS09 shows no such sensitivity. Although, in high frequency band both show similar responses.

I make the following recommendations for future works:

- The block matrix method that I have utilized may present numerical instability in the computation due to singular matrix inversions. For such cases, a different approach may be utilized to improve the results. Also, inhomogeneous plane wave decomposition may be employed.

- In order to compare the theory, I recommend carrying out calculations of reflection and transmission coefficients as well as energy flux with the original field variables, i.e., fluid and solid displacement fields.

- The numerical simulator that I have developed can compute reflection and transmission coefficients at any frequency for any angle of incidence. This may be utilized to design a variety of laboratory experiments to run validity check on the results of the two sets of boundary conditions.

References

Aki, K. y Richard, P. (2002). *Quantitative Seismology*. University Science Books.

Biot, M. A. (1955). Theory of propagation of elastic waves in a fluid-saturated porous solid i. low-frequency range. *JASA*, **28**(2): 168–178.

Biot, M. A. (1962). Mechanics of deformation and acustic propagation in porous media. *J. Appl. Phys.*, **33**(1482).

de la Cruz, V. y Spanos, T. (1989). Seismic boundary conditions for porous media. *JGR*, **94**: 3025–3029.

de la Cruz, V. y Spanos, T. (1992). Reflection and transmission of seismic waves at the boundaries of porous media. *Wave Motion*, **94**(16): 323–328.

Deresiewicz, H. y Skalak, R. (1963). On uniqueness in dynamic poroelasticity. *BSSA*, **53**(783).

Dutta, N. y Odé, H. (1983). Seismic reflections for a gas-water contact. *Geophysics*, **48**(148).

Mavko, G. Mukerji T. y Dvorkin, J. (2009). *The Rock Physics Handbook*. Cambridge University Press.

Sahay, P. (1995). Nature of waves in deformable porous media. *SPIE Proceedings: Mathematical Methods in Geophysical Imaging III*, **2571**: 247–255.

Sahay, P. (1996). Elastodynamics of deformable porous media. *Proc. R. Soc. Lond. A*, **452**(1950): 1517–1529.

Sahay, P. (2001). Dynamic greenś function for homogeneous and isotropic porous media. *Geophysical J. Int.*, **147**: 622–629.

Sahay, P. (2008). On the biot slow s-wave. *Geophysics*, **73**(19): 19–33.

Sahay, P. (2009). Personal communications.

Appendix A

SYMBOLS

Table IV. Biot theory field quantities

$\hat{\mathbf{e}}_j$		unit vector in jth direction
$\mathbf{u}^{\mathrm{s}}$	$= \hat{\mathbf{e}}_j \mathrm{u}^{\mathrm{s}}_j$	averaged displacement field vector of solid-frame
$\mathrm{u}^{\mathrm{s}}_{jk}$	$= \frac{1}{2}(\mathrm{u}^{\mathrm{s}}_{j,k} + \mathrm{u}^{\mathrm{s}}_{k,j})$	solid-frame strain tensor
$\breve{\mathrm{u}}^{\mathrm{s}}_{jk}$	$= \mathrm{u}^{\mathrm{s}}_{jk} - \frac{1}{3}\mathrm{u}^{\mathrm{s}}_{ll}\delta_{jk}$	trace-free part of solid-frame strain tensor
$\mathbf{u}^{\mathrm{f}}$	$= \hat{\mathbf{e}}_j \mathrm{u}^{\mathrm{f}}_j$	averaged displacement field vector of fluid
$\mathrm{v}^{\mathrm{f}}_{jk}$	$= \partial_t \mathrm{u}^{\mathrm{f}}_{jk} = \frac{1}{2}(\partial_t \mathrm{u}^{\mathrm{f}}_{j,k} + \partial_t \mathrm{u}^{\mathrm{f}}_{k,j})$	fluid (macroscopic) strain-rate tensor
$\breve{\mathrm{v}}^{\mathrm{f}}_{jk}$	$= \mathrm{v}^{\mathrm{s}}_{jk} - \frac{1}{3}\mathrm{v}^{\mathrm{s}}_{ll}\delta_{jk}$	trace-free part of macroscopic fluid strain-rate tensor
ζ	$= -\eta_0(\mathrm{u}^{\mathrm{f}}_{jj} - \mathrm{u}^{\mathrm{s}}_{jj})$	increase of fluid content
τ^{s}_{jk}		macroscopic solid stress tensor
τ^{f}_{jk}		macroscopic fluid stress tensor
p^{f}	$= -\frac{1}{3\eta_0}\tau^{\mathrm{f}}_{jj}$	macroscopic fluid pressure

Table V. Dynamical field quantities

$\mathrm{u}^{\mathrm{m}}_{j}$	$= \mathrm{m}^{\mathrm{s}}\mathrm{u}^{\mathrm{s}}_{j} + \mathrm{m}^{\mathrm{f}}\mathrm{u}^{\mathrm{f}}_{j}$	center-of-mass displ. field
$\mathrm{u}^{\mathrm{i}}_{j}$	$= \mathrm{u}^{\mathrm{s}}_{j} - \mathrm{u}^{\mathrm{f}}_{j}$	internal displacement field
$\mathrm{u}^{\mathrm{m}}_{jk}$	$= \mathrm{m}^{\mathrm{s}}\mathrm{u}^{\mathrm{s}}_{jk} + \mathrm{m}^{\mathrm{f}}\mathrm{u}^{\mathrm{f}}_{jk}$	centre-of-mass strain tensor
$\mathrm{u}^{\mathrm{i}}_{jk}$	$= \mathrm{u}^{\mathrm{s}}_{jk} - \mathrm{u}^{\mathrm{f}}_{jk}$	internal strain tensor
$\breve{\mathrm{u}}^{\mathrm{m}}_{jk}$	$= \mathrm{u}^{\mathrm{m}}_{jk} - \frac{1}{3}\mathrm{u}^{\mathrm{m}}_{ll}\delta_{jk}$	trace-free part of centre-of-mass strain tensor
$\breve{\mathrm{u}}^{\mathrm{i}}_{jk}$	$= \bar{\mathrm{u}}^{\mathrm{m}}_{jk} - \frac{1}{3}\bar{\mathrm{u}}^{\mathrm{m}}_{ll}\delta_{jk}$	trace-free part of internal strain tensor
τ^{m}_{jk}	$= \tau^{\mathrm{s}}_{jk} + \tau^{\mathrm{f}}_{jk}$	total stress tensor of porous medium
τ^{i}_{jk}	$= \mathrm{m}^{\mathrm{f}}\tau^{\mathrm{s}}_{jk} - \mathrm{m}^{\mathrm{s}}\tau^{\mathrm{f}}_{jk}$	internal stress tensor of porous medium
$\mathbf{u}_{j}$	$= (\mathrm{u}^{\mathrm{m}}_{j} \;\; \mathrm{u}^{\mathrm{i}}_{j})^{\mathrm{T}}$	
$\mathbf{u}_{jk}$	$= (\mathrm{u}^{\mathrm{m}}_{jk} \;\; \mathrm{u}^{\mathrm{i}}_{jk})^{\mathrm{T}}$	
$\boldsymbol{\tau}_{jk}$	$= (\tau^{\mathrm{m}}_{jk} \;\; \tau^{\mathrm{i}}_{jk})^{\mathrm{T}}$	

Table VI. Microscopic parameters

ρ_{s}	$=$	solid unperturbed density
ρ_{f}	$=$	pore fluid unperturbed density
K_{s}	$=$	solid-mineral bulk modulus
μ_{s}	$=$	solid-mineral shear modulus
K_{f}	$=$	pore fluid bulk modulus
ξ_{f}	$=$	pore fluid bulk viscosity
μ_{f}	$=$	pore fluid shear viscosity

Table VII. Macroscopic parameters

K_0		dry solid-frame bulk modulus
μ_0		dry solid-frame shear modulus
η_0		unperturbed porosity
ϕ_0	$= 1 - \eta_0$	unperturbed volume fraction of solid
κ		permeability
S		tortuosity factor

Table VIII. Derived parameters

$\alpha_{_K}$	$= 1 - \frac{K_0}{K_\mathrm{s}}$	Biot bulk coefficient
M	$= (\frac{\eta_0}{K_\mathrm{f}} + \frac{\alpha_{_K} - \eta_0}{K_\mathrm{s}})^{-1}$	fluid storage coefficient
α_μ	$= 1 - \frac{\mu^0}{\mu^\mathrm{s}}$	Biot shear coefficient
ρ_m	$= \phi_{_0}\rho_\mathrm{s} + \eta_{_0}\rho_\mathrm{f}$	total density
ρ_r	$= (1/\phi_{_0}\rho_\mathrm{s} + 1/\eta_{_0}\rho_\mathrm{f})^{-1}$	reduced density
ρ_{12}	$= -(S-1)\eta_0\rho_\mathrm{f}$	induced mass-coefficient
ρ_i	$= \rho_\mathrm{r} - \rho_{12} = (S - m_\mathrm{f})\eta_{_0}\rho_\mathrm{f}$	modified reduced density
m_s	$= \phi_{_0}\rho_\mathrm{s}/\rho_\mathrm{m}$	solid mass fraction
m_f	$= \eta_{_0}\rho_\mathrm{f}/\rho_\mathrm{m}$	fluid mass fraction
d_s	$= \phi_{_0}\rho_\mathrm{s}/\rho_\mathrm{i} = \frac{m_\mathrm{s}}{m_\mathrm{f}}\frac{1}{S - m_\mathrm{f}}$	
d_f	$= \eta_{_0}\rho_\mathrm{f}/\rho_\mathrm{i} = \frac{1}{S - m_\mathrm{f}}$	
ν_f	$= \mu_\mathrm{f}/\rho_\mathrm{f}$	fluid kinematic shear viscosity
H_0	$= K_0 + \frac{4}{3}\mu_0$	dry-frame P-wave elastic modulus
H_c	$= K_0 + \frac{4}{3}\mu_0 + \alpha_{_K}^2 M$	Gassmann P-wave elastic modulus
Ω_b	$= \eta_{_0}\nu_\mathrm{f}/\kappa$	Biot critical frequency
Ω_i	$= d_\mathrm{f}\Omega_\mathrm{b}$	Biot relaxation frequency
Ω_fP	$= K_\mathrm{f}/(\xi_\mathrm{f} + \frac{4}{3}\mu_\mathrm{f})$	free-fluid compressional relaxation frequency
Ω_flP	$= \eta_{_0} M/(\frac{\eta_0 M}{K_\mathrm{f}}\xi_\mathrm{f} + \frac{4}{3}\mu_\mathrm{f})$	fluid comp. relax. freq. in the deformable frame
Ω_α	$= H_\mathrm{c}/(\frac{\eta_0 M}{K_\mathrm{f}}\xi_\mathrm{f} + \frac{4}{3}\mu_\mathrm{f})$	saturated-frame comp. relaxation frequency
Ω_fS	$= K_\mathrm{f}/\mu_\mathrm{f}$	free-fluid shear relaxation frequency

Table IX. Derived parameters (Continuation)

Ω_{flS}	$=\eta_{_0} M/\mu_{\mathrm{f}}$	fluid shear relax. freq. in the deformable frame
Ω_{β}	$=\mu_0/\mu_{\mathrm{f}}$	saturated-frame shear relaxation frequency
α^2_{s}	$=\frac{K_{\mathrm{s}}+\frac{4}{3}\mu_{\mathrm{s}}}{\rho_{\mathrm{s}}}$	miniral P-wave velocity (squared)
β^2_{s}	$=\frac{\mu_{\mathrm{s}}}{\rho_{\mathrm{s}}}$	miniral S-wave velocity (squared)
$\alpha^2_{_0}$	$=\frac{H_0}{\phi_0\rho_{\mathrm{s}}}$	dry-frame P-wave velocity (squared)
$\beta^2_{_0}$	$=\frac{\mu^0}{\phi_0\rho_{\mathrm{s}}}$	dry-frame S-wave velocity(squared)
α^2_{c}	$=\frac{H_{\mathrm{c}}}{\rho_{\mathrm{m}}}$	Gassmann P-wave velocity (squared)
β^2_{c}	$=\frac{\mu_0}{\rho_{\mathrm{m}}}$	Gassmann S-wave velocity(squared)
α^2_{I}		fast P-wave velocity (squared)
α^2_{II}		slow P-wave velocity (squared)
β^2_{I}		fast S-wave velocity (squared)
β^2_{II}		slow S-wave velocity (squared)

Appendix B

VISCOSITY-EXTENDED BIOT THEORY

In this chapter for completeness, at first, I summarize the elements of equations of motion of the Biot theory. Thereafter, the viscosity-extended Biot theory is summarized, which is based upon Sahay (2008) and Solorza and Sahay (2009).

B.1 Biot Theory

For homogeneous and isotropic elastic solid matrix with interconnected pores filled with a newtonian fluid, the theory of wave propagation was developed by Biot (1956). The governing equations of motion are

$$\phi_{_0}\rho^{\mathrm{s}}_{_0}\frac{\partial^2 \mathrm{u}^{\mathrm{s}}_j}{\partial t^2} = \tau^{\mathrm{s}}_{jk,k} + \mathrm{I}_j, \tag{125}$$

$$\eta_{_0}\rho^{\mathrm{f}}_{_0}\frac{\partial^2 \mathrm{u}^{\mathrm{f}}_j}{\partial t^2} = \tau^{\mathrm{f}}_{jk,k} - \mathrm{I}_j. \tag{126}$$

Here $(\mathrm{u}^{\mathrm{s}}_j)$ and $(\mathrm{u}^{\mathrm{f}}_j)$ are the averaged displacement fields of solid-frame and fluid respectively. $\eta_{_0}$ is the unperturbed porosity and $\phi_{_0} = 1 - \eta_{_0}$ is the unperturbed volume fraction of solid phase. $\rho^{\mathrm{s}}_{_0}$ and $\rho^{\mathrm{f}}_{_0}$ are the solid and fluid density respectively.

The Biot stress tensor are constructed utilizing the concept of elastic deformation energy potential. They are stated in the notation of Biot (1962) as follows

$$\tau^{\mathrm{s}}_{jk} = \mathrm{K}^0\mathrm{u}^{\mathrm{s}}_{ll}\delta_{jk} + 2\mu^0\breve{\mathrm{u}}^{\mathrm{s}}_{jk} - \left(\alpha_{_{\mathrm{K}}} - \eta_{_0}\right)\mathrm{p}^{\mathrm{f}}\delta_{jk}. \tag{127}$$

$$\tau^{\mathrm{f}}_{jk} = -\eta_{_0}\mathrm{p}^{\mathrm{f}}\delta_{jk} \tag{128}$$

where K^0 and μ^0 the bulk and shear modulus respectively, and the everage fluid pressure, p^{f}, is

$$\mathrm{p}^{\mathrm{f}} = -\mathrm{M}\left(\alpha_{\mathrm{K}}\mathrm{u}^{\mathrm{s}}_{ll} - \zeta\right). \tag{129}$$

The solid-frame strain tensor, $\mathrm{u}^{\mathrm{s}}_{jk}$, is $\frac{1}{2}\left(\mathrm{u}^{\mathrm{s}}_{j,k} + \mathrm{u}^{\mathrm{s}}_{k,j}\right)$, and $\breve{\mathrm{u}}^{\mathrm{s}}_{jk}$ is its trace free part, expressed by

$$\breve{\mathrm{u}}^{\mathrm{s}}_{jk} = \mathrm{u}^{\mathrm{s}}_{jk} - \frac{1}{3}\mathrm{u}^{\mathrm{s}}_{ll}\delta_{jk}. \tag{130}$$

ζ is interpreted as increase of fluid content and it is the divergence of the difference of fluid and solid displacements, that is

$$\zeta = -\eta_{_0}\left(\mathrm{u}^{\mathrm{f}}_{ll} - \mathrm{u}^{\mathrm{s}}_{ll}\right). \tag{131}$$

The Biot bulk coefficient, α_{K}, and the fluid storage coefficient, M, are linked to the bulk moduli of the constituent solid, K^{s}, and the constituent fluid, K^{f}, as

$$\alpha_{\mathrm{K}} = 1 - \frac{\mathrm{K}^0}{\mathrm{K}^{\mathrm{s}}}, \tag{132}$$

and

$$\frac{1}{\mathrm{M}} = \frac{\eta_{_0}}{\mathrm{K}^{\mathrm{f}}} + \frac{\alpha_{\mathrm{K}} - \eta_{_0}}{\mathrm{K}^{\mathrm{s}}}, \tag{133}$$

with $\eta_{_0} \leq \alpha_{\mathrm{K}} \leq 1$.

I_j is the drag force that the two phases impart on each other in equal but opposite direction. Biot constructed the drag force term utilizing the concepts of dissipation function and kinetic energy density function, expressed as follows

$$\mathrm{I}_j = -\eta_{_0}\rho^{\mathrm{f}}_{_0}\Omega^{\mathrm{b}}\frac{\partial}{\partial t}\left(\mathrm{u}^{\mathrm{s}}_j - \mathrm{u}^{\mathrm{f}}_j\right) + \rho^{12}\frac{\partial^2}{\partial t^2}\left(\mathrm{u}^{\mathrm{s}}_j - \mathrm{u}^{\mathrm{f}}_j\right). \tag{134}$$

$\Omega^{\mathrm{b}} = \eta_{_0}\nu^{\mathrm{f}}/K$, where ν^{f} is the pore-fluid kinematic shear viscosity (i. e. fluid shear viscosity scaled by its density) and K is the permeability, which is known as the Biot

critical frequency. The ρ^{12} is the induced mass-coefficient which is linked to tortuosity, S, as

$$\rho^{12} = -(\mathrm{S}-1)\eta_0\rho_0^{\mathrm{f}}. \tag{135}$$

Biot theory excludes the fluid viscous stress part in its macroscopic fluid stress tensor (equation 128), therefore, viscous loss mechanism within the pore fluid is not taken into account here. For a porous medium filled with a highly viscous fluid, such as heavy crude oil or bitumen, the viscous loss within the pores fluid may be of importance.

Furthermore, the lack of viscous loss mechanism within the pores fluid makes the framework mathematically inconsistent or incomplete, because it makes two (out of six) degrees of freedom redundant. The usual practices have been to ignore these redundant degrees of freedom and to analyze this theory in the domain of the remaining four degrees of freedom. As the result, one assumes the existence of only three waves, two compression waves and a shear-wave.

B.1.1 Constitutive equations by volume-averaging method

By employing averaging theorems developed by Slatery (1967) and Whitaker(1967), the constitutive equations at macro-scale are established by averaging poro-scale constitutive equations (de la Cruz and Spanos, 1985; Sahay et al., 2001, Spanos 2002). This is an alternative method to construct poroelastic constitutive equations.

The constitutive equations for the solid and fluid constituents at the pore scale are

described by the linear elasticity and the newtonian rheology, respectively, as follows

$$\sigma^{\mathrm{s}}_{jk} = \mathrm{K}^{\mathrm{s}}\delta_{jk}\mathrm{u}^{\mathrm{s}}_{ll} + 2\mu^{\mathrm{s}}\breve{\mathrm{u}}^{\mathrm{s}}_{jk}. \tag{136}$$

$$\sigma^{\mathrm{f}}_{jk} = -\mathrm{p}^{\mathrm{f}}\delta_{jk} + \pi^{f}_{jk}, \tag{137}$$

where $\breve{\mathrm{u}}^{\mathrm{s}}_{jk}$ is the trace-free part of the pore-scale solid strain tensor, $\breve{\mathrm{u}}^{\mathrm{s}}_{jk} = \mathrm{u}^{\mathrm{s}}_{jk} - \frac{1}{3}\mathrm{u}^{\mathrm{s}}_{ll}\delta_{jk}$, and the pore-scale fluid pressure is

$$\partial_t \mathrm{p}^{\mathrm{f}} = -\mathrm{K}^{\mathrm{f}}\mathrm{v}^{\mathrm{f}}_{ll}, \tag{138}$$

where $\mathrm{v}^{\mathrm{f}}_j = \partial_t \mathrm{u}^{\mathrm{f}}_j$. K^{s} and and μ^{s} are the bulk and shear moduli of solid grain; K^{f} is the bulk modulus of pore fluid.

The viscous stress tensor π^{f}_{jk} incorporates viscous relaxation within the pore fluid. It is taken to be related to fluid strain-rate tensor as below

$$\pi^{f}_{jk} = \xi^{\mathrm{f}}\delta_{jk}\mathrm{v}^{\mathrm{f}}_{ll} + 2\mu^{\mathrm{f}}\breve{\mathrm{v}}^{\mathrm{f}}_{jk}, \tag{139}$$

where ξ^{f} and μ^{f} are the bulk and shear viscosities of the fluid and $\breve{\mathrm{v}}^{\mathrm{f}}_{jk}$ is the trace-free part of pore-scale fluid strain-rate tensor $\breve{\mathrm{v}}^{\mathrm{f}}_{jk} = \mathrm{v}^{\mathrm{f}}_{jk} - \frac{1}{3}\mathrm{v}^{\mathrm{f}}_{ll}\delta_{jk}$.

When the macroscopic constitutive equations are deduced from the constitutive equations for solid and fluid constituents at the microscopic scale by using the the method of volume averaging, the fluid strain-rate term is introduced in a natural way. They was first derived by de la Cruz and Spanos (1985). They are

$$\tau^{\mathrm{s}}_{jk} = \mathrm{K}^{\mathrm{s}}\delta_{jk}\left[\phi_{_0}\mathrm{u}^{\mathrm{s}}_{ll} - \left(\eta - \eta_{_0}\right)\right] + 2\mu^{\mathrm{s}}\left(\phi_{_0}\breve{\mathrm{u}}^{\mathrm{s}}_{jk} + D_{jk}\right), \tag{140}$$

$$\tau^{\mathrm{f}}_{jk} = -\eta_{_0}\mathrm{p}^{\mathrm{f}}\delta_{jk} + \underline{\xi^{\mathrm{f}}\delta_{jk}\left(\eta_0\mathrm{v}^{\mathrm{f}}_{ll} + \partial_t\eta\right) + 2\mu^{\mathrm{f}}\left(\eta_{_0}\breve{\mathrm{v}}^{\mathrm{f}}_{jk} - \partial_t D_{jk}\right)}. \tag{141}$$

where the underline piece is the incorporated fluid viscous loss term. The macroscopic fluid-pressure equation obtained by the method of volume averaging reads

$$\eta_{_0}\partial_t\bar{\mathrm{p}}^{\mathrm{f}} = -\mathrm{K}^{\mathrm{f}}\left(\eta_0\mathrm{v}^{\mathrm{f}}_{ll} + \partial_t\eta\right). \tag{142}$$

The term $\eta - \eta_{_0}$ is

$$\eta - \eta_{_0} = -\frac{1}{\mathrm{V}}\int_{\mathrm{A}^{\mathrm{sf}}} \mathrm{u}^{\mathrm{s}}_l\hat{n}_l \; dA, \tag{143}$$

and the A^{sf} represents the pore interface contained in the averaging volume V and the unit normal $\hat{\mathrm{n}}_l$ points from solid to fluid phase.

The term $\eta - \eta_{_0}$ is the area integral of dilatation motion, i.e. motion perpendicular to the pore boundaries. Hence, it is interpreted as the sum of motion of pore interfaces in its normal direction, per unit volume of the porous medium.

The term D_{ij} is viewed as the sum over the pore-boundary deviatoric motion, i.e., the sum of interfacial motion along itself, in a unit volume of the porous medium, expressed as follows

$$D_{ij} = \frac{1}{\mathrm{V}}\int_{\mathrm{A}^{\mathrm{sf}}} \frac{1}{2}\left(\mathrm{u}^{\mathrm{s}}_i\hat{n}_j + \mathrm{u}^{\mathrm{s}}_j\hat{n}_i - \frac{2}{3}\delta_{ij}\mathrm{u}^{\mathrm{s}}_l\hat{n}_l\right) dA. \tag{144}$$

The terms $\eta - \eta_{_0}$ and D_{ij} are yet to be defined to complete the description at macro-scale.

B.1.2 Viscosity-extended Biot theory

By assuming the area integral term of dilatation motion of pore interface $\eta - \eta_{_0}$ to be related to the difference of the solid and fluid pressure as

$$\eta - \eta_{_0} = -\phi_{_0}\frac{\left(\alpha_k - \eta_{_0}\right)}{\mathrm{K}^0}\left(\mathrm{p}^{\mathrm{s}} - \mathrm{p}^{\mathrm{f}}\right) \tag{145}$$

and the area integral of the deviatoric motion of the pore interface D_{ij} to be solely linearly dependent of the deviatoric (or trace free-part) part of solid stress τ^{s}_{ij} as

$$D_{ij} = -\frac{\left(\alpha_k - \eta_{_0}\right)}{2\mu^0}\tau^{\mathrm{s}}_{jk} \tag{146}$$

where α_μ is the Biot shear coefficient and its explicit form is

$$\alpha_k = 1 - \frac{\mu^0}{\mu^{\mathrm{s}}} \tag{147}$$

Sahay (2008) showed that the V-A expressions for solid stress (eq 12) are reduced to Biot's expressions for solid stress (eq 3) and fluid pressure (eq 5).

Substituting the expression for p^{f} from equation 15 and the expression for p^{s} from equation 13, using the identity $\phi_{_0}\mathrm{p}^{\mathrm{s}}\tau^{\mathrm{s}}_{ll}$ permits it to be rewritten in terms of solid macroscopic dilatation and fluid macroscopic pressure as

$$\eta - \eta_{_0} = -\left(\alpha_k - \eta_{_0}\right)\left(\mathrm{u}^{\mathrm{s}}_{ll} + \frac{1}{\mathrm{K}^{\mathrm{s}}}\mathrm{p}^{\mathrm{f}}\right). \tag{148}$$

Likewise, obtaining the expression for the deviatoric (or trace free-part) of solid stress τ^{s}_{jk} f (eq 13) and substituting it into equation 19, the pore-boundary deviatoric term D_{jk} is rewritten as

$$D_{ij} = -\left(\alpha_k - \eta_{_0}\right)\breve{\mathrm{u}}^{\mathrm{s}}_{jk}. \tag{149}$$

Equation 15 renders the Biot fluid-pressure equation 5 when the porosity equation 21 is substituted into it. Plugging the expression for porosity equation(eq 21) and pore-boundary deviatoric term (eq 22) into equation 11, we obtain the Biot solid-stress tensor (eq 3). When equations 21 and 22 are substituted into equation 14, the fluid-stress tensor is obtained as

$$\tau^{\mathrm{f}}_{jk} \;=\; -\eta_{_0}\mathrm{p}^{\mathrm{f}}\delta_{jk} \underline{- \eta_{_0}\frac{\xi^{\mathrm{f}}}{\mathrm{K}^{\mathrm{f}}}\partial_t\mathrm{p}^{\mathrm{f}}\delta_{jk} + 2\mu^{\mathrm{f}}\left\{\eta_{_0}\partial_t\breve{\mathrm{u}}^{\mathrm{f}}_{jk} + \left(\alpha_\mu - \eta_{_0}\right)\partial_t\breve{\mathrm{u}}^{\mathrm{s}}_{jk}\right\}}, \tag{150}$$

where $\mathrm{v}^{\mathrm{s}} = \partial_t \mathrm{u}^{\mathrm{s}}$. The underlined piece is the incorporated fluid viscous stress-tensor term, thus, the link with the Biot's equations is established. It shows that the pressure rate as well as the fluid and solid shear strain rate play an important role in fluid stress when the pore-fluid viscosities are taken into account, and this approach is called Viscosity-extended Biot theory.

The modified Biot constitutive equations (eq 3 and eq 23), on eliminating pressure terms by solid and fluid volumetric strains using equation 5, then reads in compact notation as

$$\begin{pmatrix} \tau^{\mathrm{s}}_{jk} \\ \tau^{\mathrm{f}}_{jk} \end{pmatrix} = \left(\mathbf{K}^{\mathrm{b}} + \boldsymbol{\xi}^{\mathrm{b}}\partial_t\right) \begin{pmatrix} \mathrm{u}^{\mathrm{s}}_{ll} \\ \mathrm{u}^{\mathrm{f}}_{ll} \end{pmatrix} \delta_{jk} + 2\left(\boldsymbol{\mu}^{\mathrm{b}} + \boldsymbol{\nu}^{\mathrm{b}}\partial_t\right) \begin{pmatrix} \breve{\mathrm{u}}^{\mathrm{s}}_{jk} \\ \breve{\mathrm{u}}^{\mathrm{f}}_{jk} \end{pmatrix}, \tag{151}$$

where the following definitions have been employed

$$\begin{pmatrix} \mathrm{K}^0 + \left(\alpha_{\mathrm{K}} - \eta_0\right)^2 \mathrm{M} & (\alpha_{\mathrm{K}} - \eta_0)\eta_0 \mathrm{M} \\ (\alpha_{\mathrm{K}} - \eta_0)\eta_0 \mathrm{M} & \eta_0^2 \mathrm{M} \end{pmatrix} \equiv \mathbf{K}^{\mathrm{b}}, \tag{152}$$

$$\begin{pmatrix} 1 & 0 \\ 0 & 0 \end{pmatrix} \mu^0 \equiv \boldsymbol{\mu}^{\mathrm{b}}, \tag{153}$$

$$\begin{pmatrix} 0 & 0 \\ \alpha_{\mathrm{K}} - \eta_0 & \eta_0 \end{pmatrix} \frac{\eta_0 \mathrm{M}}{\mathrm{K}^{\mathrm{f}}} \xi^{\mathrm{f}} \equiv \boldsymbol{\xi}^{\mathrm{b}}, \tag{154}$$

and

$$\begin{pmatrix} 0 & 0 \\ \alpha_{\mu} - \eta_0 & \eta_0 \end{pmatrix} \mu^{\mathrm{f}} \equiv \boldsymbol{\nu}^{\mathrm{b}}. \tag{155}$$

By setting the bulk and shear viscosities vanishing, the matrices incorporating fluid viscous relaxation processes, $\boldsymbol{\xi}^{\mathrm{b}}$ and $\boldsymbol{\nu}^{\mathrm{b}}$, are dropped and the classical Biot constitutive relation is recovered. The incorporation of fluid viscous relaxation terms render the form of this modified constitutive relation to be a 2×2 matrix generalization of viscoelastic

constitutive relation.

B.1.3 Viscosity-extended Biot theory in terms of natural dynamical fields

The above are expressed in terms of solid and fluid displacement, however, seismic sensors do not register solid and fluid phase motions solely, but they in fact register the mass weighted vector sum of the motion of fluid and solid constituents (Sahay, 1995; Sahay, 1996). The proper fields of dynamical purposes are the mass weighted vector sum and vector difference of solid and fluid displacement fields. They are known as centre-of-mass and internal displacement fields, respectively.

Center-of-mass ($\mathrm{u}^{\mathrm{m}}_j$) and internal ($\mathrm{u}^{\mathrm{i}}_j$) fields defined as

$$\left(\mathbf{u}^{\mathrm{m}}_j \quad \mathbf{u}^{\mathrm{i}}_j\right)^{\mathrm{T}} \;=\; \mathbf{m}^{-1}\left(\mathbf{u}^{\mathrm{s}}_j \quad \mathbf{u}^{\mathrm{f}}_j\right)^{\mathrm{T}}, \tag{156}$$

and its stresses are given by

$$\left(\tau^{\mathrm{m}}_{jk} \quad \tau^{\mathrm{i}}_{jk}\right)^{\mathrm{T}} \;=\; \mathbf{m}^{\mathrm{T}}\left(\tau^{\mathrm{s}}_{jk} \quad \tau^{\mathrm{f}}_{jk}\right)^{\mathrm{T}}, \tag{157}$$

where $^{\mathrm{T}}$ denotes transpose. The transformation matrix is defined by

$$\mathbf{m} \;=\; \begin{pmatrix} 1 & m_{\mathrm{f}} \\ 1 & -m_{\mathrm{s}} \end{pmatrix}, \tag{158}$$

and the solid- and fluid- mass fractions are expressed as

$$m_{\mathrm{s}} = \frac{\phi_0 \rho_{\mathrm{s}}}{\rho_{\mathrm{m}}}, \tag{159}$$

$$m_{\mathrm{f}} = \frac{\eta_0 \rho_{\mathrm{f}}}{\rho_{\mathrm{m}}}, \tag{160}$$

where ρ_{m} and ρ_{r} are the total and reduced densities of the porous medium given by

$$\rho_{\mathrm{m}} \;=\; \phi_0 \rho_{\mathrm{s}} + \eta_0 \rho_{\mathrm{f}}, \tag{161}$$

$$1/\rho_{\mathrm{r}} \;=\; 1/\phi_0 \rho_{\mathrm{s}} + 1/\eta_0 \rho_{\mathrm{f}}, \tag{162}$$

where the modified reduced density is expressed as

$$\rho_{\mathrm{i}} = \rho_{\mathrm{r}} - \rho_{12}. \tag{163}$$

The viscosity-extended constitutive relation (eq 151) is reformulated in terms of natural dynamical fields as

$$\begin{pmatrix} \tau^{\mathrm{m}}_{jk} \\ \tau^{\mathrm{i}}_{jk} \end{pmatrix} = (\mathbf{K} + \boldsymbol{\xi}\partial_t) \begin{pmatrix} \mathrm{u}^{\mathrm{m}}_{ll} \\ \mathrm{u}^{\mathrm{i}}_{ll} \end{pmatrix} \delta_{jk} + 2\,(\boldsymbol{\mu} + \boldsymbol{\nu}\partial_t) \begin{pmatrix} \breve{\mathrm{u}}^{\mathrm{m}}_{jk} \\ \breve{\mathrm{u}}^{\mathrm{i}}_{jk} \end{pmatrix}, \tag{164}$$

where

$$\mathbf{m}^{\mathrm{T}}\mathbf{K}_{\mathrm{b}}\mathbf{m} \equiv \mathbf{K},\ \mathbf{m}^{\mathrm{T}}\boldsymbol{\xi}_{\mathrm{b}}\mathbf{m} \equiv \boldsymbol{\xi},\ \mathbf{m}^{\mathrm{T}}\boldsymbol{\mu}_{\mathrm{b}}\mathbf{m} \equiv \boldsymbol{\mu},\ \text{and}\ \mathbf{m}^{\mathrm{T}}\boldsymbol{\nu}_{\mathrm{b}}\mathbf{m} \equiv \boldsymbol{\nu}. \tag{165}$$

Utilizing the identity

$$\begin{pmatrix} \phi_0\rho_{\mathrm{s}} & 0 \\ 0 & \eta_0\rho_{\mathrm{f}} \end{pmatrix} \mathbf{m} = (\mathbf{m}^{\mathrm{T}})^{-1} \begin{pmatrix} \rho_{\mathrm{m}} & 0 \\ 0 & \rho_{\mathrm{r}} \end{pmatrix} \tag{166}$$

the equations of motion (125 and 126) in terms of natural dynamical field are expressed as

$$\begin{pmatrix} \rho_{\mathrm{m}} & 0 \\ 0 & \rho_{\mathrm{r}} \end{pmatrix} \partial_t^2 \begin{pmatrix} \mathrm{u}^{\mathrm{m}}_j \\ \mathrm{u}^{\mathrm{i}}_j \end{pmatrix} = \begin{pmatrix} 1 & 0 \\ 0 & 1 \end{pmatrix} \begin{pmatrix} \tau^{\mathrm{m}}_{jk,k} \\ \tau^{\mathrm{i}}_{jk,k} \end{pmatrix} + \begin{pmatrix} 0 & 0 \\ 0 & 1 \end{pmatrix} \mathrm{I}_j, \tag{167}$$

where the drag force term, I_j, in terms of the dynamical fields, is

$$\mathrm{I}_j = -\eta_0\rho_{\mathrm{f}}\Omega_{\mathrm{b}}\ \partial_t \mathrm{u}^{\mathrm{i}}_j + \rho_{12}\ \partial_t^2 \mathrm{u}^{\mathrm{i}}_j. \tag{168}$$

Introducing the notation

$$\mathbf{u}_j = \begin{pmatrix} \mathrm{u}^{\mathrm{m}}_j & \mathrm{u}^{\mathrm{i}}_j \end{pmatrix}^{\mathrm{T}}, \tag{169}$$

and

$$\boldsymbol{\tau}_{jk} = \begin{pmatrix} \tau^{\mathrm{m}}_{jk} & \tau^{\mathrm{i}}_{jk} \end{pmatrix}^{\mathrm{T}}, \tag{170}$$

the equations of motion are rewritten in compact form as

$$\boldsymbol{\rho}\ \partial_t^2 \mathbf{u}_j + \eta_0\rho_{\mathrm{f}}\Omega_{\mathrm{b}}\ \mathbf{I}_0\ \partial_t \mathbf{u}_j = \boldsymbol{\tau}_{jk,k}, \tag{171}$$

where $\boldsymbol{\rho}$ is the density matrix

$$\boldsymbol{\rho} = \begin{pmatrix} \rho_{\mathrm{m}} & 0 \\ 0 & \rho_{\mathrm{i}} \end{pmatrix}, \tag{172}$$

and $\mathbf{I}_0$ is 2×2 matrix whose element (2,2) is unity and rest of the elements are equal to zero, that is

$$\mathbf{I}_0 = \begin{pmatrix} 0 & 0 \\ 0 & 1 \end{pmatrix}. \tag{173}$$

The constitutive relation (eq 164) is rewritten as

$$\boldsymbol{\tau}_{jk} = \left(\mathbf{K} + \boldsymbol{\xi}\partial_t\right)\mathbf{u}_{ll}\delta_{jk} + 2\left(\boldsymbol{\mu} + \boldsymbol{\nu}\partial_t\right)\breve{\mathbf{u}}_{jk}. \tag{174}$$

Notationally the equations of motion (171) and the constitutive relation (174) are analog to equations in elasticity theory, however density and elastic parameters in poroelasticity are 2×2 matrices. Plugging eq (174) into eq (171), and introducing the "extended dynamical vector" $\mathbf{u}$ whose elements are centre-of-mass and internal field vectors,

$$\mathbf{u} = \hat{\mathbf{e}}_j \mathbf{u}_j = \hat{\mathbf{e}}_j (\mathrm{u}_j^{\mathrm{m}} \;\; \mathrm{u}_j^{\mathrm{i}})^{\mathrm{T}}, \tag{175}$$

where $\hat{\mathbf{e}}_j$ is the unit vector in jth direction, and applying $\boldsymbol{\rho}^{-1}$ from the left, the viscosity-extended Biot equations of motion (171) are cast in vectorial notation. They read

$$\mathbf{I}\partial_t^2\mathbf{u} + \Omega_{\mathrm{i}}\mathbf{I}_0\partial_t\mathbf{u} = \left(\mathbf{C}_\alpha + \mathbf{N}_\alpha\partial_t\right)\nabla\left(\nabla\cdot\mathbf{u}\right) - \left(\mathbf{C}_\beta + \mathbf{N}_\beta\partial_t\right)\nabla\times\nabla\times\mathbf{u} \tag{176}$$

where

$$\frac{\eta_0\rho_{\mathrm{f}}}{\rho_{\mathrm{i}}} \equiv d_{\mathrm{f}} \tag{177}$$

$$\frac{\phi_0\rho_{\mathrm{s}}}{\rho_{\mathrm{i}}} \equiv d_{\mathrm{s}} \tag{178}$$

and Biot relaxation frequency corresponding to the dissipation due to fluid flow with respect to the solid-frame and contains a permeability term. Its explicit expression is

$$d_{\mathrm{f}}\Omega_{\mathrm{b}} \equiv \Omega_{\mathrm{i}}. \tag{179}$$

$\mathbf{I}$ is the 2×2 identity matrix,

$$\boldsymbol{\rho}^{-1}\left(\mathbf{K} + \frac{4}{3}\boldsymbol{\mu}\right) \equiv \mathbf{C}_{\alpha}, \tag{180}$$

$$\boldsymbol{\rho}^{-1}\boldsymbol{\mu} \equiv \mathbf{C}_{\beta}, \tag{181}$$

$$\boldsymbol{\rho}^{-1}\left(\boldsymbol{\xi} + \frac{4}{3}\boldsymbol{\nu}\right) \equiv \mathbf{N}_{\alpha}, \tag{182}$$

and

$$\boldsymbol{\rho}^{-1}\boldsymbol{\nu} \equiv \mathbf{N}_{\beta}. \tag{183}$$

The elements of the second-order $\mathbf{C}_{\alpha}$ and $\mathbf{C}_{\beta}$ matrices have dimensions of velocity squared and they contain the frame shear modulus and frame and fluid densities. The elements of the second-order $\mathbf{N}_{\alpha}$ and $\mathbf{N}_{\beta}$ matrices have dimensions of kinematic viscosity and they contain the fluid shear viscosity. After some rearrangements, the explicit expressions of these are

$$\mathbf{C}_{\alpha} = \alpha_{\mathrm{c}}^2 \begin{pmatrix} 1 & m_{\mathrm{f}}\left(1 - \frac{\alpha_K}{\eta_0}\frac{\alpha_{\mathrm{fl}}^2}{\alpha_{\mathrm{c}}^2}\right) \\ d_{\mathrm{f}}\left(1 - \frac{\alpha_K}{\eta_0}\frac{\alpha_{\mathrm{fl}}^2}{\alpha_{\mathrm{c}}^2}\right) & d_{\mathrm{f}}\left(m_{\mathrm{f}} + \varepsilon\right) \end{pmatrix} \tag{184}$$

$$\mathbf{N}_{\alpha} = \alpha_{\mathrm{c}}^2 \begin{pmatrix} \Upsilon & -\left(\eta_0 - m_{\mathrm{f}}\Upsilon\right) \\ -d_{\mathrm{s}}\Upsilon & d_{\mathrm{s}}\left(\eta_0 - m_{\mathrm{f}}\Upsilon\right) \end{pmatrix} \frac{1}{\Omega_{\alpha}} \tag{185}$$

$$\mathbf{C}_{\beta} = \beta_{\mathrm{c}}^2 \begin{pmatrix} 1 & m_{\mathrm{f}} \\ d_{\mathrm{f}} & d_{\mathrm{f}}m_{\mathrm{f}} \end{pmatrix} \tag{186}$$

$$\mathbf{N}_{\beta} = \beta_{\mathrm{c}}^2 \begin{pmatrix} \alpha_{\mu} & -\left(\eta_0 - m_{\mathrm{f}}\alpha_{\mu}\right) \\ -d_{\mathrm{s}}\alpha_{\mu} & d_{\mathrm{s}}\left(\eta_0 - m_{\mathrm{f}}\alpha_{\mu}\right) \end{pmatrix} \frac{1}{\Omega_{\beta}}. \tag{187}$$

The details of the derivations of eqs (184-185) are in Appendices A and B, respectively. The derivations of (186) and (187) are straightforward.

$$\alpha_{\mathrm{c}}^2 = \frac{H_{\mathrm{c}}}{\rho_{\mathrm{m}}} \tag{188}$$

and

$$\beta_{\mathrm{c}}^2 = \frac{\mu_0}{\rho_{\mathrm{m}}} \tag{189}$$

are called Gassmann P- and S- wave speed (squared), respectively.

$$\Omega_\alpha = \frac{H_{\mathrm{c}}}{\frac{\eta_0 M}{K_{\mathrm{f}}}\xi_{\mathrm{f}} + \frac{4}{3}\mu_{\mathrm{f}}}. \tag{190}$$

$$\Omega_\beta = \frac{\mu_0}{\mu_{\mathrm{f}}} \tag{191}$$

are the saturated-frame relaxation frequency for P- and S- process, respectively.

Here,

$$H_{\mathrm{c}} = K_0 + \frac{4}{3}\mu_0 + \alpha_{K}^2 M, \tag{192}$$

is the Gassmann P-wave elastic modulus.

The term

$$\varepsilon = \left(1 - 2\frac{\alpha_{K} m_{\mathrm{f}}}{\eta_0}\right)\frac{\alpha_{\mathrm{fl}}^2}{\alpha_{\mathrm{c}}^2} \tag{193}$$

is a positive quantity less than unity, and the term

$$\Upsilon = \alpha_{K} + (\alpha_\mu - \alpha_{K})\frac{4}{3}\frac{\Omega_{\mathrm{flP}}}{\Omega_{\mathrm{flS}}} \tag{194}$$

is bounded as $\alpha_{K} \le \Upsilon \le \alpha_\mu$.

$$\alpha_{\mathrm{fl}}^2 = \frac{\eta_0 M}{\rho_{\mathrm{f}}} \tag{195}$$

is identified as the velocity (squared) of sound in fluid in the presence of deformable solid-frame.

$$\Omega_{\mathrm{flP}} = \frac{\eta_0 M}{\frac{\eta_0 M}{K_{\mathrm{f}}}\xi_{\mathrm{f}} + \frac{4}{3}\mu_{\mathrm{f}}} \tag{196}$$

and

$$\Omega_{\mathrm{flS}} = \frac{\eta_0 M}{\mu_{\mathrm{f}}} \tag{197}$$

are identified as, respectively, fluid P-modulus and fluid S-modulus relaxation frequencies in the presence of deformable solid-frame.

The factorization of velocity (square) and relaxation frequency terms in eqs 184-187 enable the elements of the resulting matrices to be bounded by unity, which provide an easement in mathematical analysis.

B.1.4 Frequency domain representation

In frequency domain eq (176) reads as

$$\boldsymbol{\alpha}\nabla\left(\nabla\cdot\mathbf{u}\right) - \boldsymbol{\beta}\nabla\times\nabla\times\mathbf{u} + \omega^2\mathbf{u} \;=\; 0 \tag{198}$$

where $\boldsymbol{\alpha}$ and $\boldsymbol{\beta}$ are non-symmetric second-order matrices associated with P- and S-motion, respectively, whose elements are dimentionally equal to velocity squared. They are expressed as follows

$$\boldsymbol{\alpha} \;= \boldsymbol{\Omega}^{-1}\left(\mathbf{C}_\alpha - i\omega\mathbf{N}_\alpha\right) \;\equiv \begin{pmatrix} \alpha^{\mathrm{mm}} & \alpha^{\mathrm{mi}} \\ \alpha^{\mathrm{im}} & \alpha^{\mathrm{ii}} \end{pmatrix}, \tag{199}$$

$$\boldsymbol{\beta} \;= \boldsymbol{\Omega}^{-1}\left(\mathbf{C}_\beta - i\omega\mathbf{N}_\beta\right) \;\equiv \begin{pmatrix} \beta^{\mathrm{mm}} & \beta^{\mathrm{mi}} \\ \beta^{\mathrm{im}} & \beta^{\mathrm{ii}} \end{pmatrix}, \tag{200}$$

where $\mathbf{\Omega}$ is a 2×2 diagonal matrix associated with the Biot relaxation frequency Ω^{i}

$$\mathbf{I} + i\,\frac{\Omega_{\mathrm{i}}}{\omega}\,\mathbf{I}_0 \;\equiv\; \mathbf{\Omega}. \tag{201}$$

where $\mathbf{I}$ is the 2×2 identity matrix and $\mathbf{I}_0$ is the diagonal matrix $\mathrm{diag}(0,1)$. Utilizing the definitions (180-183), the stresses (174) now read

$$\boldsymbol{\tau}_{jk} \;=\; \boldsymbol{\rho}\left[\left\{(\mathbf{C}_\alpha - i\omega\mathbf{N}_\alpha) - 2\,(\mathbf{C}_\beta - i\omega\mathbf{N}_\beta)\right\}\mathrm{u}_{ll}\delta_{jk} + 2\,(\mathbf{C}_\beta - i\omega\mathbf{N}_\beta)\,\breve{\mathrm{u}}_{jk}\right]$$

which, in the view of definitions (199-200), are expressed as

$$\boldsymbol{\tau}_{jk} \;=\; \mathbf{\Omega}\boldsymbol{\rho}\left\{(\boldsymbol{\alpha} - 2\boldsymbol{\beta})\,\mathrm{u}_{ll}\delta_{jk} + 2\boldsymbol{\beta}\;\breve{\mathrm{u}}_{jk}\right\}. \tag{202}$$

Appendix C

SEISMIC BOUNDARY CONDITIONS IN POROUS MEDIA

The boundary conditions define the field quantities across the surface of a material discontinuity. For the case wherein there is no imbedded sources or sinks of energy at the interface, they are simply the statements of the conservation of the fundamental quantities, namely, mass, linear momentum, angular momentum and energy.

In classical elasticity, for the case of a welded contact, boundary conditions are stated as the continuity of the velocity field and the traction field. The conservation of mass across an interface requires the continuity of normal component of velocity. The continuity of tractions is the statement about the conservation of linear momentum across an interface. The conservation of angular momentum further requires the continuity of tangential components of velocity field; although in literature this continuity is often ascribed to kinematic requirement of "no-slip". The continuity of energy flux is required for conservation of energy, which is automatically satisfied on account of the continuity of velocity and traction fields. In the context of classical elasticity, if the conservation of energy hold true at an interface, it automatically guarantees the conservation of mass and linear momentum.

For a porous-porous welded contact, the two interacting continua nature of the media pose two additional complexities. Firstly, given the fluid-fluid and solid-solid contact

surfaces may move away from each other as media deform, how an unique interface, in a macroscopic sense, is to be defined on which conservation of total mass, total momentums and total energy would hold true. Secondly, at an interface, in a macroscopic sense, a phase (solid or fluid) from one side may exert force on the other side, not only upon a phase its own kind but the other also, one needs a basis to quantify such phasic interactions.

The earliest set of boundary conditions for porous-porous welded contact is due to Deresiewick and Skalak (1963). This work is based upon the consideration of the conservation of total energy. Although, authors do recognize that the fluid-fluid contact surface indeed separate off the solid-solid contact surface, but they heuristically take the latter to be the surface across which total energy flux is conserved. They have proposed two set of boundary conditions, namely, "open pore" and "partially open pore". The latter contains an adjustable parameter that is known as "interface permeability".

The other competing set of boundary conditions is due to de la Cruz and Spanos (1989). They have suggested that macroscopic interface has to be the surface across with total mass is conserved. They show that across this interface, the conservation of mass and linear momentum yield the continuity of normal component of mass weight vector sum of the solid and fluid velocities and total tractions; for the continuity of the tangential components of that mass weighted velocity field they invoke "no slip" condition. By utilizing Newton's third law of motion, they have quantified how the stresses on each phase interact with the stress on each of the phases across the interface and have developed two additional conditions on tractions. These equations contain a parameter to describe "overlap" among the phases on two sides of an interface.

A critical overview of the Deresiewick and Skalak (1963) boundary conditions, along with its extension that includes fluid viscous stress tensor part, is presented in the next section. Next, the de la Cruz and Spanos (1989) boundary conditions are outlined along with its extension by Sahay (2009, private communications). This extension recast them in a form in which the "overlap" parameter is no longer present. Also, in this form the conservation of total energy, which is not explicitly addressed in the original formulation, holds true. These critical overviews are from unpublished notes of Sahay.

C.1 Deresiewicz and Skalak (1963) boundary conditions

The boundary conditions due to Deresiewicz and Skalak (1963) are based upon of the conservation of total energy. They showed that to conserve total energy across an interface the normal energy flux has to remain continuous, and for which they found that

$$\left\langle \left(\tau^{\mathrm{s}}_{jk} \dot{\mathrm{u}}^{\mathrm{s}}_{j} + \tau^{\mathrm{f}}_{jk} \dot{\mathrm{u}}^{\mathrm{f}}_{j} \right) \hat{n}_k \right\rangle = 0 \tag{203}$$

must hold true. Here, $\hat{n}_k$ denotes the unit normal to the interface separating two dissimilar porous media and the bra-ket symbol, $\langle\ \rangle$, represents the jump in the quantity within its argument. To have consistency with the classical Biot theory, the viscous shear stress part of the fluid stress tensor was not taken into consideration by them. Retaining only the hydrostatic part of the fluid stress tensor, they took

$$\tau^{\mathrm{f}}_{jk} = -\eta_0 \mathrm{p}^{\mathrm{f}} \delta_{jk}. \tag{204}$$

At first, they assumed (implicitly) that the two terms in equation (203) have to be individually continuous, i. e.,

$$\left\langle \tau^{\mathrm{s}}_{jk} \dot{\mathrm{u}}^{\mathrm{s}}_{j} \hat{n}_k \right\rangle = 0, \tag{205}$$

and

$$\left\langle \eta_0 \mathrm{p}^{\mathrm{f}} \delta_{jk} \ \dot{\mathrm{u}}^{\mathrm{f}}_{j} \hat{n}_k \right\rangle = 0. \tag{206}$$

The term $\tau^{\mathrm{s}}_{jk}\hat{n}_k$ is the traction vector for solid phase. The term $\delta_{jk}\dot{\mathrm{u}}^{\mathrm{f}}_{j}\hat{n}_k = \dot{\mathrm{u}}^{\mathrm{f}}_{k}\hat{n}_k \equiv \dot{\mathrm{u}}^{\mathrm{f}}_{\perp}$ is the component of fluid velocity normal to the interface. Clearly, the expression in equation (205) is the dot product of solid phase traction vector and solid velocity field. Likewise, the expression in equation (206) is the dot product of the porosity weighted fluid pressure and the normal component of fluid velocity field. For equations (205) and (206) to hold true, each element of the products must be continuous. Those amount to the continuity of solid traction vector, solid velocity field, porosity weighted fluid pressure, and normal component of fluid velocity. They are stated as

$$\left\langle \tau^{\mathrm{s}}_{jk} \hat{n}_k \right\rangle = 0, \tag{207}$$

$$\left\langle \dot{\mathrm{u}}^{\mathrm{s}}_{j} \hat{n}_k \right\rangle = 0, \tag{208}$$

$$\left\langle \eta_0 \mathrm{p}^{\mathrm{f}} \right\rangle = 0, \tag{209}$$

$$\left\langle \dot{\mathrm{u}}^{\mathrm{f}}_{\perp} \right\rangle = 0. \tag{210}$$

Deresiewicz and Skalak (1963) concluded that the above set of boundary conditions are of limited value. It was because, on physical grounds, they insisted that mass of fluid at the interface must be conserved. For that the relative normal flow of fluid with respect to solid frame, $\eta_0 \left(\dot{\mathrm{u}}^{\mathrm{f}}_{\perp} - \dot{\mathrm{u}}^{\mathrm{s}}_{\perp} \right)$, must remain continuous across the interface. This constrain is compatible with equations (207) through (210) only if porosity remains unchanged across the interface or there is no relative motion between fluid and solid-

frame at the interface. The quantity

$$\eta_0 \left(\dot{\mathrm{u}}_j^{\mathrm{f}} - \dot{\mathrm{u}}_j^{\mathrm{s}} \right) \equiv \dot{\mathrm{w}}_j \tag{211}$$

is recognized as "fluid filtration velocity". It should be noted that the continuity of the normal component of fluid filtration velocity implicitly suggests that solid-solid contact surface has been taken as the interface which is also obvious from the cartoons presented by Deresiewicz and Skalak (see Figures 2 and 3).

C.1.1 Open pore case

In order to incorporate "fluid filtration velocity" into the statement of energy conservation, they re-wrote the expression of energy flux. In equation (203) the addition and subtraction of the term $\eta_0 \mathrm{p}^{\mathrm{f}} \delta_{jk} \dot{\mathrm{u}}_j^{\mathrm{s}}$ yields

$$\left(\tau_{jk}^{\mathrm{s}} \dot{\mathrm{u}}_j^{\mathrm{s}} - \eta_0 \mathrm{p}^{\mathrm{f}} \delta_{jk} \dot{\mathrm{u}}_j^{\mathrm{s}} + \eta_0 \mathrm{p}^{\mathrm{f}} \delta_{jk} \dot{\mathrm{u}}_j^{\mathrm{s}} - \eta_0 \mathrm{p}^{\mathrm{f}} \delta_{jk} \dot{\mathrm{u}}_j^{\mathrm{f}} \right) \hat{n}_k. \tag{212}$$

By regrouping terms for total stress, $\tau_{jk} = \tau_{jk}^{\mathrm{s}} - \eta_0 \mathrm{p}^{\mathrm{f}} \delta_{jk}$, and filtration velocity (see equation 211) it is

$$\left(\underline{\left(\tau_{jk}^{\mathrm{s}} \dot{\mathrm{u}}_j^{\mathrm{s}} - \eta_0 \mathrm{p}^{\mathrm{f}} \delta_{jk} \right)} \dot{\mathrm{u}}_j^{\mathrm{s}} - \mathrm{p}^{\mathrm{f}} \delta_{jk} \underline{\eta_0 \left(\dot{\mathrm{u}}_j^{\mathrm{f}} - \dot{\mathrm{u}}_j^{\mathrm{s}} \right)} \right) \hat{n}_k, \tag{213}$$

or

$$\left(\tau_{jk} \dot{\mathrm{u}}_j^{\mathrm{s}} - \mathrm{p}^{\mathrm{f}} \delta_{jk} \dot{\mathrm{w}}_j \right) \hat{n}_k. \tag{214}$$

In the above, assuming the continuity of each term individually they proposed

$$\left\langle \dot{\mathrm{u}}_j^{\mathrm{s}} \right\rangle = 0, \tag{215}$$

$$\left\langle \tau_{jk} \hat{n}_k \right\rangle = 0, \tag{216}$$

$$\left\langle \dot{\mathrm{w}}_{\perp} \right\rangle = 0, \tag{217}$$

$$\left\langle \mathrm{p}^{\mathrm{f}} \right\rangle = 0. \tag{218}$$

They asserted that these are the boundary conditions for the case when fluid is able to freely flow across the interface and coined the named "open pore" to this set. Their cartoon illustration of this case is reproduced in Figure 19.

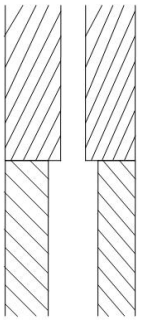

Figure 19. Open pore case, adapted from Deresiewicz and Skalak (1963)

C.1.2 Partially open pore case

Deresiewicz and Skalak (1963) further suggested that there shall be cases when fluid is not completely free to flow across the interface. As an illustration they presented the cartoon shown in Figure 20. They argued that when the hydraulic contact between

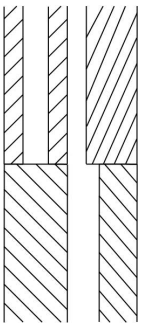

Figure 20. Partially open pores, adapted from Deresiewicz and Skalak (1963)

two porous media is imperfect, the boundary condition (218) will not hold true because of the difference in fluid pressure across the interface. On physical reasoning, they

generalized equation (218) by proposing that the differential fluid pressure must be linearly related to the normal component of filtration velocity at the interface, i. e.,

$$\left\langle \mathrm{p}^{\mathrm{f}} \right\rangle = \frac{1}{k_{\mathrm{DS}}} \dot{\mathrm{w}}_{\perp} \tag{219}$$

k_{DS} is the proportionality constant which has the dimensions of permeability and it is known as "interface permeability". It is taken to span from $0 \leq k_{\mathrm{DS}} \leq \infty$. $k_{\mathrm{DS}} = \infty$ represents the open pore case as it yields equation (218). The equations (215) through (217) and (219) are the final set of boundary conditions proposed by Deresiewicz and Skalak.

However, according to them, $k_{\mathrm{DS}} = 0$ corresponds to the seal pore case (see Figure 21). For that they suggested to take equations (215) and (216) as is, and to replace equations (217) and (219) by the conditions of the vanishing normal component of fluid filtration velocity at the interface for each side.

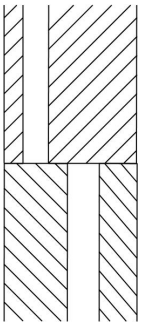

Figure 21. Close pores, adapted from Deresiewicz and Skalak (1963)

C.1.3 Generalization of Deresiewicz and Skalak (1963) boundary conditions for fluid viscous stress tensor (DS09)

In order to have consistency with the viscosity-extended Biot framework, the viscous shear stress part of the fluid stress tensor, which was dropped in equation (204), has to be re-incorporated and the boundary conditions have to be reworked. Accordingly, one finds that in the boundary equations (215 through 217 and 219) the fluid pressure term has to be replaced by the fluid stress tensor term and the normal component of fluid filtration velocity has to be replaced by the filtration velocity vector. The derivations are straightforward. The viscosity generalized Deresiewicz and Skalak (1963) boundary conditions read

$$\left\langle \dot{\mathrm{u}}_j^{\mathrm{s}} \right\rangle = 0, \tag{220}$$

$$\left\langle \tau_{jk}\hat{n}_k \right\rangle = 0, \tag{221}$$

$$\left\langle \dot{\mathrm{w}}_j \right\rangle = 0, \tag{222}$$

$$\left\langle \sigma_{\mathrm{jk}}^{\mathrm{f}}\hat{\mathrm{n}}_{\mathrm{k}} \right\rangle = \frac{1}{k_{\mathrm{DS}}}\dot{\mathrm{w}}_j \tag{223}$$

where $\sigma_{jk}^{\mathrm{f}} = \frac{\tau_{jk}^{\mathrm{f}}}{\eta_0}$, and it is the fluid stress per unit area. For mathematical convenience later, equations (220) and (222) on velocity fields are lumped as

$$\left\langle \begin{array}{c} \dot{\mathrm{u}}_j^{\mathrm{s}} \\ \dot{\mathrm{w}}_j \end{array} \right\rangle = \begin{pmatrix} 0 \\ 0 \end{pmatrix}, \tag{224}$$

and equations (221) and (223) on tractions are viewed as

$$\left\langle \begin{array}{c} \tau_{jk}\hat{n}_k \\ \sigma_{jk}^{\mathrm{f}}\hat{n}_k \end{array} \right\rangle = \begin{pmatrix} 0 & 0 \\ 0 & \frac{1}{k_{\mathrm{DS}}} \end{pmatrix} \begin{pmatrix} \dot{\mathrm{u}}_j^{\mathrm{s}} \\ \dot{\mathrm{w}}_j \end{pmatrix} \tag{225}$$

C.1.4 DS09 boundary conditions in term of natural dynamical fields

Transformation matrices

By using the definition of fluid filtration velocity given in equation (211), the state vector in Deresiewicz and Skalak (1963) framework, $(\mathrm{u}_j^{\mathrm{s}} \;\; \mathrm{w}_j)^{\mathrm{T}}$, is found to be related to Biot theory state vector, $(\mathrm{u}_j^{\mathrm{s}} \;\; \mathrm{u}_j^{\mathrm{f}})^{\mathrm{T}}$, as follows

$$\begin{pmatrix} \mathrm{u}_j^{\mathrm{s}} \\ \mathrm{u}_j^{\mathrm{f}} \end{pmatrix} = \mathbf{B} \begin{pmatrix} \mathrm{u}_j^{\mathrm{s}} \\ \mathrm{w}_j \end{pmatrix}, \qquad \mathbf{B} = \begin{pmatrix} 1 & 0 \\ 1 & \frac{1}{\eta_0} \end{pmatrix}. \tag{226}$$

In the above, employing the transformation (156) between the Biot theory state vector,$(\mathrm{u}_j^{\mathrm{s}} \;\; \mathrm{u}_j^{\mathrm{f}})^{\mathrm{T}}$, and the natural dynamical state vectors, $(\mathrm{u}_j^{\mathrm{m}} \;\; \mathrm{u}_j^{\mathrm{i}})^{\mathrm{T}}$, yields

$$\begin{pmatrix} \mathrm{u}_j^{\mathrm{s}} \\ \mathrm{w}_j \end{pmatrix} = \underbrace{\mathbf{B^{-1}M}}_{\mathbf{T}^{-1}} \begin{pmatrix} \mathrm{u}_j^{\mathrm{m}} \\ \mathrm{u}_j^{\mathrm{i}} \end{pmatrix}, \tag{227}$$

where the matrix $\mathbf{M}$ is defined in (158). After some algebraic multiplications, the transformation matrix $\mathbf{T}$ is

$$\mathbf{T}^{-1} = \begin{pmatrix} 1 & m_{\mathrm{f}} \\ 0 & -\eta_0 \end{pmatrix}, \tag{228}$$

where mass fractions, m_{f} and m_{s}, are defined in equations (160) and (159), respectively. In here, the identity $m_{\mathrm{s}} + m_{\mathrm{f}} = 1$ has been employed for symplicifcations. Likewise, after some algebraic manipulations, the traction vector in Deresiewicz and Skalak (1963) framework, $(\tau_{jk}\hat{n}_k \;\; \sigma_{jk}^{\mathrm{f}}\hat{n}_k)^{\mathrm{T}}$, is found to be related to the traction vector in natural dynamical framework, $(\tau_{jk}^{\mathrm{m}}\hat{n}_k \;\; \tau_{jk}^{\mathrm{i}}\hat{n}_k)^{\mathrm{T}}$, as follows

$$\begin{pmatrix} \tau_{jk}\hat{n}_k \\ \sigma_{jk}^{\mathrm{f}}\hat{n}_k \end{pmatrix} = \mathbf{T}^T \begin{pmatrix} \tau_{jk}^{\mathrm{m}}\hat{n}_k \\ \tau_{jk}^{\mathrm{i}}\hat{n}_k \end{pmatrix}, \tag{229}$$

where

$$\mathbf{T}^{\mathrm{T}} \quad = \quad \begin{pmatrix} 1 & 0 \\ \frac{m_{\mathrm{f}}}{\eta_0} & -\frac{1}{\eta_0} \end{pmatrix}. \tag{230}$$

In the above, the transformation relation (157) is employed, and τ^{m}_{jk} and τ_{jk} are the symbols for the same quantity, the total stress.

Transformed DS09 boundary conditions

By using the transformation relations (227) and (229), the boundary equations (224) and (225) are, respectively,

$$\left\langle \mathbf{T}^{-1} \begin{pmatrix} \dot{\mathrm{u}}^{\mathrm{m}}_j \\ \dot{\mathrm{u}}^{\mathrm{i}}_j \end{pmatrix} \right\rangle \quad = \quad \begin{pmatrix} 0 \\ 0 \end{pmatrix}, \tag{231}$$

and

$$\left\langle \mathbf{T}^{\mathrm{T}} \begin{pmatrix} \tau^{\mathrm{m}}_{jk}\hat{n}_k \\ \tau^{\mathrm{i}}_{jk}\hat{n}_k \end{pmatrix} \right\rangle \quad = \quad \underbrace{\begin{pmatrix} 0 & 0 \\ 0 & \frac{1}{k_{\mathrm{DS}}} \end{pmatrix} \mathbf{T}^{-1}} \begin{pmatrix} \dot{\mathrm{u}}^{\mathrm{m}}_j \\ \dot{\mathrm{u}}^{\mathrm{i}}_j \end{pmatrix} \tag{232}$$

where

$$\mathbf{D} \quad = \begin{pmatrix} 0 & 0 \\ 0 & \frac{1}{k_{\mathrm{DS}}} \end{pmatrix} \mathbf{T}^{-1} = \begin{pmatrix} 0 & 0 \\ 0 & -\frac{\eta_0}{k_{\mathrm{DS}}} \end{pmatrix}. \tag{233}$$

By setting $\begin{pmatrix} \mathrm{u}^{\mathrm{m}}_j & \mathrm{u}^{\mathrm{i}}_j \end{pmatrix}^T \equiv \mathbf{u}$ and $\begin{pmatrix} \tau^{\mathrm{m}}_{jk} & \tau^{\mathrm{i}}_{jk} \end{pmatrix}^{\mathrm{T}} \equiv \boldsymbol{\tau}_{jk}$, introduced earlier in (169) and (171), and $\begin{pmatrix} 0 & 0 \end{pmatrix}^{\mathrm{T}} \equiv \mathbf{0}$, the above are written in a compact form as

$$\left\langle \mathbf{T}^{-1}\dot{\mathbf{u}} \right\rangle \quad = \quad \mathbf{0}, \tag{234}$$

$$\left\langle \mathbf{T}^{\mathrm{T}}\boldsymbol{\tau}_{jk}\hat{n}_j - \mathbf{D}\dot{\mathbf{u}} \right\rangle \quad = \quad \mathbf{0} \tag{235}$$

Equations (234) and (235) shall be referred as DS09 boundary conditions, henceforth.

C.2 de la Cruz and Spanos (1989) boundary conditions

The boundary conditions due de la Cruz and Spanos (1989) are based upon conservation of total mass and total linear momentum and the application of Newton's third law of motion to describe how the stresses on each phase interact with the stress on each of the phases across the boundary.

C.2.1 Continuity of total mass

de la Cruz and Spanos started with the well established equations of mass balance for multi-phasic medium. For the solid and fluid bi-phasic medium, those equations read as below

$$\frac{\partial}{\partial t}((1-\eta)\rho_{\mathrm{s}}) = \partial_j((1-\eta)\rho_{\mathrm{s}}\dot{\mathrm{u}}^{\mathrm{s}}_j), \tag{236}$$

$$\frac{\partial}{\partial t}(\eta\rho_{\mathrm{f}}) = \partial_j(\eta\rho_{\mathrm{f}}\dot{\mathrm{u}}^{\mathrm{f}}_j). \tag{237}$$

They showed that by adding the above two equations one obtains

$$\frac{\partial}{\partial t}(\underbrace{(1-\eta)\rho_{\mathrm{s}}+\eta\rho_{\mathrm{f}}}_{\rho_{\mathrm{m}}}) = \partial_j(\underbrace{(1-\eta)\rho_s\dot{\mathrm{u}}^{\mathrm{s}}_j+\eta\rho_f\dot{\mathrm{u}}^{\mathrm{f}}_j}_{\rho_{\mathrm{m}}\ (m_{\mathrm{s}}\dot{\mathrm{u}}^{\mathrm{s}}_j+m_{\mathrm{f}}\dot{\mathrm{u}}^{\mathrm{f}}_j)}). \tag{238}$$

The term, $(1-\eta)\rho_{\mathrm{s}}+\eta\rho_{\mathrm{f}}$, on the left-hand side of equation, is recognized as total density of poro-continuum, ρ_{m}. On right-hand side of equation, ρ_{m} is factored out and the remaining term, with the aid of mass fractions introduced earlier in (160) and (159), is written as $m_{\mathrm{s}}\dot{\mathrm{u}}^{\mathrm{s}}_j+m_{\mathrm{f}}\dot{\mathrm{u}}^{\mathrm{f}}_j$, which is the vector sum of mass weighted solid and fluid velocity fields. They pointed out that since the above equation is obviously the equation of balance of total mass of poro-continuum, the vector sum of mass weighted solid and fluid velocity fields has to be recognized as the velocity associated with the

linear momentum flux. Thereupon, they suggested that if total mass of poro-continuum has to conserve across the interface, then the normal component of this velocity field must remain continuous, i. e.,

$$\left\langle m_{\mathrm{s}}\dot{\mathrm{u}}^{\mathrm{s}}_{\perp} + m_{\mathrm{f}}\dot{\mathrm{u}}^{\mathrm{f}}_{\perp}\right\rangle = 0. \tag{239}$$

They argued that the macroscopic interface between two porous media has to be taken as the surface across which total mass is conserved, not the fluid-fluid or solid-solid contact surfaces. Furthermore, on the basis of the macroscopic nonslip, they assumed that tangential component of this velocity field should also remain continuous which lead to

$$\left\langle m_{\mathrm{s}}\dot{\mathrm{u}}^{\mathrm{s}}_{j} + m_{\mathrm{f}}\dot{\mathrm{u}}^{\mathrm{f}}_{j}\right\rangle = 0. \tag{240}$$

C.2.2 Continuity of total linear momentum

de la Cruz and Spanos (1989) showed that by adding the equation of motion for solid frame and fluid constituent given in equations (125) and (126), respectively, one obtains

$$\frac{\partial}{\partial t}(\rho(m_{\mathrm{s}}\dot{\mathrm{u}}^{\mathrm{s}}_{j} + m_{\mathrm{f}}\dot{\mathrm{u}}^{\mathrm{f}}_{j})) = \partial_k(\tau^{\mathrm{s}}_{jk} + \tau^{\mathrm{f}}_{jk}). \tag{241}$$

They argued since the left-hand side term is the rate of change of total linear momentum, equation (241) is the statement of conservation total of linear momentum, therefore, the sum,$\tau^{\mathrm{s}}_{jk} + \tau^{\mathrm{f}}_{jk}$, has to be taken as the total stress[1], τ^{m}_{jk}, of poro-continuum. Thereupon, they suggested that if the total linear momentum has to be conserved across the interface, then total traction of poro contimuum must remain continuous, i. e.,

$$\left\langle \left(\tau^{\mathrm{s}}_{jk} + \tau^{\mathrm{f}}_{jk}\right)\hat{n}_k\right\rangle \;=\; 0. \tag{242}$$

[1] τ_{jk} and τ^{m}_{jk} are notations for the same quantity, the total stress of poro-continuum.

C.2.3 Newton's third law of motion and balance of phasic forces

Equation (242) implies that the total forced exerted on the interface by a side is balanced by an equal and opposite force exerted on the interface by the other side. This is the statement of Newton's third law of motion. de la Cruz and Spanos (1989) have asserted that as Newton's third law is operational on the totality of the phasic forces, it must hold true for how phasic forces are individually balanced at the interface. On this basis they suggested two additional conditions on tractions as below.

At interface, a given phase from one side overlaps with the both phases on the other side. Say, η_a be average area, per unit circle, of the fluid phase in the side "a" that is in contact with the fluid and solid phases in the side "b". Without loss of generality, it may be viewed as the unperturbed porosity of the side "a". Let P and Q be the average area of the overlap of the fluid in the side "a" with the fluid and solid phases in the side "b", respectively. Then, force exerted by medium "b" on the fluid phase in "a" is

$$P\sigma_{jk}^{\mathrm{f}(b)}\hat{n}_k + Q\sigma_{jk}^{\mathrm{s}(b)}\hat{n}_k, \tag{243}$$

where $\sigma_{jk}^{\mathrm{f}(b)}\hat{n}_k$ and $\sigma_{jk}^{\mathrm{s}(b)}\hat{n}_k$ stand for force exerted, per unit area, by fluid and solid phases on the side "b", respectively. Clearly, in the view of Newton's third law, this must be balanced by forces exerted by the fluid phase in the side "a", i. e.,

$$P\sigma_{jk}^{\mathrm{f}(b)}\hat{n}_k + Q\sigma_{jk}^{\mathrm{s}(b)}\hat{n}_k = \eta_a\sigma_{jk}^{\mathrm{f}(a)}\hat{n}_k, \tag{244}$$

where $\sigma_{jk}^{\mathrm{f}(a)}\hat{n}_k$ is the force exerted, per unit area, by the fluid phase on the side "b". The reciprocal interaction, the balance of forces exerted by medium "a" on fluid in medium

"b" and vice-versa, results into

$$P\sigma_{jk}^{\mathrm{f}(a)}\hat{n}_k + R\sigma_{jk}^{\mathrm{s}(a)}\hat{n}_k = \eta_b\sigma_{jk}^{\mathrm{f}(b)}\hat{n}_k, \tag{245}$$

where η_b is the average area per unit circle of the fluid phase in the side "b" and R is the average area of overlap of the fluid in the side "b" with the solid phase in the side "a".

By definition, $P + Q = \eta_a$ and $P + R = \eta_b$. Setting the average area of overlap of the fluids on two side, $P = \eta_a\eta_b\beta$, where β spans from $0 \leq \beta \leq \frac{1}{\eta_{[a/b]}}$ and $\eta_{_{[a/b]}}$ stands for the greater of η_a and η_b, one finds $Q = \eta_a(1 - \eta_b\beta)$ and $R = \eta_b(1 - \eta_a\beta)$. Using these definitions of overlap areas, and employing the notations of phasic stresses

$$\tau_{jk}^{\mathrm{f}(a)} = \eta_a\sigma_{jk}^{\mathrm{f}(a)}, \tau_{jk}^{\mathrm{s}(a)} = (1 - \eta_a)\sigma_{jk}^{\mathrm{s}(a)} \text{ etc.}, \tag{246}$$

equations (244) and (245) are written as

$$\tau_{jk}^{\mathrm{f}(a)}\hat{n}_k = \eta_a\beta\tau_{jk}^{\mathrm{f}(b)}\hat{n}_k + \frac{\eta_a\,(1 - \eta_b\beta)}{1 - \eta_b}\tau_{jk}^{\mathrm{s}(b)}\hat{n}_k, \tag{247}$$

$$\tau_{jk}^{\mathrm{f}(b)}\hat{n}_k = \eta_b\beta\tau_{jk}^{\mathrm{f}(a)}\hat{n}_k + \frac{\eta_b\,(1 - \eta_a\beta)}{1 - \eta_a}\tau_{jk}^{\mathrm{s}(a)}\hat{n}_k, \tag{248}$$

Equations (240), (242), (247) and (248) constitute the set of boundary conditions of the de la Cruz and Spanos (1989) framework.

C.2.4 Reformulated de la Cruz and Spanos boundary conditions (dCS09)

By convention, boundary conditions must be such that they also conserve total energy at the interface. de la Cruz and Spanos (1989) have not touched upon this issue explicitly. Sahay (2009, private communications) has showed that by subjecting equations (247) and (248) to the continuity of total traction (242), one finds that they are simply

the statement about continuity of fluid traction acting on per unit area. The continuity of solid traction (per unit area) is also implicit with the continuity of the total traction and fluid traction (per unit area), and thus it in not an independent condition. Furthermore, he has shown that given total mass, total traction, and fluid traction (per unit area) are continuous, the conservation of energy requires that the fluid velocity field must also remain continuous. The derivations are shown below.

By using the identities $\tau_{jk}^{\mathrm{f}(a)} + \tau_{jk}^{\mathrm{s}(a)} = \tau_{jk}^{(a)}$, and $\tau_{jk}^{\mathrm{f}(b)} + \tau_{jk}^{\mathrm{s}(b)} = \tau_{jk}^{(b)}$ in equations (247) and (248), the solid traction parts are eliminated. Upon further rearrangements they read, in terms of fluid traction and total traction, as

$$\tau_{jk}^{\mathrm{f}(a)}\hat{n}_k - \frac{\eta_a(\beta-1)}{1-\eta_b}\tau_{jk}^{\mathrm{f(b)}}\hat{n}_k = \eta_a\left(1 - \frac{\eta_b(\beta-1)}{1-\eta_b}\right)\tau_{jk}^{\mathrm{(b)}}\hat{n}_k, \tag{249}$$

$$\tau_{jk}^{\mathrm{f}(b)}\hat{n}_k - \frac{\eta_b(\beta-1)}{1-\eta_a}\tau_{jk}^{\mathrm{f(a)}}\hat{n}_k = \eta_b\left(1 - \frac{\eta_a(\beta-1)}{1-\eta_a}\right)\tau_{jk}^{\mathrm{(a)}}\hat{n}_k. \tag{250}$$

On the basis of the continuity of total traction (242), setting $\tau_{jk}^{(a)}\hat{n}_k = \tau_{jk}^{(b)}\hat{n}_k \equiv \tau_{jk}\hat{n}_k$ in the above and solving for the fluid stresses yields

$$\tau_{jk}^{\mathrm{f}(a)}\hat{n}_k = \eta_a\tau_{jk}\hat{n}_k, \tag{251}$$

$$\tau_{jk}^{\mathrm{f}(b)}\hat{n}_k = \eta_b\tau_{jk}\hat{n}_k. \tag{252}$$

Recalling that τ_{jk}^{f} is the force extered by the fluid phase upon η part of the unit area (see 246), the above equations may be viewed as the continuity of $\sigma_{jk}^{\mathrm{f}}\hat{n}_k$, the force exerted by the fluid phase upon an unit area,

$$< \sigma_{jk}^{\mathrm{f}}\hat{n}_k > = 0, \tag{253}$$

which the final form of equations (247) and (248). It is to be noted that overlap parameter, β, is no longer present in this form. Finally, subjecting the continuity of

normal energy flux (203) to the conditions of (240), (242), and (253), yields

$$\left\langle (m_{\mathrm{f}} - \eta) \left(\dot{\mathrm{u}}_j^{\mathrm{s}} - \dot{\mathrm{u}}_j^{\mathrm{f}} \right) \right\rangle \;=\; 0. \tag{254}$$

Thus, equations (240), (242), (253) and (254) are the reformulated de la Cruz and Spanos boundary conditions.

Using the definition for fluid mass fraction (159)

$$(m_{\mathrm{f}} - \eta) = -\eta \left(1 - \frac{\rho_{\mathrm{f}}}{\rho_{\mathrm{m}}} \right) = -\eta(1-\eta)\frac{\rho_{\mathrm{s}} - \rho_{\mathrm{f}}}{\rho_{\mathrm{m}}} = -\eta \Delta_\rho, \tag{255}$$

where $(1-\eta)\frac{\rho_{\mathrm{s}} - \rho_{\mathrm{f}}}{\rho_{\mathrm{m}}} \equiv \Delta_\rho$ may be view as buoyancy of the poro-continuum, equation (260) can be viewed in terms of filtration velocity (equation 211) as

$$\langle \Delta_\rho \mathrm{w}_j \rangle = 0. \tag{256}$$

C.2.5 dCS09 boundary conditions in terms of natural dynamical fields

By using the transformation introduced in (156) and (157), the reformulated de la Cruz and Spanos (equations 240, 242, 253 and 254), in terms of natural dynamical field variables, are as follows

$$\left\langle \mathrm{u}_j^{\mathrm{m}} \right\rangle \;=\; 0, \tag{257}$$

$$\left\langle \tau_{jk}^{\mathrm{m}} \hat{n}_j \right\rangle \;=\; 0, \tag{258}$$

$$\left\langle \left((m_{\mathrm{f}} - \eta)\, \tau_{jk}^{\mathrm{m}} - \tau_{jk}^{\mathrm{i}} \right) \hat{n}_j \right\rangle \;=\; 0, \tag{259}$$

$$\left\langle (m_{\mathrm{f}} - \eta)\, \mathrm{u}_j^{\mathrm{i}} \right\rangle \;=\; 0. \tag{260}$$

Equations (257) and (260) are viewed in a matricial form as

$$\left\langle \underbrace{\begin{pmatrix} 1 & 0 \\ 0 & m_{\mathrm{f}} - \eta \end{pmatrix}}_{\mathbf{G}} \begin{pmatrix} \mathrm{u}_j^{\mathrm{m}} \\ \mathrm{u}_j^{\mathrm{i}} \end{pmatrix} \right\rangle = \begin{pmatrix} 0 \\ 0 \end{pmatrix}, \quad \text{or } \langle \mathbf{G}\ \mathbf{u} \rangle = \mathbf{0}. \tag{261}$$

where $\left(\mathrm{u}_j^{\mathrm{m}} \;\; \mathrm{u}_j^{\mathrm{i}}\right)^T \equiv \mathbf{u}$ introduced earlier in 169 and $(0 \;\; 0)^{\mathrm{T}} \equiv \mathbf{0}$. Likewise, equations (258) and (259) in a matricial form are

$$\left\langle \underbrace{\begin{pmatrix} 1 & 0 \\ m_{\mathrm{f}} - \eta & -1 \end{pmatrix}}_{\mathbf{H}} \begin{pmatrix} \tau_{jk}^{\mathrm{m}} \hat{n}_j \\ \tau_{jk}^{\mathrm{i}} \hat{n}_j \end{pmatrix} \right\rangle = \begin{pmatrix} 0 \\ 0 \end{pmatrix} \quad \text{or } \langle \mathbf{H}\ \boldsymbol{\tau}_{jk} \hat{n}_j \rangle = \mathbf{0}. \tag{262}$$

where $\left(\tau_{jk}^{\mathrm{m}} \;\; \tau_{jk}^{\mathrm{i}}\right)^{\mathrm{T}} \equiv \boldsymbol{\tau}_{jk}$ (see 171). Henceforth, equations (261) and (262) are referred as dCS09 boundary conditions.

Appendix D

PHYSICAL PROPERTIES

The following data are used in the numerical computation.

Table X. Solid-frame properties

solid density:	ρ_{s}	=	$2.65 \times 10^{+03}$	$\left(\frac{kg}{m^3}\right)$,
mineral frame P-velocity:	$\mathrm{v}_{\mathrm{p}_{\mathrm{s}}}$	=	$5.694 \times 10^{+03}$	$\left(\frac{m}{s}\right)$,
mineral frame S-velocity:	$\mathrm{v}_{\mathrm{s}_{\mathrm{s}}}$	=	$3.796 \times 10^{+03}$	$\left(\frac{m}{s}\right)$,
dry frame P-velocity:	$\mathrm{v}_{\mathrm{p}_0}$	=	$1.500 \times 10^{+03}$	$\left(\frac{m}{s}\right)$,
dry frame S-velocity:	$\mathrm{v}_{\mathrm{s}_0}$	=	$1.700 \times 10^{+03}$	$\left(\frac{m}{s}\right)$,
permeability	K	=	10×10^{-13}	(m^2),
porosity:	η_0	=	0.3,	
tortuosity factor:	S	=	$\frac{4}{3}$,	

Table XI. Fluid properties

Gas				
density:	ρ_0^{f}	=	$100 \times 10^{+03}$	$\left(\frac{kg}{m^3}\right),$
shear viscosity:	μ^{f}	=	15.0×10^{-06}	$(Pa{\cdot}s),$
bulk viscosity:	ξ^{f}	=	35×10^{-06}	$(Pa{\cdot}s),$
bulk modulus:	K^{f}	=	$22 \times 10^{+08}$	$(Pa),$
Air				
density:	ρ_0^{f}	=	$.121 \times 10^{+03}$	$\left(\frac{kg}{m^3}\right),$
shear viscosity:	μ^{f}	=	18.0×10^{-06}	$(Pa{\cdot}s),$
bulk viscosity:	ξ^{f}	=	35×10^{-06}	$(Pa{\cdot}s),$
bulk modulus:	K^{f}	=	$15 \times 10^{+06}$	$(Pa),$
Oil				
density:	ρ_0^{f}	=	$.900 \times 10^{+03}$	$\left(\frac{kg}{m^3}\right),$
shear viscosity:	μ^{f}	=	1.00×10^{-03}	$(Pa{\cdot}s),$
bulk viscosity:	ξ^{f}	=	2.8×10^{-03}	$(Pa{\cdot}s),$
bulk modulus:	K^{f}	=	$0.5 \times 10^{+09}$	$(Pa),$
Water				
density:	ρ_0^{f}	=	$1.00 \times 10^{+03}$	$\left(\frac{kg}{m^3}\right),$
shear viscosity:	μ^{f}	=	1.00×10^{-03}	$(Pa{\cdot}s),$
bulk viscosity:	ξ^{f}	=	2.8×10^{-03}	$(Pa{\cdot}s),$
bulk modulus:	K^{f}	=	$2.4 \times 10^{+09}$	$(Pa),$

Appendix E

NATURE OF WAVE FIELDS

In order to illustrate the nature of wave fields, for a sample of Berea sandstone saturated with different fluids, namely, water, oil and gas, velocity and attenuation (Figure 22) along with the associated ratio of centre-of-mass and internal displacement fields (Figure 23) as well as the ratio of solid and fluid displacement fields (Figure 24) are shown. The Biot critical frequencies for each kind of fluid are marked by a down arrow on the frequency axis in their corresponding colors. The physical properties of the sample are listed in Appendix A.

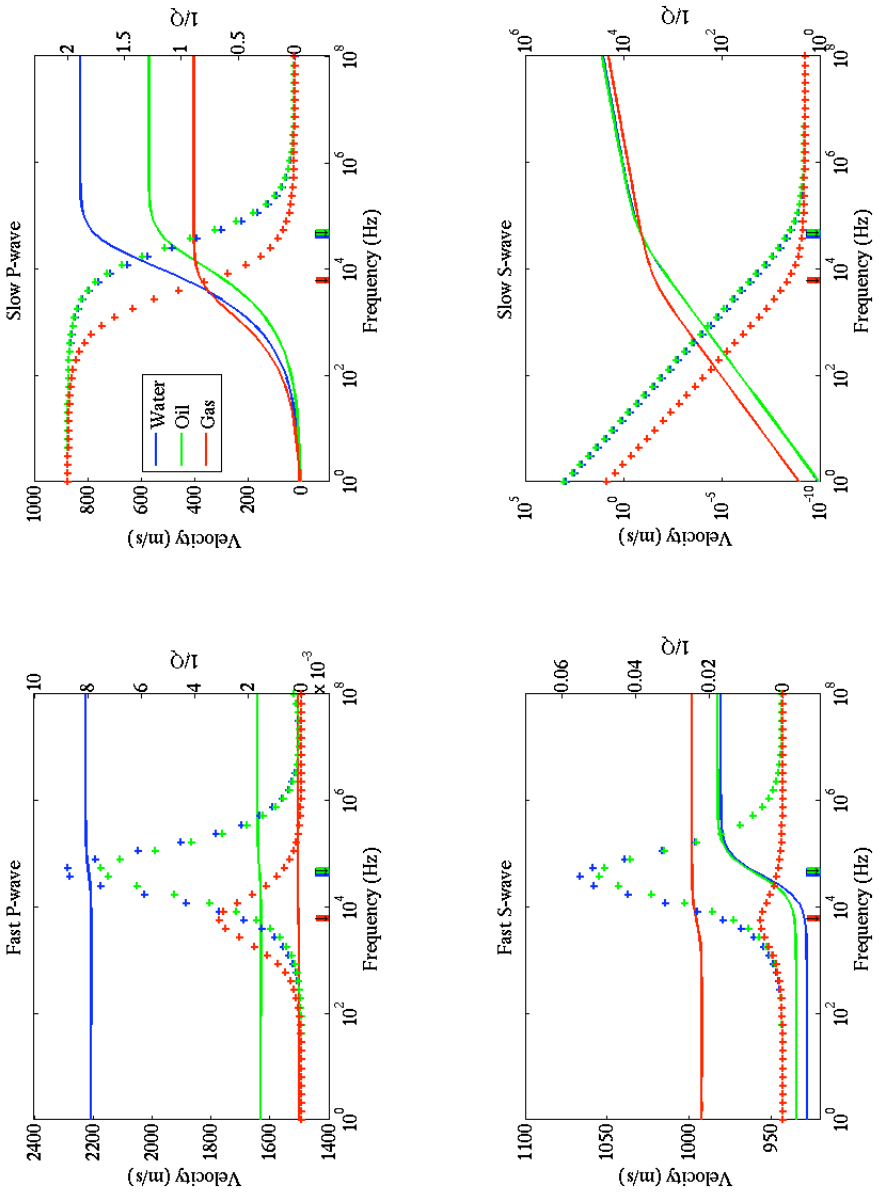

Figure 22. Velocity and attenuation are shown, respectively, in solid and crossed curves. In all plots, the scales of velocities and phases are shown on the left and right vertical axes.

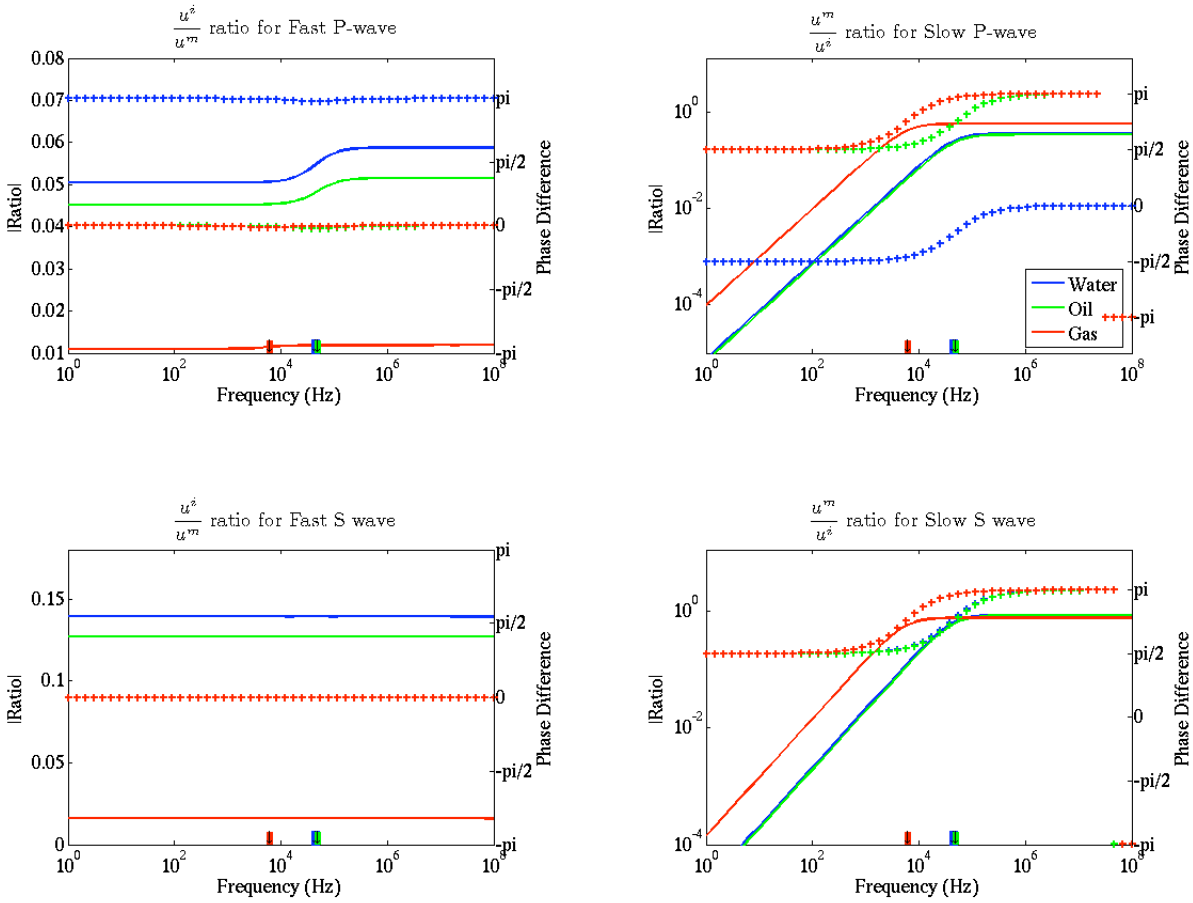

Figure 23. Amplitude and phase parts of the ratio of internal to center of mass associated with fast P-wave. The modulus and phases are plotted in solid and crossed lines, respectively. In all plots, the scales of modulus and phases are shown on the left and right vertical axes.

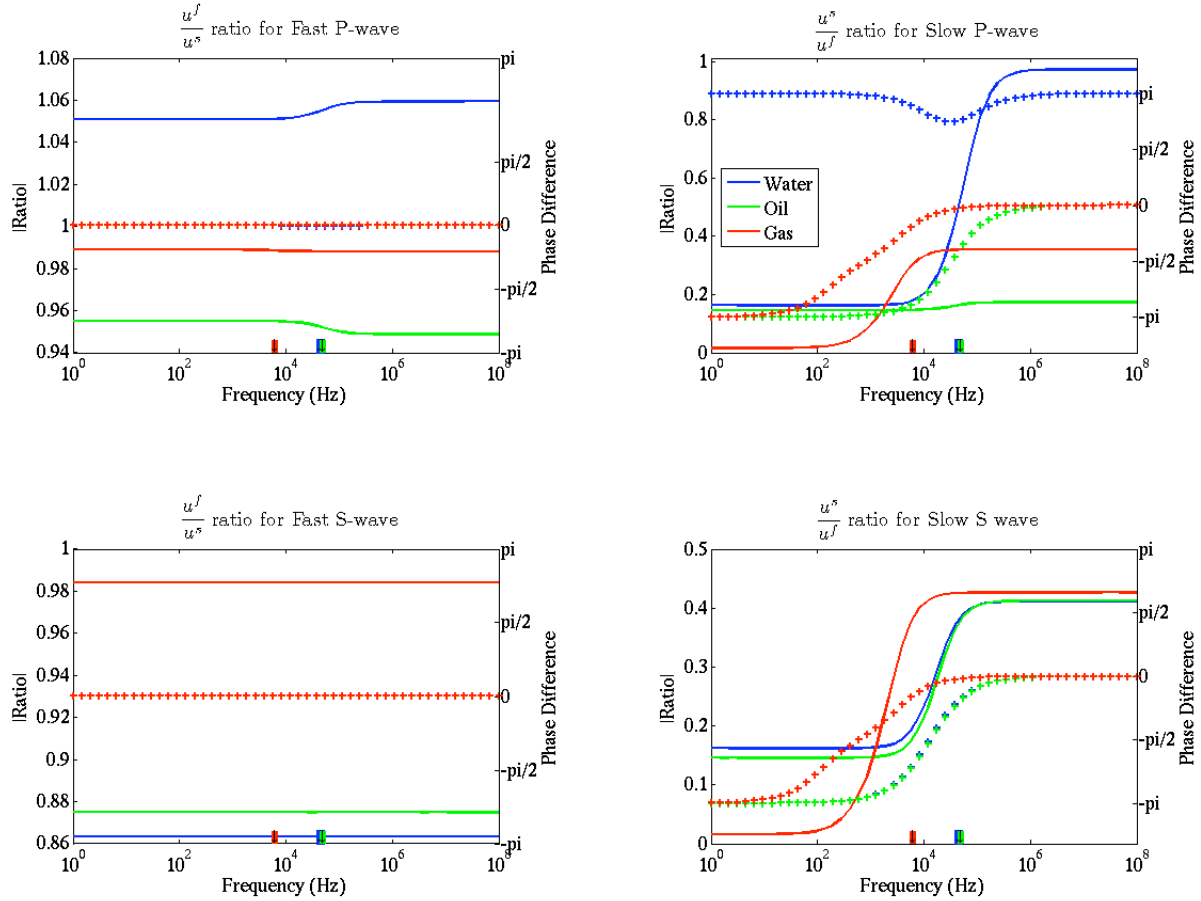

Figure 24. Amplitude and phase parts of the ratio of solid to fluid motions associated with fast P-wave plotted in solid and crossed lines, respectively. In all plots, the scales of modulus and phases are shown on the left and right vertical axes.